EXPERIMENTAL ANALYSIS OF LIMITATIONS IN THE STRUT-AND-TIE METHOD

Niels Bailleul
Mikael Wahlgren

LUNDS UNIVERSITET
Lunds Tekniska Högskola

2016

Report TVBK-5249
ISSN 0349-4969
ISRN: LUTVDG/TVBK-16/5249 (118p)

Master's thesis
Supervisors: Oskar Larsson and Kent Kempengren
Examiner: Annika Mårtensson

May 2016

DIVISION OF STRUCTURAL ENGINEERING
FACULTY OF ENGINEERING
MASTER'S THESIS

EXPERIMENTAL ANALYSIS OF LIMITATIONS IN THE STRUT-AND-TIE METHOD

EXPERIMENTELL ANALYS AV BEGRÄNSNINGARNA I FACKVERKSMETODEN FÖR HÖGA BETONGELEMENT

NIELS BAILLEUL and MIKAEL WAHLGREN

Supervisors: OSKAR LARSSON, Div. of Structural Engineering, LTH and
KENT KEMPENGREN, Div. of Structural Engineering, LTH

Examiner: Professor ANNIKA MÅRTENSSON, Div. of Structural Engineering, LTH

Keywords: *Strut-and-Tie method, Reinforced concrete, Concrete Damaged Plasticity, Fracture energy,*

Nyckelord: *Fackverksmetoden, Armerad betong, Sprickenergi*

ABSTRACT

One of the overall main purposes for a structural engineer is to design structures and structural elements so that they meet society's safety requirements, yet use as little material as possible. In order to do so, the designer has to understand and simplify a complex reality. The strut-and-tie method is such a simplification model which allows engineers to design reinforced concrete structures where basic beam theory is not applicable, e. g. high beams or discontinuity regions near supports and loads.

When designing according to the strut-and-tie method, several assumptions have to be made regarding the structural behavior. Questions exists whether current recommendations regarding these assumptions are conservative – the assumed internal truss system for ultimate limit state calculations is usually based on the linear-elastic stress field. This despite stress redistribution due to cracking and plastic deformations is possible. Accounting for the stress redistribution would yield a higher load-bearing capacity in the ultimate limit state. The conservative approach derives from uncertainties regarding the materials plastic deformation capacities and serviceability limit state considerations.

The aim of this report is to investigate the effects on the stress distribution of a simply supported high concrete beam when loaded to failure, investigating the redistribution capacity of the member. In the design of the specimen, extreme cases were chosen, e.g. a structure with a very small amount of reinforcement. Thus, the scope of the project also includes limitations in the strut-and-tie method.

Studies were performed on four specimen with different amount of reinforcement; three members with increasing amount of reinforcement and a fourth reinforced with a minimum reinforcement mesh in accordance with Eurocode. The beams were simply supported and subjected to two-point loading. Laboratory results were compared with computer simulations and hand calculations.

Analyzing the results from the simulations indicated a rise of the internal lever arm, in three out of four cases. The laboratory test results clearly showed two types of behavior; a brittle failure for the 'insufficiently reinforced' and a ductile response from the one with minimum reinforcement installed. Comparing the results from the lab and the model gave diverse results in terms of stiffness.

SAMMANFATTNING

Ett av de övergripande syftena för en konstruktör är att utforma konstruktioner och konstruktionselement så att de uppfyller samhällets säkerhetskrav, samtidigt som materialanvändandet är sparsamt. För att klara av detta måste konstruktören förstå och förenkla en komplex verklighet. Fackverksmetoden är en modell som gör det möjligt för konstruktörer att utforma betongkonstruktioner där grundläggande balkteori inte är tillämplig, t.ex. höga balkelement eller diskontinuitetsregioner nära stöd och laster.

Vid dimensionering enligt fackverksmetoden måste flera antaganden göras om konstruktionens beteende. Frågor huruvida nuvarande rekommendationer gällande dessa antaganden är konservativa finns – den interna hävarmen för beräkningar i brottgränstillstånd är baserad på det linjär-elastiska spänningsfältet. Detta trots att ett tillgodoräknande av spänningsomfördelning på grund av sprickor och plastiska deformationer är möjligt för dimensionering i brottgränstillstånd. Ett sådant tillgodoräknande skulle ge högre bärförmåga. Det konservativa förhållningssättet härstammar från osäkerheter gällande materialens plastiska deformationskapacitet och dess respons i bruksgränstillstånd.

Syftet med denna rapport är att undersöka effekterna på spänningsfördelningen av en fritt upplagd hög betongbalk när den belastas till brott och därigenom undersöka konstruktionens kapacitet att omlagra spänningar. Vid utformningen av försöken valdes extrema fall, exempelvis konstruktioner med mycket låg armeringsmängd. Således ingår också analyser av begränsningar i metoden.

Studier utfördes på fyra prov med varierande armeringsmängd; tre provkroppar med ökande mängd armering och en fjärde förstärkt med minimiarmeringsnät i enlighet med Eurocode. Balkarna utsattes för tvåpunktsbelastning och var fritt upplagda. Laboratorieresultat jämfördes med datorsimuleringar och handberäkningar.

När resultaten från simuleringen analyserades kunde utvecklingen av den inre hävarmen enkelt konstateras. Resultaten från laborationen gav indikationer på två typer av beteende; ett sprött brott i balken med minst armering, samt ett duktilt beteende hos balken försedd med minimiarmering. När resultaten från de två metoderna jämfördes uppvisades dock stora skillnader vad gäller styvhet.

ACKNOWLEDGEMENTS

This master's thesis was made at the Division of Structural Engineering at the Faculty of Engineering LTH at Lund University during the spring of 2016, starting in January and finalized in May.

We would like to thank first and foremost our supervisors Dr. Oskar Larsson, who initiated the idea for this thesis and for all valuable comments and hints and Ph.D. student Kent Kempengren who we have shared a lot of headaches with in the computer modelling process and who have always helped us when in need. We would also like to thank Prof. Emeritus Sven Thelandersson who have offered his expertise and knowledge throughout the process.

A special thanks to research engineer Per-Olof Rosenkvist for all help and good times in the lab; and research engineer Bengt Nilsson for the help in the advanced 'fracture energy' testing.

Most importantly we would like to thank each other. For enduring this process, always striving forward and for motivating and helping one another.

This concludes a five year journey at Lund University. A time period that have shaped us to the individuals we are today. One last thanks therefore goes to everyone that have enriched this time, especially during the last year – the late nights in school, the ping pong tournaments and all the interesting discussions. Thank you.

LUND, MAY 2016

Engineering is the art of modelling materials we do not wholly understand, into shapes we cannot precisely analyze so as to withstand forces we cannot properly assess, in such a way that the public has no reason to suspect the extent of our ignorance.

– Dr AR Dykes

CONTENTS

1 INTRODUCTION

1.1 Background

In order to meet safety requirements which society has set upon the construction business, structural engineers need to design structures with a certain reliability. A balanced solution in which sufficient reliability and proper material utilization should be chosen. Designing a structure safely requires adequate understanding of the behavior of structural elements as well as the structure as a whole. In order to understand this, there are several ways to simplify a complex reality. Many of these simplifications are subject to deeper investigations.

A structural element most designers encounter during their career is the reinforced concrete member, such as a beam, slab, wall or column. The challenges of these structural elements are typically the combination of reinforcing steel and concrete. In many cases this is not an issue as simple calculation models exist which are easy to understand. Generally, 'normal' beams are convenient to analyze. However, these may consist of so-called discontinuity regions where the standard beam theories are not applicable. This is where the strut-and-tie method comes in handy, supplying the engineer with a method to design the discontinuity regions in a convenient and understandable way.

The strut-and-tie method allows the engineer to estimate the response of such a discontinuity region. This is done by assuming a fictitious truss, where the compressive regions are simplified as struts and the tensile regions are simplified as ties, hence the name of the method. Questions whether the strut-and-tie method is overly conservative or not may be raised. The struts and ties are often arranged according to the linear-elastic stress field. However, taking into account a fully plastic stress field, with regard to stress redistribution due to cracking and plasticity of materials, would allow a higher load-bearing capacity of discontinuity regions.

1.2 Objective

The main objective of this thesis is to investigate the stress behavior when test specimen are incrementally loaded to failure. From this, conclusions about how the internal lever arm in the fictive truss develops may be drawn. The objective is also to investigate limitations in the strut-and-tie method.

One of the potential outcomes is an indication on the stress redistribution capacity of a high concrete beam. Recommended design angle is today $\alpha = 60°$, based on theory of elasticity, which may be considered as conservative. Including the stress redistribution capacity of the concrete structure, due to plastic deformations of materials as well as cracking, a higher angle would be obtained, thus leading to smaller dimensions and better utilization of material.

1.3 Scope & Limitations

The scope of this master thesis is to review chosen angles and limitations in the strut-and-tie method.

Within the scope is also to verify if theory and practice conform. The investigation is limited to hand calculations, a laboratory practical of four test specimens and computer simulations.

The thesis will not study the impact of different concrete classes, nor the influence of different types of reinforcement. Solely one geometry will be tested to investigate the behavior of the theoretical model.

1.4 Method

After the initiating literature study, where knowledge upon previous discoveries, theories and tests were gained, decisions were made upon desired dimensions and design of the high beams that were tested. Three different analysis were compared:

- Hand calculations for design of deep concrete members, using the strut-and-tie method
- Laboratory testing of designed specimens
- Computer modelling of designed specimens

The hand calculations were made iteratively in the decision making process to make sure the chosen specimen had desired capacity.

Three different reinforcement arrangements were chosen, T1, T2 and T3 with increasing amount of reinforcement. Applying the strut-and-tie method, the capacity of the three different specimen were calculated with internal angles of 45°, 60° and ~70°. A fourth specimen was made, using the same reinforcement configuration as T2, to study the effect of the recommended minimum reinforcement in the specimen.

The results achieved in the laboratory testing were compared with the results from the strut-and-tie method. Results from the computer modelling made in the software *BRIGADE/Plus* was also matter of comparison.

1.4.1 Literature study

The literature study may be divided into a set of theoretical areas:

- Basic theory of materials and their properties
- Codes and literature regarding the strut-and-tie method and previous testing
- Theory on which computer modelling is based

1.4.2 Hand calculations

Calculations made by hand were made using the simplified strut-and-tie method. These were made as a primary step in the project as well as a final evaluating step following the laboratory testing results.

1.4.3 Laboratory testing

Laboratory tests were made using the laboratory hall and belonging equipment and knowledge of the staff. Measurements and documentation of the entire process were made thoroughly. Testing of main specimens and material properties were carried out.

1.4.4 Computer modelling

Computer modelling was carried out using the finite element software *BRIGADE/Plus*, which uses the *Abaqus* interface and solver with additional features specialized towards civil engineering applications. The simulations provided a theoretical response of the test specimens.

1.5 Tested model

The load case applied throughout this project is shown in Figure 1-1. The total load, *F*, applied in the laboratory work will be divided into two point loads, more details in chapter 4. A displacement-controlled loading was applied in the laboratory process. Thus, when modelling in the finite element program *BRIGADE/Plus* the 'forces' were applied as displacements at the top of the beam resulting in reaction forces in the supports, equal to the, forces on top according to Newton's third law [1]. Details concerning the computer modelling are presented in chapter 5.

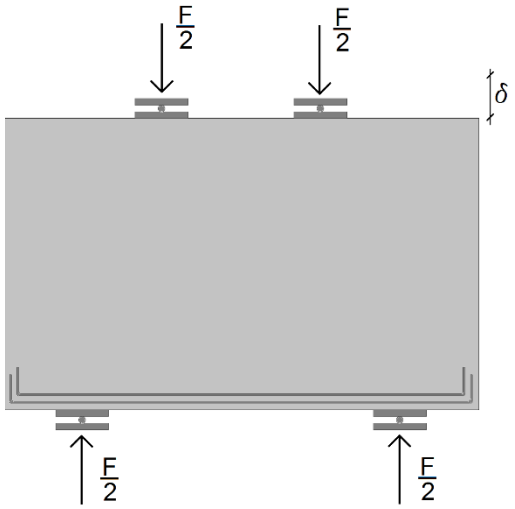

Figure 1-1: Deformation and reaction forces

Four different beam configurations were tested. The loading of each specimen was identical, the same goes for the boundary conditions and materials used. The overall design of the specimens is shown in Figure 1-2. What varied was the amount of primary reinforcement installed in the bottom of beams T1-T3. The fourth one, T4, was equipped with the same amount of primary reinforcement as T2, but with additional minimum reinforcement according to the standards.

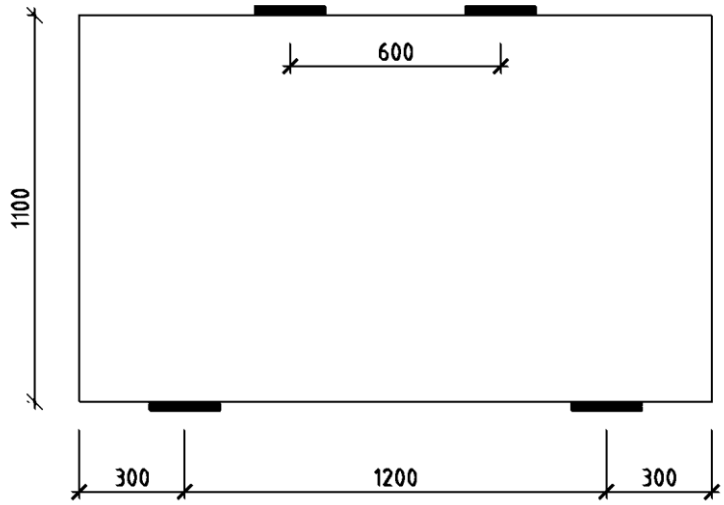

Figure 1-2: Overall setup of beams, depth 200 mm

The different setups are presented in Table 1-1. The reinforcement used got a diameter of $\phi 8\ mm$ and the number of reinforcement bars used originates from internal angles, α, of $45°, 60°\ and\ \sim 70°$. The calculations leading up to these results are presented in Appendix B.

*Table 1-1: Number of reinforcement bars in each beam *T4 also contains minimum reinforcement*

	Nr of reinforcement layers	Nr of reinforcement bars/ layer
T1	1	2
T2	2	2
T3	2	3
T4*	2	2

2 BACKGROUND THEORY

The following chapter briefs the reader about some essential theory applied in the project. Some basic beam theory together with properties of included materials is discussed. The strut-and-tie method is explained, including its development as well as the hypothesis concerning the internal angle from where this master thesis originate. Finally, constitutive modelling and theoretical basis of the computer model is explained.

2.1 Materials

Beside the geometry, the most influential and obvious factor which contribute to the strength and serviceability of a beam or bearing member, is the properties of the materials. The material structure, their individual strength in tension and compression as well as their relationship to each other and the collaboration between the different materials are decisive parts in a structures load-bearing capacity. These parameters and the behavior is what will briefly be explained in the following subsections.

2.1.1 Concrete

One commonly used building material is concrete, which is made up of cement, aggregates, water and occasionally additives to obtain desired properties of the final product.

Concrete is a convenient building material to use because of its compressional strength and versatility. Once a cast is made it is easy to pour the concrete, let it set and then make use of the structure. A weakness of the material is its tensile strength - concrete has significantly different behavior depending on how the load is applied. This fact makes it more complex to analyze in terms of structural strength.

The difference between the materials anisotropic strengths is due to the fact of micro cracks in the concrete, often in the face between the aggregate and the mortar, leaving the concrete composite with a reduced tensile strength [2]. The solution to the low tensile strength is reinforcement in the tensile areas, e.g. steel bars, subsection 2.1.3.

Furthermore, like many other materials, the behavior of the material is afflicted by the multiaxial stress state, i.e. simultaneously stressing concrete in different directions will severely affect the strength of the material.

Uniaxial state of stress – compression

An idealized stress-strain relationship for concrete in uniaxial compression is shown in Figure 2-1. Despite concrete often being referred to as a brittle material, it has some plastic capacity. When the concrete member is loaded, the stress-strain relationship is nearly linear to about $\sigma = 0.3f_c$. During this stage, the strain energy (the energy stored by a deformed structure) is less than the energy required to form new crack surfaces, meaning that the cracking of the concrete will be unchanged and a linear-elastic behavior is observed. When the stress rises above $0.3f_c$, to a level of approximately $0.5f_c$, the strain energy and crack-inducing energy is the same, meaning a stable crack growth occurs. If the applied load remains unchanged, cracks will grow quickly to their final extent. From $0.5f_c$ to $0.75f_c$ cracks start to merge and in the meantime cracks between mortar and aggregates, continue to slowly arise. [2]

If a constant load is applied, crack propagation will slowly occur until cracks have reached their final lengths. Finally, for compressive stresses above $0.75f_c$, unstable crack propagation is induced. The strain energy is on a level above the energy required to form cracks. In such a case, even though loading remain constant, rupture might occur. If the concrete is subjected purely to compressive stresses the micro cracks will grow and propagate until failure. [2]

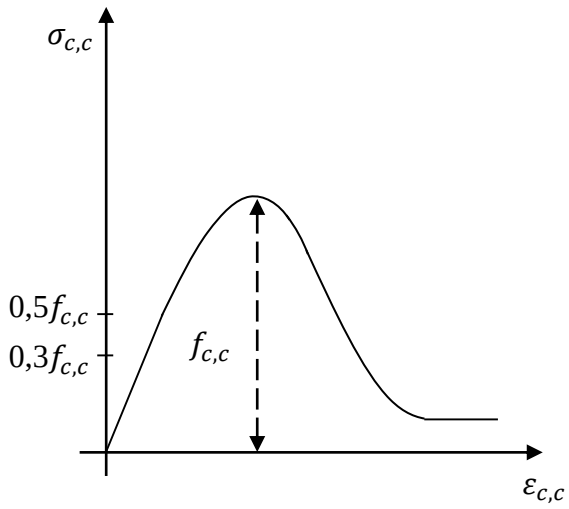

Figure 2-1: Idealized stress-strain relationship of concrete subjected to uniaxial compression

Despite the relationship being linear up to $0.3f_c$, in accordance with Burström [3], the linear modulus of elasticity in compression is normally defined as the secant modulus at 30-40% of the concrete strength f_c'. According to the codes [4] E_{cm} may defined as the modulus of elasticity defined at $0.4f_c$. The secant modulus of elasticity is then calculated as shown in Equation (2.1) [4], Figure 2-2.

$$E_{cm} = \frac{0{,}4f_c}{\varepsilon_{0{,}4f_c}} = \tan\alpha \qquad (2.1)$$

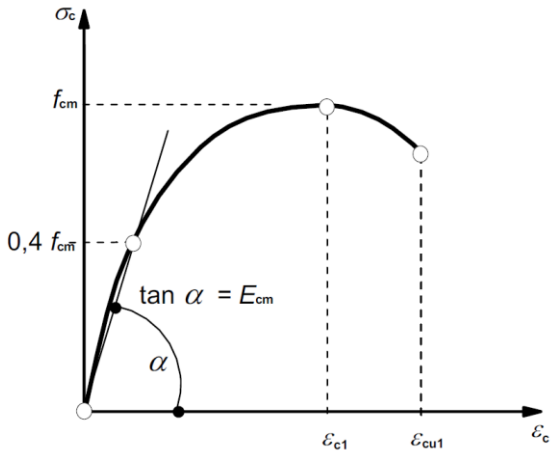

Figure 2-2: Idealized compressive stress-strain relationship for assessment of modulus of elasticity of concrete [4]

This idealization, adopted from [4], is used for non-linear analysis of structures. The expression for the curve is found in Equation (2.2).

$$\sigma_c = f_{cm} \cdot \frac{k\eta - \eta^2}{1 + (k-2) \cdot \eta} \qquad (2.2)$$

Where:

f_{cm} is according to the codes the mean strength of concrete

E_{cm} is according to the codes the mean modulus of elasticity of concrete, decided according to Equation (2.1) above

ε_{c1} is the strain when the maximum strength is reached, according to Eurocode defined as $\varepsilon_{c1} = 0.7 f_{cm}^{0.31} \leq 2.8$ ‰

$\eta = \varepsilon_c / \varepsilon_{c1}$

$k = 1.05\, E_{cm} \cdot |\varepsilon_{c1}| / f_{cm}$

This relation is valid for $0 < |\varepsilon_c| < |\varepsilon_{cu1}|$, where ε_{cu1} is the crushing strain of the concrete, according to the code 3.5 ‰ for concrete classes $< C50$.

Uniaxial state of stress – tension

When concrete is subjected to uniaxial tensile stresses it behaves different from the compressive state. The stress-strain relationship looks similar, however the tensile strength is significantly lower than the compressive strength and the material has a longer linear branch until reaching the tensile strength.

The elastic stress-strain relation, seen in Figure 2-3, lasts until about $0.6f_t$ [2], i.e. the level of micro cracks remain relatively unchanged. From approximately $0.6f_t$ to $0.75f_t$ crack propagation is regarded as stable. Above this level crack propagation is regarded as unstable. Tensile stresses will, apart from compressive stresses induce fewer, but larger, cracks transverse the stress direction. [2]

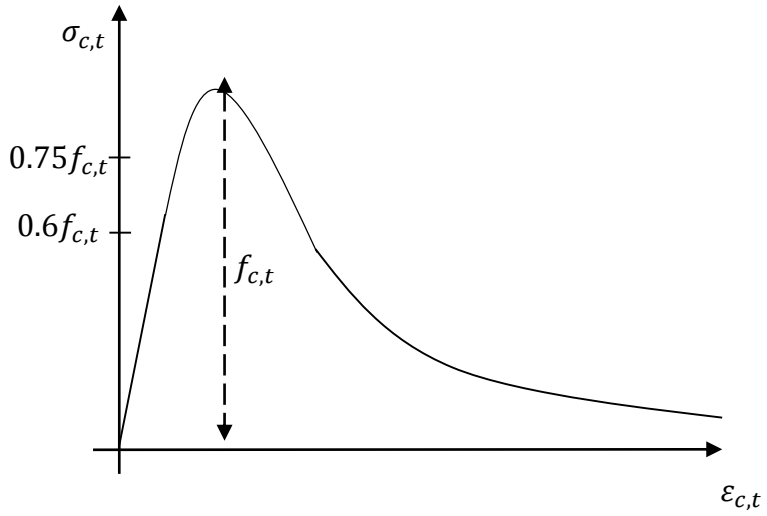

Figure 2-3: Uniaxial stress-strain relationship of concrete in tension

The tensile strength is somewhat unpredictable [3]. According to Neville [5] several relationships may be chosen, often on empirical basis and chosen as

$$f_t = k(f_c)^n \tag{2.3}$$

Where suggested values of n varies between $0.5 - 0.75$. Neville [5] suggests a relationship according to Equation (2.4):

$$f_t = 0.3(f_c)^{2/3} \tag{2.4}$$

Whilst Chen [2] suggests a relationship of Equation (2.5):

$$f_t = \frac{4}{145.0377} \cdot \sqrt{f_c} \tag{2.5}$$

Due to the uncertainties in deciding tensile strengths from the compressive strength further evaluation is preferred. A way of deciding the tensile strength is by so-called tensile splitting cylinder tests, Brazilian tests. In order to fully capture the tensile behavior, a fracture energy criterion is complementing the pure tensile strength. This fracture energy criterion is explained in subsection 2.6.1. Tests of the material properties are described in subsection 4.1.1.

Biaxial state of stress

A concrete member subjected to a biaxial stress state will have an impact on its behavior. Due to the different response from tensile and compressive stresses, differences exists whether the member is under compressive-compressive (CC), compressive-tensile (CT) or tensile-tensile stresses (TT) [2]. Generally, a CC-stress state yields a higher strength than uniaxial compressive strength, a CT-stress state a lower strength than uniaxial compressive strength and a TT-state a lower or approximately same strength compared to uniaxial tensile strength.

2.1.2 Reinforcing Steel

In contrary with concrete, steel is a homogeneous material, meaning that its material properties are similar in every direction. To achieve desired properties one may treat steel in different ways, most commonly hot- or cold rolled [3]. A hot-rolled steel is a ductile material and when studying the stress-strain curve it is obvious that the behavior of the material is somewhat non-linear.

A curve describing the behavior of hot-rolled steel is presented in Figure 2-4. The initial part of the curve, from 0-A, is the elastic region of the material, i.e. the material will regain its original state after loading. Part A-B of the first slope is also elastic, but the materials response to loading is no longer linear [6]. Reaching the first peak of the stress-strain curve, B, indicates the elastic limit of the material also known as the yield point. Exceeding this stress and the material will start to yield and adopt a deformed shape. Passing the initial yield stress decreases the strength of the material leaving it to yield at a lower stress, C. From this point a constant load will strain the material up to a certain point D [6]. Beyond this point the material is both elastic and plastic and the slope of the curve is continuously decreasing until the ultimate strength level, E [6]. Exceeding this point and failure will be imminent.

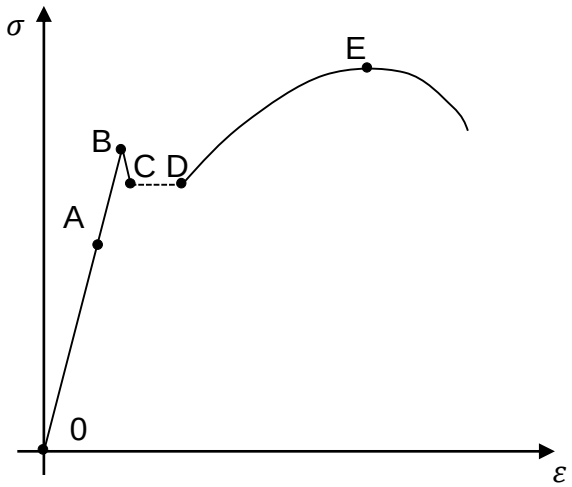

Figure 2-4: Stress-strain relationship of hot-rolled steel

One shall though keep in mind that in most cases the behavior from the elastic limit, B, to the far point of the flow zone, D, can be hard to distinguish. The yield stress is instead defined as the point where the material assumes a plastic deformation of *0.2%*, Figure 2-5. [6]

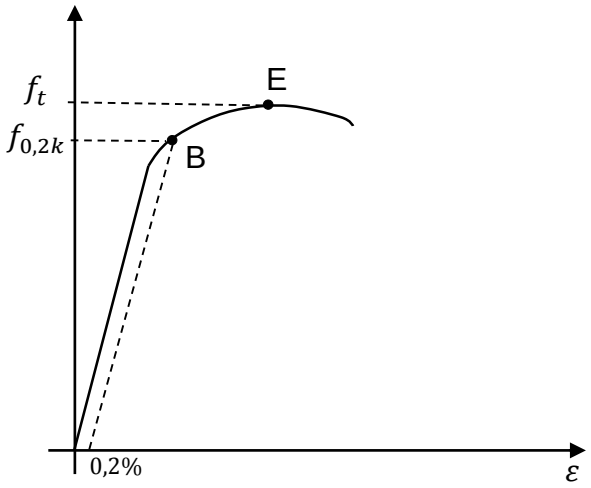

Figure 2-5: Idealized stress-strain curve of Steel

2.1.3 Reinforced concrete

As mentioned, due to the weak tensile strength, concrete structures need reinforcement. Most structures are subjected to some kind of tension and/or shear [7]. In modern day design of concrete, structures likely to be subjected only to compression are also reinforced in order to reach satisfactory level of reliability [7].

A reinforced concrete structure may be designed in several ways. A variety of alternatives exists, such as using reinforcement steel without prestress, prestressing wires, post-tensioning, and even carbon fiber solutions.

When reinforcement is introduced, the interaction between the two materials has to be considered. Steel is stiffer than concrete ($E_s > E_c$). Thus, steel will attract a higher amount of stress compared to concrete. Furthermore, in many applications concrete is assumed to have negligible tensile strength. In order to reach composite action between the two materials the strain of the concrete and the reinforcement bars has to be equal. This will lead to cracks in the tensile regions in the concrete.

To reach the composite action desired, sufficient bond strength between steel and concrete has to be reached. Bond is normally achieved through adhesion and friction [8]. This requirement is normally met by anchoring the bars to a certain extent and, if needed, they may be bent to offer satisfactory anchorage length.

2.2 Stress distribution

This section briefly discusses the stresses within a structure subjected to a load.

2.2.1 Linear stress distribution

In basic beam theory, also known as Bernoulli-Euler beam theory, it is often assumed that plane sections remain plane, sections remain perpendicular to its center line and that the strains varies linearly over the entire cross-section. One basic case is presented in Figure 2-6, where a column with the cross-sectional area *A* is subjected to a concentrated force *F*. The force is assumed to be carried by the entire cross-section from the point of loading. This yields the basic stress situation stated in Equation (2.6):

$$\sigma = \frac{F}{A} \tag{2.6}$$

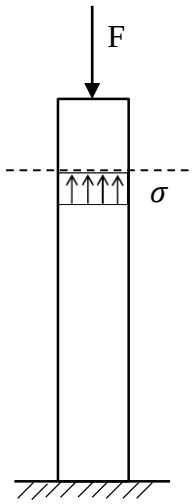

Figure 2-6: Point load and subsequent stress on column

Consider a simply supported beam element subjected to an evenly distributed load according to Figure 2-7. If the Bernoulli-Euler beam theory as above is used, the applied load *q* induces a bending moment that the cross-section has to resist, leaving the top of the beam subjected to compressive stresses and the bottom subjected to tensile stresses. Important to notice is the linear elastic stress variation over the height of the cross-section.

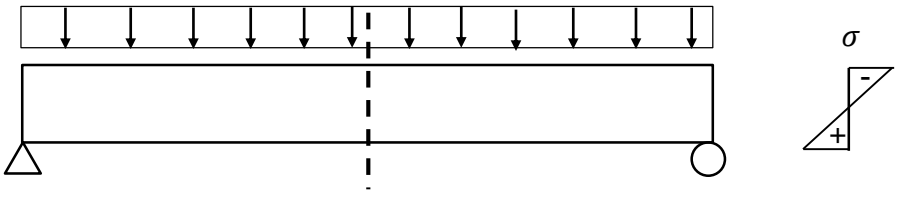

Figure 2-7: Stress in cross-section in center of beam

These two cases may be added together, e.g. in a column subjected to a distributed wind load or a pre-stressed concrete beam. The well-known Navier's formula [9] used in these cases, Equation (2.7).

$$\sigma = \frac{N}{A} + \frac{M_y}{I_y} y \qquad (2.7)$$

These formulas are only applicable if the Bernoulli assumptions are true, i.e. if the structural member has a span-to-height ratio ≥ 3. Bernoulli beam theory cannot be used when dealing with high beams. Furthermore, when a structure is subjected to a concentrated load the stress distribution will not be evenly distributed over the entire cross-section at once. The same effect also occurs when dealing with geometrical discontinuities. This means that designers have to take these regions, the discontinuity regions, into consideration when designing. Especially when working with concrete, 'unexpected' tensile stresses might occur. Making calculations by hand regarding these nonlinearities is analytically difficult. A common solution to this problem is the strut-and-tie method, section 2.4. [8]

2.2.2 Non-linear stress distribution

When designing structures, load and stress situations which yield non-linear behavior may occur. This means that the Bernoulli principle cannot be used. For example, the column shown in Figure 2-6 will not have a uniform stress throughout the cross-section just below the point of impact. It will take a certain distance for the load to be distributed over the entire cross-section, see Figure 2-8, where the top part is the so called discontinuity region (D-region) and the lower part is referred to as the continuity region (Bernoulli region; B-region) [8].

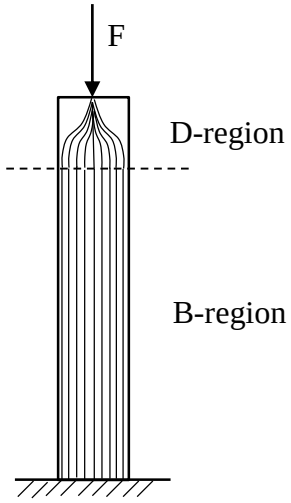

Figure 2-8: D-region & B-region in column

Comparing the beam subjected to the uniformly distributed load in Figure 2-7, where plane sections are assumed to remain plane and therefore a linear stress distribution is achieved, a high beam will behave differently. The stress distribution becomes non-linear over the entire cross-section and conventional beam theory cannot be applied [8], Figure 2-9. This is true also before the concrete has started to crack or any material has started to yield, i.e. a linear elastic behavior of the material results in a non-linear stress distribution.

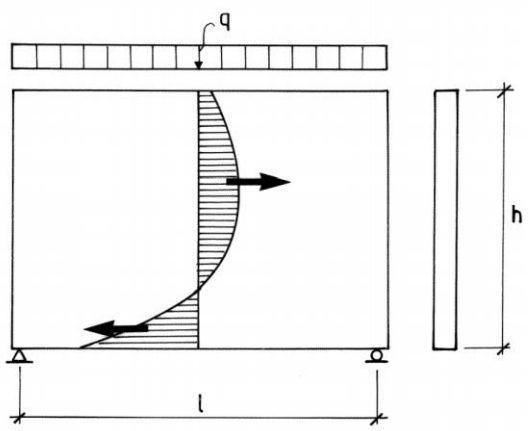

Figure 2-9: Stress distribution in high beam [8]

Basic knowledge concerning D-regions is the foundation of the strut-and-tie method, analyzing the flow of forces and the reaction of the structure.

2.3 Design based on plasticity

A structure is statically determinate or indeterminate on a global scale. When determining sectional forces, a simply supported beam on two supports is statically determinate and a continuous beam on three supports is statically indeterminate. The first example may conveniently be solved using equilibrium condition. The latter must be complemented with constitutive relations and compatibility conditions, e.g. linear relation between the moment and curvature in a section. These rules are applicable also for deep beams. [8]

When determining internal stresses from the sectional forces, the problem is statically indeterminate regardless of the static character of the structure on a global scale. When sectional forces are known, assumptions about the material response have to be made. In a Bernoulli beam this is usually done by assuming a linear strain distribution and a corresponding material behavior. If material behavior based on plasticity is assumed, higher capacities than assumptions based on pure linear-elastic behavior may be reached. Since the linear strain distribution is used and simplified elastic-plastic material models are possible to use, Bernoulli beams are also convenient to analyze in plastic design [8].

However, high beams cannot be assessed on the premise of plane sections remaining plane. This condition means that no compatibility condition may be found – and no way to analyze the internal stresses by hand. A linear-elastic finite element analysis may be used for the linear-elastic stage, before concrete cracking occurs. When the concrete starts to crack and materials start to yield, fracture mechanics, i.e. the non-linear response of the materials and the interaction between reinforcement and concrete, has to be accounted for. These non-linear analyses are advanced – but the plastic design is necessary since the ultimate limit state capacity would be heavily underestimated if cracking and plasticity is not taken into account. The plastic design can be made upon two premises: lower or upper bound solution [8].

Lower bound solution

A lower bound solution is based on a model which is possible due to equilibrium and no overstressing of material [8]. This yields a possible solution where the capacity cannot be lower, hence its name. The results from a lower bound solution is in all cases on the ‘safe side’.

Upper bound solution

The upper bound solution is based on a model which assumes a collapse mechanism. It has to be possible from a kinematic perspective [8]. This yields a solution where the capacity cannot be higher, and is therefore a design process on the ‘unsafe side’. If the lower and upper bound solution coincide, the ‘true’ solution is found.

2.4 The strut-and-tie method

Solving the complexities of discontinuity regions, described in subsection 2.2.2 and section 2.3, can be made using the strut-and-tie method in the ultimate limit state (ULS). The discontinuity regions may occur close to concentrated loads or geometrical discontinuities. These regions extends approximately as far as the width of the cross-section, often making the region more or less quadratic [8], Figure 2-10.

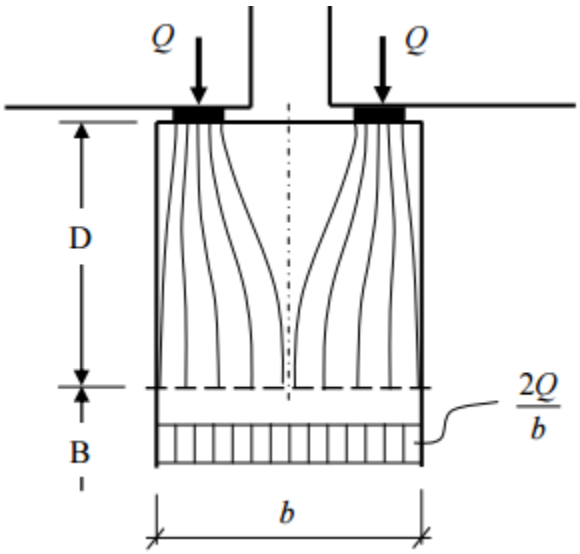

Figure 2-10: Discontinuity region and continuity region of column head [8]

The applied load *Q* spreads out, and the load (stress) may be followed by flow lines all the way to the continuity region. At the B-region a linear stress condition is assumed [10]. Continuity regions may be designed using a linear approach such as described in subsection 2.2.1.

The load can be simplified and divided into struts and ties upon two premises: either from the 'load path method' or from a linear finite element analysis. The load path method is used to represent the stress field by smoothly shaped curves. This is a simplification of the true stress field, however, it allows the designer to quickly realize the internal truss of the discontinuity region.

An example of the load path method is given. If the stress trajectories in Figure 2-10 above are followed from the concentrated force down, two turns in the trajectories may be distinguished, one close to the concentrated load and one closer to the B-region. These two bends are needed to achieve equilibrium within the structure, as shown in Figure 2-11.

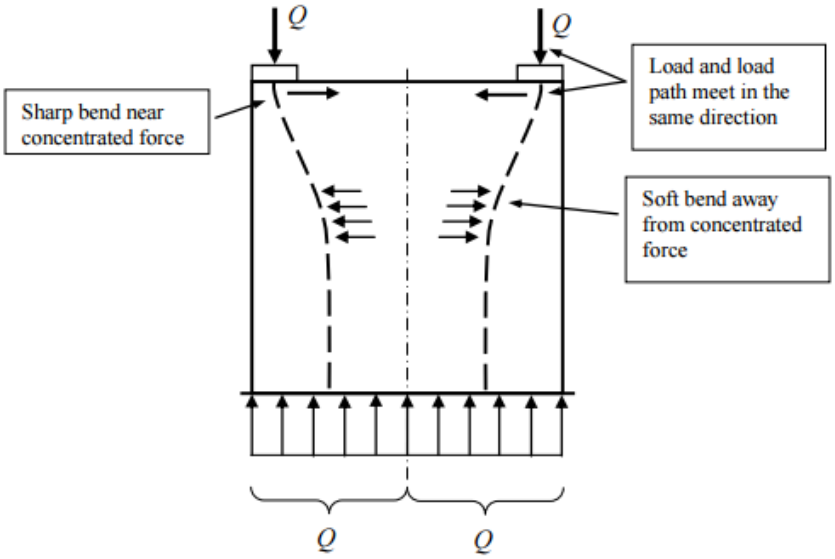

Figure 2-11: Equilibrium forces required to change direction of loads [8]

These forces originate from either a compressive or a tensile stress within the structure. Reinforcement may be added in tensile regions. In Figure 2-12 the linear-elastic stress field is shown, with corresponding struts and ties. The interested reader may find more information regarding choice of load paths in [8] and [10]. A selection of principles related to this project are listed below, adopted from [8]:

- The angle between a concentrated strut and a tie should not be less than 45°, preferably 60°
- Load paths should adopt smooth bends away from uniformly distributed loads
- Stresses under concentrated forces should be spread out as near the force as possible, in a sharp bend, with a deviation angle of preferably 30°, not exceeding 45°

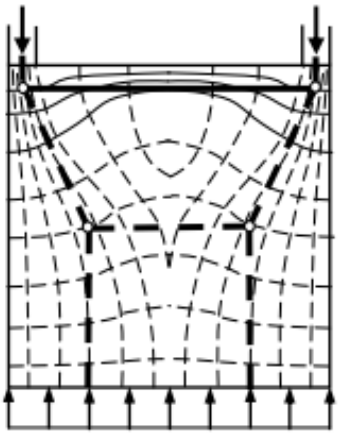

Figure 2-12: Flow of forces in D-region, linear-elastic stress field [8]

The strut-and-tie model should, according to recommendations, be based on the linear elastic stress field. Using a linear elastic finite element model is a relatively convenient procedure, as the only needed information is gross geometry and placement of supports and nodes. From the stress trajectories in the finite element model struts and ties can then be fitted with the stress field acting on the geometry.

Once the orientation and direction of each of the inner members have been set, i.e. struts and ties, the forces which they are subjected to may be calculated. These are calculated from a basic equilibrium of moment, according to Figure 2-13 [8], and Equations (2.8) & (2.9).

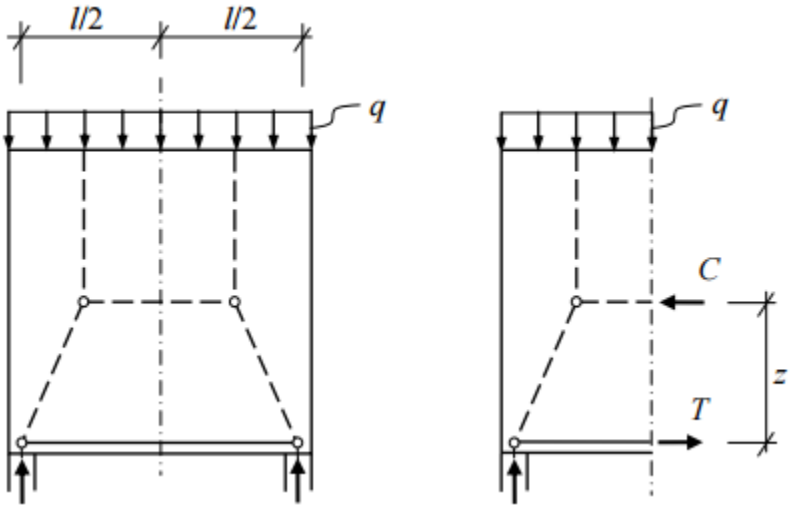

Figure 2-13: Equilibrium in D-region [8]

$$M_E = q \cdot \frac{l}{2} \cdot \frac{l}{4} \tag{2.8}$$

$$M_R = C \cdot z \tag{2.9}$$

Leaving a horizontal equilibrium, Equation (2.10).

$$C = T \tag{2.10}$$

To control the resistance of the concrete struts the compressive force *C* is considered over an area of the fictive strut. This area is dependent both on the internal angle α and the size of the external supports where the force *F* is applied. In a regular design situation this effective stress is compared with the design strength of the member according to Equation (2.11).

$$f_{cd} > \sigma_c = \frac{F}{A_{strut}} \tag{2.11}$$

Designing the tensile member follows the same principle as above. When the force T is known it is divided by the cross-sectional area of the reinforcement A_r. The stress must be less than the yielding point of the steel, Equation (2.12).

$$f_y > \sigma_s = \frac{T}{A_r} \tag{2.12}$$

To prevent failure of any structure the resistance of any member must be greater than the stress it is subjected to. The observant reader realizes that the internal lever arm of the high concrete member will have a major impact on the resistance of the member, combining Equations (2.8)-(2.10) the lever arm expressed in Equation (2.13) is retrieved.

$$z = \frac{ql^2}{8} \cdot \frac{1}{T} \tag{2.13}$$

Since T got a maximum value, originating from the yielding point of the steel, it is evident that a higher internal lever arm z makes a higher value of the load q possible.

Furthermore, for a given amount of reinforcement A_s the capacity only depends on the lever arm. This lever arm is dependent on the internal angle from which the struts form within the high concrete member as can be seen in Figure 2-14 below, and expressed in Equation (2.14).

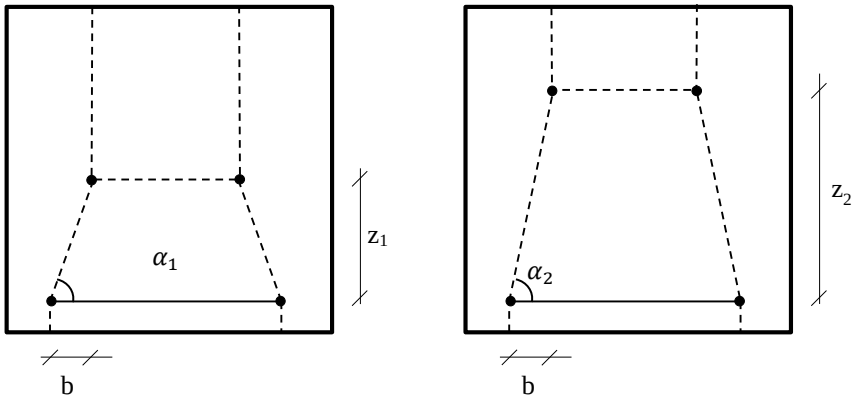

Figure 2-14: Internal lever arm depending on angle

$$z = \tan(\alpha) \cdot b \tag{2.14}$$

As mentioned, the strut-and-tie model is based on a linear-elastic stress field. Allowing a stress redistribution due to cracking and plastic deformations, higher capacities could be reached in the ultimate limit state. Questions exist on the redistribution ability of concrete structures.

2.4.1 Examples of applications of the strut-and-tie method

The strut-and-tie approach can be applied in cases other than high beams. A few examples will be given in this subsection to present the widespread usage of the method.

Corbel

A structure often used to bear floor slabs in buildings are so called corbels, columns with cantilevering edges in either two or four directions. Applying the previously mentioned ‘load path method’ the truss system can easily be assumed, and through equilibrium in each node the direction regarding the magnitude of the applied forces, internal forces may be determined. This is presented in Figure 2-15, where the red lines indicate tension, i.e. where one preferably places reinforcement, and the dashed blue lines indicates compressive struts.

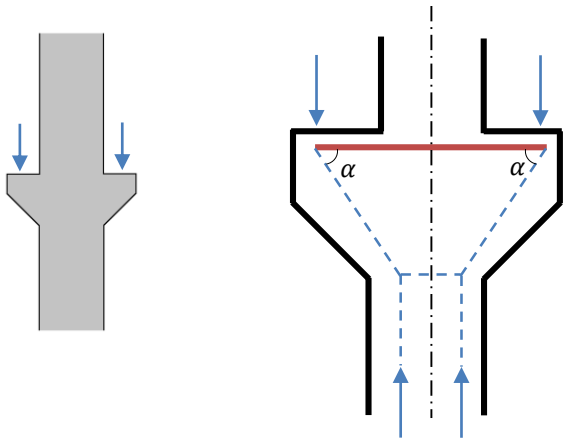

Figure 2-15: Strut-and-tie model in corbel

End of post-tensioned concrete beam

Post-tensioned concrete beams needs to be reinforced in order to prevent them from splitting due to the tensile stresses that form. The angle α is used according to the standards, and a reinforced tie is needed where that stress-line meets the center of each half of the beam, Figure 2-16.

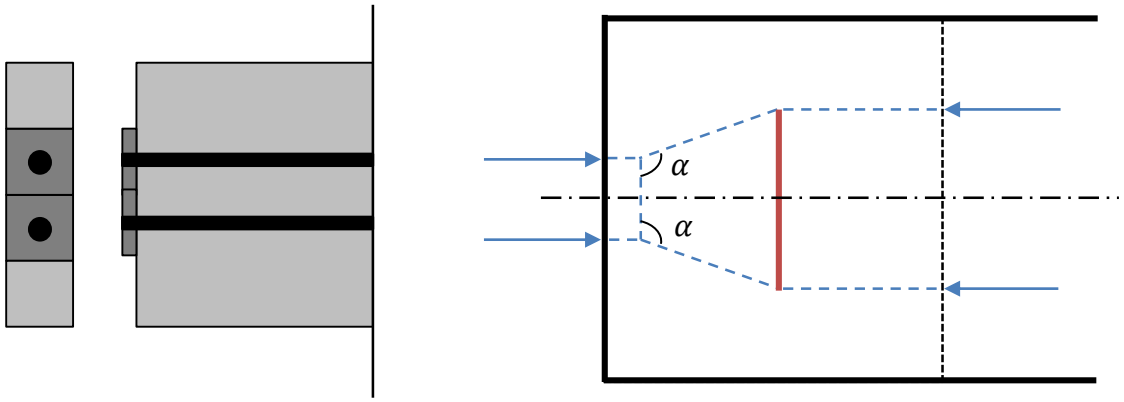

Figure 2-16: Strut-and-tie model in post-tensioned beam

Footing of a wall

A footing of a foundation or column may also be analyzed using the strut-and-tie method. In a corresponding manner the ground pressure acts as a distributed force, resulting in a pressure line on each side of the symmetry axis. With an assumption of an angle α, they meet the pressure lines from the wall or column from above, Figure 2-17.

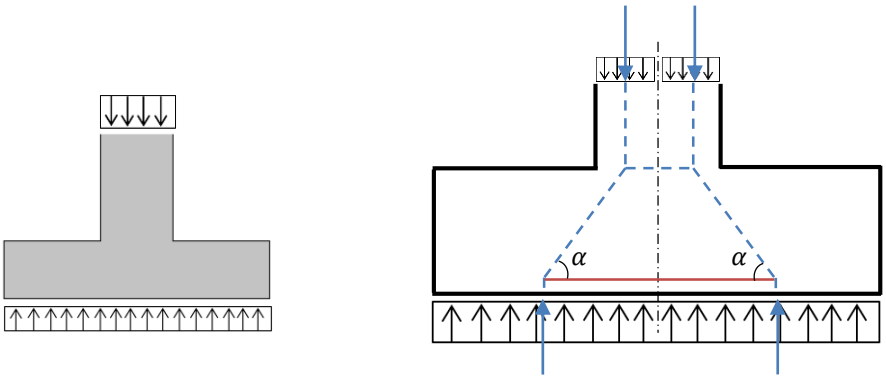

Figure 2-17: Strut-and-tie model of wall footing

2.4.2 Stress redistribution in discontinuity regions

The strut-and-tie method models a structure when it is on the verge of collapse [8], i.e. an approach for ultimate limit state design.

As long as the stresses are below the tensile capacity of the concrete cracks will be infinitesimally small, also named micro cracks. Since these cracks are so small, and stresses are below the tensile strength, this is known as the 'uncracked state'. The reinforcement has no significant impact on the structural behavior.

When the tensile stress exceeds the tensile strength significant cracking occurs. This cracking will lead to an increased stress level in the reinforcement - as the concrete loses stiffness, stresses will redistribute to stiffer areas**.** This phenomena is called 'stress redistribution due to cracking' [8]. As stresses re-arrange when loads increase, non-linear behavior of the member occurs despite the material response being linear-elastic. This state is known as the cracked state. Hence, if one wants to predict the member's behavior during this stage non-linear analysis is required.

When one of the materials reaches significant non-linear behavior, i.e. plastic behavior, the ultimate state is reached [8]. In composite concrete structures a characteristic event is yielding of the reinforcement. If a member starts to yield the member is described to have lost its stiffness, resulting in higher stresses in stiffer areas. This is known as 'plastic stress redistribution'.

When the structure has reached its final capacity the 'ultimate limit state' is reached. The strut-and-tie method is considered as a 'lower bound' solution. The definition of failure in a

discontinuity region using the strut-and-tie method is when one member reaches plastic stresses. However, as a discontinuity region is statically undetermined, stress redistribution is still possible despite a member or material reaching plastic stresses. The deformations and especially plastic strains will grow and develop and as long as further loading is kinematically possible failure is not truly reached [8].

An example is the high beam member subjected to a uniformly distributed load presented in Figure 2-13. Firstly, a linear-elastic stress field will develop in the member. When the tensile strength of the concrete is reached, cracks occur. Cracking of the concrete causes a stress redistribution, as stiffer regions attract more stresses. When the tie starts to yield, the uncracked concrete starts to attract more stresses. As plastic strains in the tie increases cracks will be forced upwards. As the internal lever arm increases due to the two types of redistribution, the capacity of the beam increases, i.e. the loads can still increase despite a plastic and cracked response.

Several stress fields are possible to achieve, and the selected stress field governs the reinforcement arrangements. Thus, the designer has freedom to choose a stress field which yields a certain capacity or reinforcement amount. Recommendations exists and ‘impossible stress fields’ should be avoided [8]. However, even for the simple case of a simply supported member several angles can be chosen in the internal truss system.

Considering what is mentioned above the advantages of the strut-and-tie method become more obvious. Only gross geometry, loads and plastic resistance is needed. It may be used early in the design process and provides adequate hand calculations to compare with more advanced finite element analysis.

2.5 Risk assessment and safety factors

Usually when designing a structure characteristic strength values are used for the members included to assure a safe structure, i.e., the real strength has a probability of 95% to be higher than the one assumed in the design process. The strength of the members is assumed to be normally distributed.

In the same manner the load applied is often assumed to be in the top 2%, leaving an acceptable level of probability of failure.

However in this project the mean strength is used when the primary calculations are made. The reason for this is the laboratory testing process where it is most likely to receive strength values close to the mean strength.

Safety factors are normally used when designing structures to provide an acceptable probability of failure. When the primary calculations were made the authors were looking for a certain type of failure to clearly show the 'strut-and-tie behavior'. This means that safety factors were used when designing struts, nodes and reinforcement anchorage lengths to prevent undesirable failures, but not when the ties were designed.

In practice, the following relations are used in this project when calculations have been made (Equation (2.15)-(2.18)):

$$f_{cd} = \frac{f_{cm}}{\gamma_C} \tag{2.15}$$

$$f_{cm} = f_{ck} + 8\ [MPa] \tag{2.16}$$

$$f_{ct,d} = \frac{f_{ctm}}{\gamma_C} \tag{2.17}$$

$$f_{yd} = f_{yk} \tag{2.18}$$

2.6 Finite element model

The program used, BRIGADE/Plus, is a finite element software. Dividing a defined structure into a number of smaller numerical part, i.e. finite elements, simulations can be performed over the region. Nonlinear behavior of an entire structure may be considered linearly within each small element, all of these elements together is called a finite element mesh [11]. The simulations are stated as numerical approximations of differential equations, and each element effect the behavior of its neighbors, leading to increased number of calculations depending on the size of the structure and how coarse of a mesh is used [11].

The stress situation in a 3D solid element is shown in Figure 2-18, with different stresses acting in each direction.

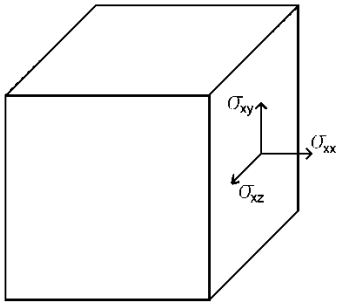

Figure 2-18: Stresses in the cross-section of a generic solid

Considering the entire stress situation of such an element mentioned above it follows Equation (2.19) [11].

$$S = \begin{bmatrix} \sigma_{xx} & \sigma_{xy} & \sigma_{xz} \\ \sigma_{yx} & \sigma_{yy} & \sigma_{yz} \\ \sigma_{zx} & \sigma_{zy} & \sigma_{zz} \end{bmatrix} \tag{2.19}$$

Since in the laboratory testing, the forces are applied through the use of thick steel plates, load is spread through the entire depth of the cross-section resulting in no need to take stresses in the z-direction into account. The matrix above can then be reduced to Equation (2.20). This is called a plane stress situation [11], meaning that the computational power needed may be reduced without neglecting any results.

$$S = \begin{bmatrix} \sigma_{xx} & \sigma_{xy} & 0 \\ \sigma_{yx} & \sigma_{yy} & 0 \\ 0 & 0 & 0 \end{bmatrix} \tag{2.20}$$

Basically, non-linearities in finite element modelling can be divided into two parts; one part which regards geometrical non-linearities (large displacements) and one part which regards material non-linearities. As displacements remain low, non-linear geometry is not of interest. However, to truly capture the behavior of the concrete during cracking and plasticity, advanced constitutive modelling is necessary.

2.6.1 Constitutive modeling using Concrete Damaged Plasticity model

In order to capture the behavior of the stress redistribution due to cracking and plasticity, the model has to consider some advanced theory; plasticity, damage theory and fracture mechanics. Plasticity in terms of pure material behavior has been presented in sections above. The constitutive model used is the Concrete Damaged Plasticity model.

Fracture mechanics

As the strut-and-tie method takes into account plastic redistribution due to cracking, cracking has to be considered when modelling, using fracture mechanics. In this project non-linear fracture mechanics was used. However to provide the reader with a more thorough understanding the more convenient linear elastic case is presented initially. Conventional fracture mechanics requires an existing crack, whereas fracture mechanics used in the Concrete Damaged Plasticity model does not.

In conventional fracture mechanics stresses and strains are assumed to propagate towards infinity, of course an unrealistic assumption. If a crack is subjected to a perpendicular stress, the stress close to a crack tip is described by Equation (2.21) [12].

$$\sigma_y = \frac{K}{\sqrt{2\pi x}} \tag{2.21}$$

Where x is the distance from the crack tip and K is the stress intensity factor calculated as Equation (2.22).

$$K = Y\sigma\sqrt{a} \tag{2.22}$$

Where a is the crack length, σ is the stress acting on a corresponding crack free area and Y is a dimensionless factor depending on structure, loading, crack length, usually set as 2.

Using this theory stresses in crack tips cannot be compared with material strength. Therefore, a crack is assumed to propagate when a critical value of K is reached, denoted K_c. This theory cannot handle uncracked material as stresses become zero if the crack length is zero. To handle uncracked material, comparison between stresses and strengths has to be made. Also, different theories based on cracked or uncracked material behavior have to be used. This proves to be unbeneficial when analyzing concrete [12].

In general, the fact that the stresses at crack tips theoretically reaches infinity may cause severe discontinuities in certain applications why an expanded theory is needed. Another approach based on the tensile stress-strain curve of concrete has been proposed by Hillerborg [12] and is today implemented and used in *Abaqus* and *BRIGADE/Plus* [13].

Considering a tensile concrete test, the stress-elongation relationship (similar behavior as stress-strain relationship) may be seen to the left in Figure 2-19. According to Hillerborg [12], a suitable way to model cracking of concrete would be to divide the behavior into two parts; one which

represents the behavior until strength of material is reached and one which models the behavior after strength of material is reached. The latter is often referred to as the 'tension softening curve' [12].

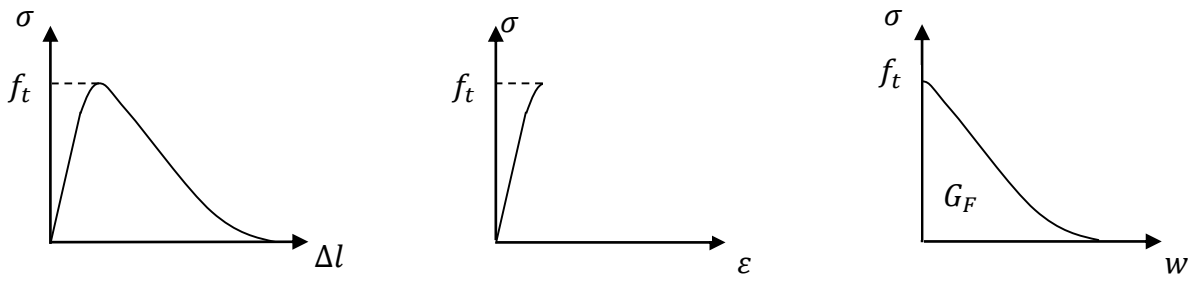

Figure 2-19: a) Stress-elongation relationship b) Stress-strain relationship until failure tensile stress c) Tension softening branch expressed in stress-displacement domain

After peak stress has been reached, micro cracks will propagate to macro cracks. When the stress in a certain area has reached zero, a crack is considered to have been formed. A fracture energy criterion can be used to analyze cracks. This energy, G_F, is calculated from the integral of the $\sigma - w$ graph Figure 2-19c, Equation (2.23).

$$G_f = \int \sigma \, dw \ [\mathrm{Nm/m^2}] \qquad (2.23)$$

Where σ is the tensile stress and dw is the crack length increment. Several alternatives to model the tension softening curve exists. It can be modelled directly by the stress-strain relationship according to Malm [13], however this may result in high mesh sensitivity if cracking occurs in unreinforced regions. In such a case fracture energy or stress-crack opening displacement representation is considered a better choice [13].

A fracture energy representation is defined by simply assigning cracking displacements as material properties in *BRIGADE/Plus*. A simplification of the stress-crack opening displacement curve, Figure 2-19c, can be represented by a bi-linear curve, from Hillerborg [14]:

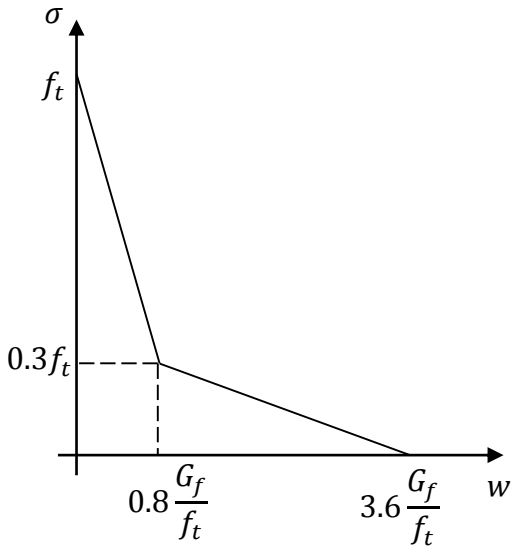

Figure 2-20: Idealized stress-displacement diagram of tension softening using fracture energy criteria [14]

Figure 2-20 represents the softening part of the tensile stress-strain relationship. G_f and f_t are properties possible to determine from laboratory testing.

Plasticity and Damage Theory

To be able to model a stress-strain relationship including plastic strains, some functions which captures load history has to be defined. As can be seen in subsection 2.1.1, some plasticity has to be accounted for. Firstly, the strain rate is defined as a function of elastic and plastic strains. $\dot{\boldsymbol{\varepsilon}}$ represents the total strain rate (the differential of the strain over time), $\dot{\boldsymbol{\varepsilon}}^{el}$ the elastic part of the strain rate and $\dot{\boldsymbol{\varepsilon}}^{pl}$ the plastic part of the strain rate, Equation (2.24).

$$\dot{\boldsymbol{\varepsilon}} = \dot{\boldsymbol{\varepsilon}}^{pl} + \dot{\boldsymbol{\varepsilon}}^{el} \tag{2.24}$$

To capture the plastic behavior, the stress-strain relationship and the yield surface has to be connected. This is represented by a flow rule. The plastic flow rule is defined according to Malm [15]:

$$\dot{\boldsymbol{\varepsilon}}^{pl} = \dot{\kappa}\frac{\partial G}{\partial \boldsymbol{\sigma}} \tag{2.25}$$

Where $\frac{\partial G}{\partial \boldsymbol{\sigma}}$ describes the direction of the vector $\dot{\varepsilon}^{pl}$ and $\dot{\kappa}$ describes the length of the vector. In Figure 2-21 the hyperbolic Drucker-Prager plastic potential function G is shown. The lower the confining pressure, the more brittle the behavior [15].

The plastic potential function uses an effective stress defined as Equation (2.26) [16].

$$\bar{\boldsymbol{\sigma}} = \boldsymbol{D}_0^{el}(\boldsymbol{\varepsilon} - \boldsymbol{\varepsilon}^{pl}) \qquad (2.26)$$

Where D_0^{el} is the elastic material stiffness matrix.

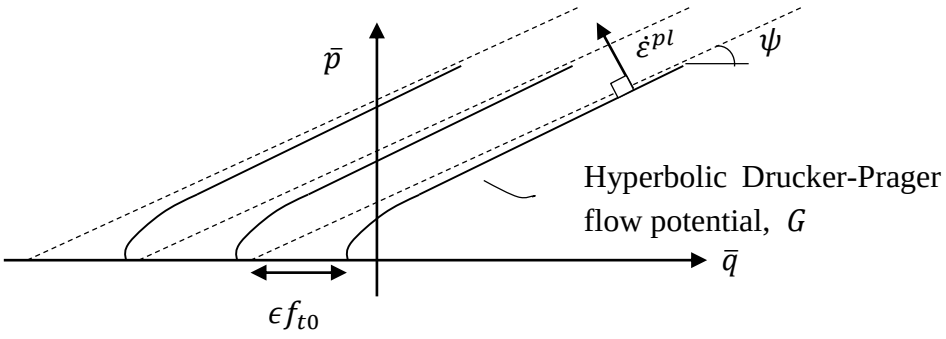

Figure 2-21: Hyperbolic Drucker-Prager flow potential, G. Adopted from [16].

The hyperbolic Drucker-Prager plastic potential function may be described by Equation (2.27) [16]:

$$G = \sqrt{(\epsilon f_t \tan\psi)^2 + \bar{q}^2} - \bar{p}\tan\psi \qquad (2.27)$$

Where:

ϵ defines at which rate the plastic potential function approaches its asymptote

ψ is the dilation angle, which describes how much volume expansion occurs at high confining pressures. A high dilation angle results in ductile behavior, low in brittle behavior.

f_t is the tensile strength of the concrete

$\bar{q}$ is the Mises equivalent effective stress as a function of the second deviatoric stress, J_2, defined as $\bar{q} = \sqrt{3J_2} = \sqrt{3(\sigma_{11}^2 + \sigma_{22}^2 - \sigma_{11}\sigma_{22})}$ for biaxial loading

$\bar{p}$ is the hydrostatic pressure stress, a function of the first stress invariant I_1, defined as $\bar{p} = -\frac{I_1}{3} = -(\sigma_{11} + \sigma_{22} + \sigma_{33})/3$ where $\sigma_{33} = 0$ for plane stress conditions.

Furthermore, the yield surfaces are described by a combination of a Drucker-Prager and Mohr-Coulomb function. In order to define all variables in the functions, the uniaxial damage is defined. The damage is of most relevance regarding cyclic loading; therefore only presented briefly.

It is not realistic that, if the material is unloaded, the stiffness of the material would remain. Therefore a damage parameter d_t and d_c are defined, which degrade the initial modulus of elasticity according to Equation (2.28) and (2.29).

$$\sigma_t = (1 - d_t)E_0(\varepsilon_t - \tilde{\varepsilon}_t^{pl}) \quad (2.28)$$

$$\sigma_c = (1 - d_c)E_0\left(\varepsilon_c - \tilde{\varepsilon}_c^{pl}\right) \quad (2.29)$$

Where $\tilde{\varepsilon}_t^{pl}$ & $\tilde{\varepsilon}_c^{pl}$ are the plastic strains which remain if the material is unloaded. As the cracks yield less load carrying area, an effective stress for uniaxial loading is defined as Equation (2.30) and (2.31):

$$\bar{\sigma}_t = E_0(\varepsilon_t - \tilde{\varepsilon}_t^{pl}) \quad (2.30)$$

$$\bar{\sigma}_c = E_0(\varepsilon_c - \tilde{\varepsilon}_c^{pl}) \quad (2.31)$$

These stresses are called the effective tensile and compressive cohesion stresses respectively.

Since no unloading and reloading of the specimens is of interest, no damage parameters are specified.

A mathematical description of the biaxial yield surface of concrete is shown Figure 2-22. The parameters are:

f_{c0} the initial uniaxial compressive yield stress

f_{b0} the initial equibiaxal compressive yield stress

f_{t0} the uniaxial tensile stress at failure

α a dimensionless coefficient described as $\alpha = \frac{f_{b0}-f_{c0}}{2f_{b0}-f_{c0}}$

β a dimensionless coefficient, described as $\beta = \frac{\bar{\sigma}_c}{\bar{\sigma}_t}(\alpha - 1) - (\alpha + 1)$

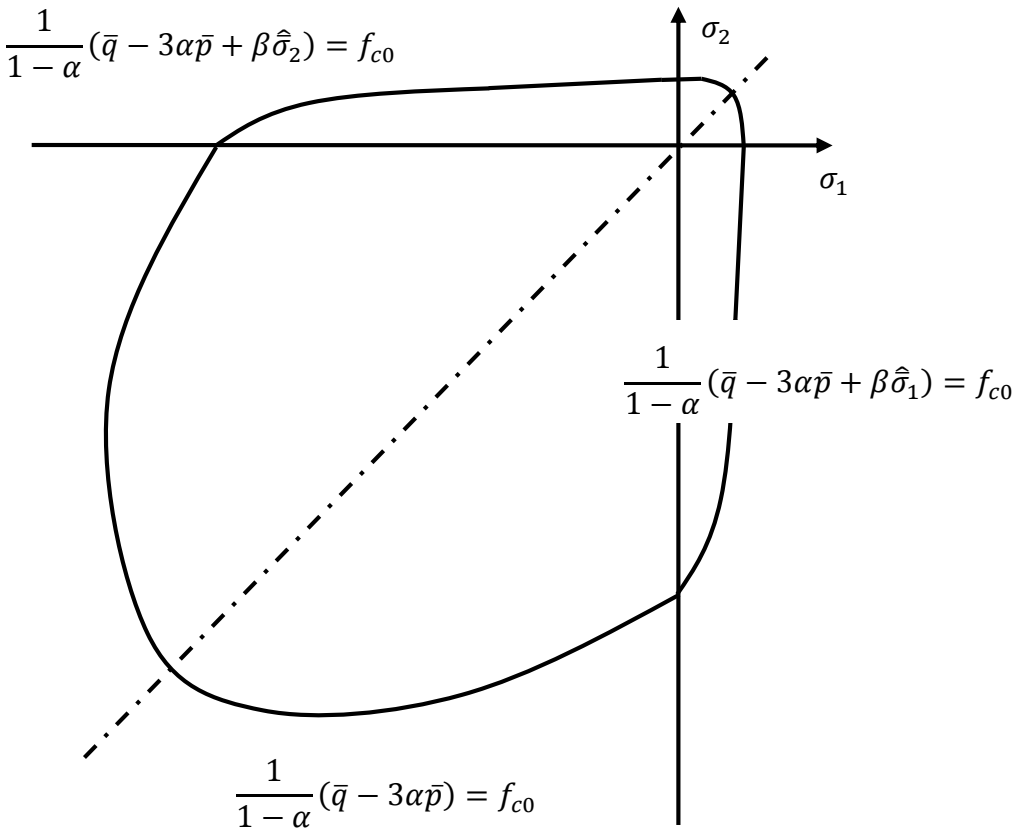

Figure 2-22: Biaxial yield surface, valid for plane stress conditions. Adopted from [16].

Furthermore, a so-called yield function needs to be defined. In *BRIGADE/Plus*, this is defined as Equation (2.32).

$$F = \frac{1}{1-\alpha}(q - 3\alpha p + \beta(\tilde{\boldsymbol{\varepsilon}}^{pl})\langle\hat{\bar{\sigma}}_{\max}\rangle - \gamma\langle\hat{\bar{\sigma}}_{\max}\rangle) - \bar{\sigma}_c(\tilde{\varepsilon}_c{}^{pl}) \leq 0 \qquad (2.32)$$

Where all parameters except γ are described above. γ is defined as Equation (2.33).

$$\gamma = \frac{3(1-K_c)}{2\,K_c - 1} \qquad (2.33)$$

K_c, which describes the relationship between the tensile meridian q_{TM} and the compressive meridian q_{CM}, according to Equation (2.34) [17] [18].

$$K_c = \frac{(\sqrt{J_2})_{TM}}{(\sqrt{J_2})_{CM}} \qquad (2.34)$$

Where J_2 is the second invariant of the stress deviator [18].

In order to reach convergence when the concrete starts to crack, a so-called viscoplastic regularization is introduced. The viscoplastic strain tensor is defined as Equation (2.35). [16]

$$\dot{\boldsymbol{\varepsilon}}_v^{pl} = \frac{1}{\mu}\left(\boldsymbol{\varepsilon}^{pl} - \boldsymbol{\varepsilon}_v^{pl}\right) \qquad (2.35)$$

Where the viscosity parameter μ represents the relaxation time of the viscoplastic system and $\boldsymbol{\varepsilon}^{pl}$ is the plastic strain as defined above.

The viscoplastic stress-strain model is defined according to Equation (2.36).

$$\sigma = (1-d_v)D^0(\varepsilon - \varepsilon_v^{pl}) \qquad (2.36)$$

The viscoplastic system converge towards the original system when $\frac{\Delta t}{\mu} \to \infty$, where Δt is the characteristic time increment.

3 CALCULATION PROCEDURE

The following chapter shows how to design a specimen according to the strut-and-tie method. The calculations regarding the specimens are presented in Appendix B. These results are based on three different angles, where $\alpha = 60°$ complies with current standards and practices.

The desired type of failure in beams *T1-T4* are so called flexure failures, i.e. the beam bends which leads to tensile strain in the primary reinforcement in the bottom and ultimately yielding and failure. In addition to the control of each strut and tie in the truss model the nodes, where these struts and ties meet, are checked. Some of these nodes are subjected purely to compression whereas some are subjected to compression and tension simultaneously. Section 3.1 - 3.3 are intended to give the reader basic knowledge in the design process using the strut-and-tie method, whilst section 3.4 presents calculations needed to determine the load-bearing capacity of the specimens.

The calculations made are presented in Appendix B. The elements designed can be seen in Figure 3-1, containing compression node, compression-tension node, compression struts and the reinforcement tie.

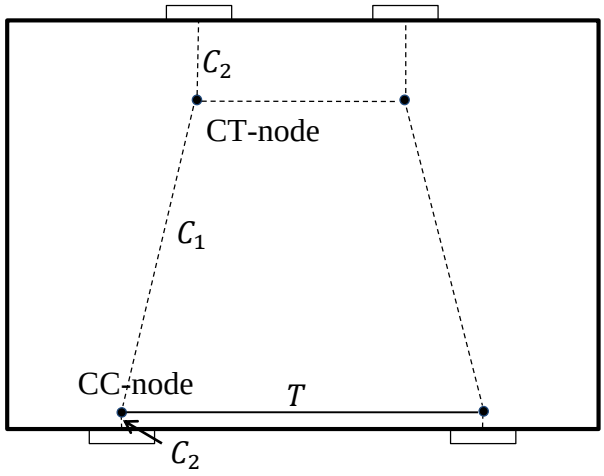

Figure 3-1: Compression-Compression node, Compression-Tension node, Struts and tie in a high beam member

3.1 Struts

As mentioned the strut-and-tie method assumes a truss within the concrete structure. The strength of these struts need to exceed the stress they are subjected to. To check this a theoretical cross-section of the strut needs to be defined. This cross-section together with the force within each member gives the current stress level. The first step however is calculating the forces acting in each strut. The forces within the cross-section can be seen in Figure 3-2.

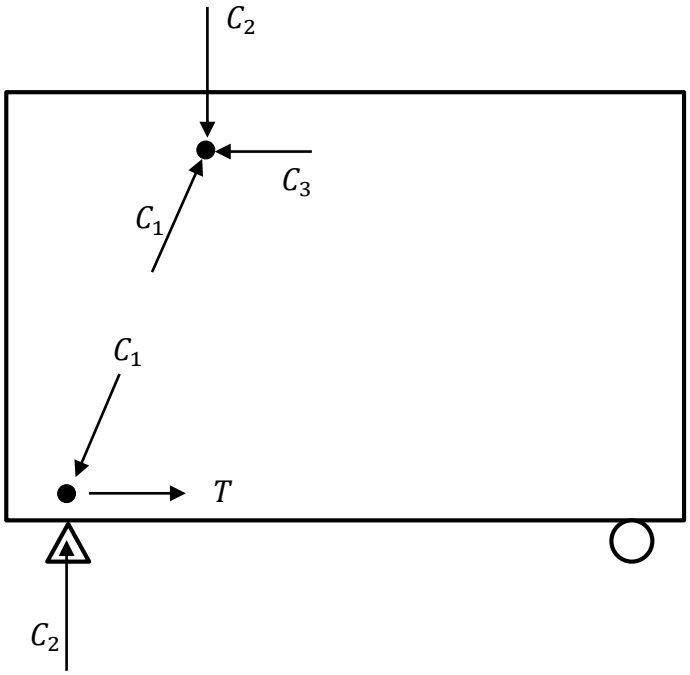

Figure 3-2: Forces acting on the nodes

3.1.1 Forces

As the forces at each node needs to be in equilibrium, each of the internal strut forces can be calculated with calculations shown below, Equations (3.1)-(3.3). The forces depends solely on the externally applied force, *F*, and the internal angle, α.

$$C_1 = \frac{F/2}{\sin \alpha} \tag{3.1}$$

$$C_2 = F/2 \tag{3.2}$$

$$C_3 = \frac{F/2}{\tan \alpha} \tag{3.3}$$

The fictive area for these struts depend primary on the area of the steel plates where the external loads are applied, as well as the steel supports.

3.1.2 Capacities

The strut strengths are normally of no concern, however, if no secondary reinforcement is provided and cracks transverse to the force direction develops this could be an issue [8]. In such a case the strut strength is calculated as Equation (3.4):

$$\sigma_{Rd,max} = 0{,}6 \cdot \nu' \cdot f_{cd} \tag{3.4}$$

Where ν' is presented later in Equation (3.6), and f_{cd} is used since failure in the struts are undesirable.

3.2 Nodes

The strength of the nodes varies depending on the type of load they are subjected to, see subsection 2.1.1. A node only subjected to compressive stresses is assumed to have a higher strength than a node subjected to tensile and compressive stresses simultaneously. The capacities should be compared to the strut forces, presented in subsection 3.1.1, acting on the faces of the nodes.

3.2.1 Capacity of 'Compression – Compression Node'

The node on the top of the beam will be subjected to compressive stresses from three directions as may be seen in Figure 3-3 below. This stress state assumes hydrostatic pressure.

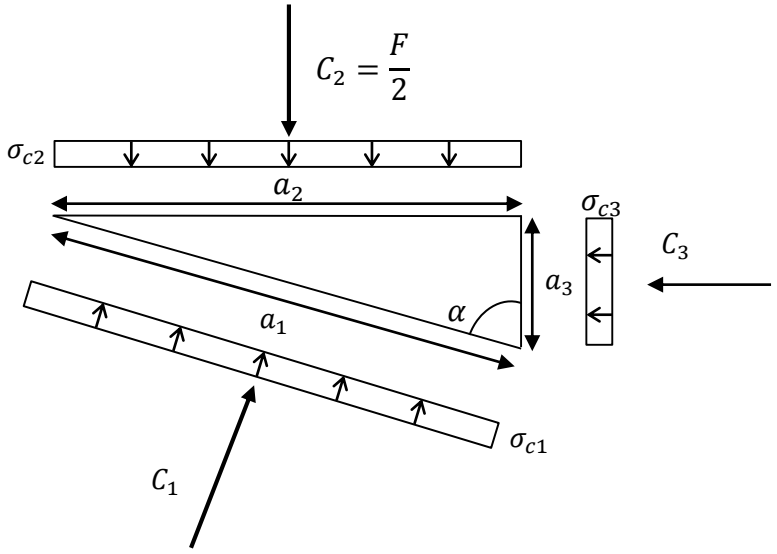

Figure 3-3: Stresses and geometry of a CC-node

The variables are: C_i compressive forces; a_i width of strut; $\sigma_{ci} = \frac{C_i}{a_i}$ stress due to compressive force; α is the angle of propagation for the internal strut.

For a Compression- Compression node (CC-node), the node resistance is calculated according to the Eurocode [4], see Equation (3.5).

$$\sigma_{Rd,max} = k_1 \cdot \nu' \cdot f_{cd} \qquad (3.5)$$

Where $k_1 = 1$ is a national parameter, in Sweden set as Eurocode's recommended value [4]. This parameter takes account for the multi-axial stress state which influences the strength, see subsection 2.1.1. Furthermore f_{cd} is used since a failure in the nodes are undesirable.

The parameter ν' is a reduction factor for concrete members with shear cracking in accordance with Eurocode 2 [4], Equation (3.6).

$$\nu' = 1 - \frac{f_{ck}}{250} \tag{3.6}$$

In order to compare stresses and strengths the node face area is needed. The geometry of the current node, the CC-node, is shown in Figure 3-3. Trigonometrical equations yields that the three quantities $a_1 - a_3$ are calculated according to Equations (3.7)-(3.9).

$$a_1 = \sqrt{a_2 + a_3} \tag{3.7}$$

$$a_2 = b_{loading\ plate} \tag{3.8}$$

$$a_3 = \frac{a_2}{\tan \alpha} \tag{3.9}$$

The node resistance is then compared with the force according to:

$$\sigma_{Rd,max} \geq \sigma_{Ci} = \frac{C_i}{a_i \cdot b} \tag{3.10}$$

Where b is the depth of the beam, C_i is the compressive force and a_i is its corresponding face length which the force acts on.

3.2.2 Capacity of 'Compression – Tension Node'

At the lower parts of the beam, where the compressive struts meets the tensile reinforcement, another node exists according to Figure 3-4.

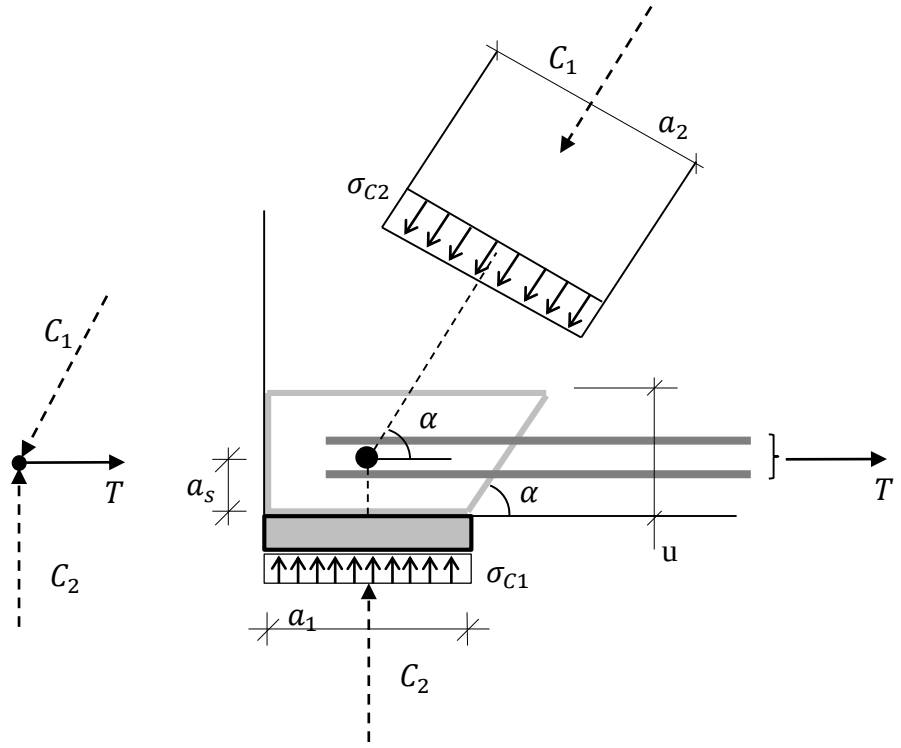

Figure 3-4: Stresses and geometry of a CT-node

The variables in the Figure above are: C_i compressive forces; T tensile force in reinforcement; R reaction force in support; a_i width of strut; $\sigma_{ci} = \frac{C_i}{a_i}$ stress due to compressive force; α is the angle of propagation for the internal strut.

For a compression-tension node (CT-node) with anchorage in one direction, the node resistance is calculated according to Equation (3.11).

$$\sigma_{Rd,max} = k_2 \cdot \nu' \cdot f_{cd} \qquad (3.11)$$

Where $k_2 = 0.85$ is a national parameter, in Sweden set as Eurocode's recommended value [4]. This parameter takes account for the multi-axial stress state which influences the strength, see subsection 2.1.1. ν' was defined in Equation (3.6).

As for the biaxial compression state of stress, geometry of the node is required, according to Equations (3.12)-(3.15) below and shown in Figure 3-4.

$$a_s = r_{tp} \tag{3.12}$$

$$u = 2a_s \tag{3.13}$$

$$a_2 = \left(a_1 + \frac{u}{\tan \alpha}\right) \sin \alpha \tag{3.14}$$

$$a_1 = b_{sup} \tag{3.15}$$

Where r_{tp} is the center of gravity for the primary reinforcement of the beam and b_{sup} is the width of the support.

The capacity of the node is then checked in accordance with Equation (3.10).

3.3 Tie

To achieve equilibrium in the truss a tie is needed. As the concrete is cracked in the ultimate limit state, the tie is considered to consist solely of reinforcement. Failure is defined as when the tie starts to yield, reaching its yield strength f_y. A free body cut of a basic structure is shown Figure 3-5.

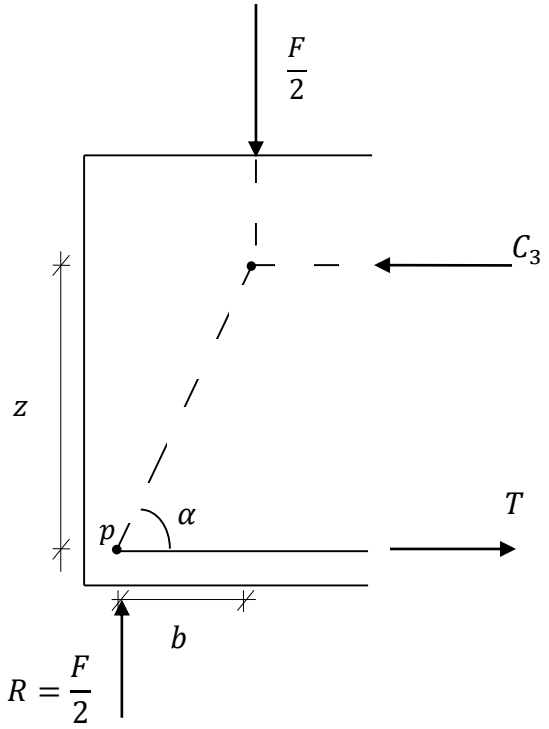

Figure 3-5: Equilibrium within high beam

The tie force is calculated in the same manner as for the struts, i.e. moment equilibrium in point p (Figure 3-5). This combined with basic trigonometry and a horizontal equilibrium yields the following results, Equation (3.16) - (3.18):

$$F/2 \cdot b = C_3 \cdot z \tag{3.16}$$

$$b = \frac{z}{\tan \alpha} \tag{3.17}$$

$$T = C_3 = \frac{F/2}{\tan \alpha} \tag{3.18}$$

The amount of reinforcement is calculated as stated in Equation (3.17).

$$A_s \geq \frac{T}{f_y} \tag{3.19}$$

Where T is the tie force and f_y the yield strength of the reinforcement bars. Choosing a dimension ϕ of the reinforcement gives the required number of bars needed to take the tensile force T where n_{rebar} is the required number of reinforcement bars according to Equation (3.20).

$$n_{rebar} = roundup\left(\frac{A_s}{A_{rebar}}\right) \tag{3.20}$$

3.4 Load bearing capacity of specimen

Assuming that anchorage failures, node failures and strut failures are prevented (see Appendix B), capacity of the beam is theoretically decided from three main variables: the internal lever arm, which is solely decided from the angle α in Figure 3-5 and the capacity of the tie, which depends on amount of reinforcement and its yield strength.

Combining Equation (3.18) and (3.19), the capacity may be calculated as:

$$F = 2 \cdot T \cdot \tan\alpha = 2 \cdot f_y \cdot A_s \cdot \tan\alpha \tag{3.21}$$

3.5 Anchorage length

In the design of a concrete member, anchorage lengths of the reinforcement bars have to be checked in order to ensure that sufficient anchorage is reached. The specimens have been designed to prevent anchorage failure in accordance with Eurocode 2 [4]. Practically, the best way to prevent anchorage failure resulted in extending the specimens lengths outside the support regions and bending the bars. The reader is referred to Appendix A for drawings and Appendix B4 for calculations.

4 LABORATORY PROCESS

In order to determine the reliability and limitations of the strut-and-tie method, verify internal angles and have results to compare with the numeric model, laboratory tests were carried out. As many parameters as possible within the time-scope of the project were tested, including compressive and tensile strength of concrete, fracture energy of the concrete and stress-strain behavior of the reinforcing steel.

The four beam specimens tested were manufactured at the location where they were to be tested to be able to supervise the entire process. The concrete was ordered from an external distributer to assure a good quality concrete with proper features in terms of strength, ratio of aggregates, adequate distribution of the aggregates throughout the mixture and ratio of water. The concrete used was of quality C30, with a maximum aggregate size of 16 mm.

The reinforcement steel was ordered and the individual bars were tested according to subsection 4.1.2.

4.1 Material properties

To make proper estimations of the internal angle in the laboratory test, several material properties of the included members must be determined. Retrieving these properties makes it possible to adapt the manual calculations as well as the simulations made in BRIGADE/Plus to the conditions present at the time of the laboratory practical to get as comparable results as possible.

4.1.1 Concrete

Three different tests of the concrete were performed in order to determine the properties of the batch of C30 concrete delivered. One in order to determine the compressive strength, one in order to determine the tensile strength and one in order to determine the fracture energy.

Compressive strength test

When ordered, a hint about the strength of the concrete was given. However, in order to get a more precise perception of the material parameters the delivered batch of concrete was tested. This was tested by subjecting a cube with a side length of 150 mm to compression, which have been left to cure for 28 days in 100% relative humidity.

From the applied force F needed to crush the specimen the strength of the concrete can be derived, see Equation (4.1).

$$f_{cc} = \frac{F}{A} \tag{4.1}$$

Tensile strength test – Brazilian test

The ideal case would be to subject the specimen to a pure tensile force but since anchoring of the specimen would prove a problem another solution is used. A spitting test, also known as a Brazilian test, was performed. This was done by subjecting a cylindrical specimen, diameter of 150 mm and height of 300 mm, to a distributed load along top and bottom perimeter [19]. The force applied generated a tension force perpendicular to the load direction due to the Poisson's effect, and eventually cause the cylinder to split down the middle. Knowing the force needed to split the specimen the concrete splitting tensile strength $f_{ct,sp}$ can be derived, Equation (4.2).

$$f_{ct,sp} = \frac{2P}{\pi DL} \tag{4.2}$$

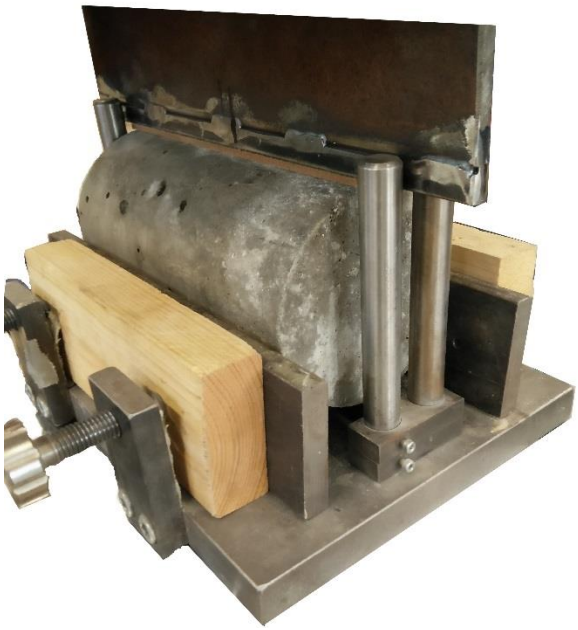

Figure 4-1: Brazilian test setup

The relation between the calculated splitting tensile strength and the approximate tensile strength of the material is decided according to Equation (4.3) [20].

$$f_{ct} = 0.9 \cdot f_{ct,sp} \tag{4.3}$$

Fracture energy test

In order to model the concrete in *BRIGADE/Plus*, a fracture energy approach is used, see subsection 2.6.1. Concrete cracking behavior is difficult to model and literature may be contradictory regarding choice of parameters. Therefore, the authors have chosen to perform a fracture energy test.

The theoretical basis of the concrete cracking behavior is described in subsection 2.6.1. According to Hillerborg [12], the best method would be to test the uniaxial tensile strength in order to get the

full stress-strain response curve of the material. However, as mentioned, these tests are difficult to perform and require advanced equipment. An alternative method proposed by Hillerborg [12] suggests that the fracture energy may be defined from a three-point bending test on a notched beam. The notch should be of length $d/2$ where d is the beam depth [12]. The beams were of size *10x10x1000 mm*^{3}, Figure 4-2.

Figure 4-2: Fracture energy test setup, without force applying piston

The fracture energy G_f is calculated according to Equation (4.4) [21].

$$G_f = \frac{U_0 + mgd_0}{A} \tag{4.4}$$

Where A is the ligament area, i.e. the width of the beam multiplied with the un-notched height $(W - a_0)$, Figure 4-3. Furthermore d_0 is the deflection of the loading point at fracture, i.e. when the load has reached zero.

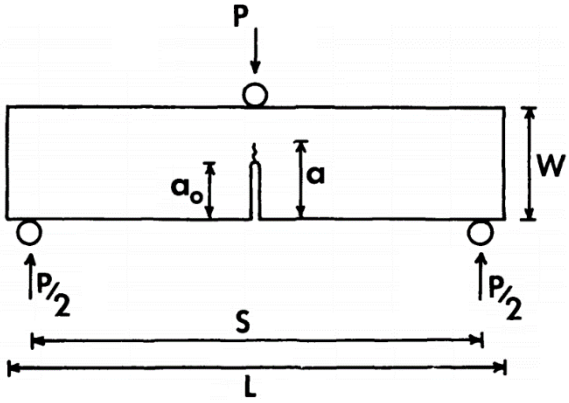

Figure 4-3: Parameters of fracture energy test [21]

Finally the variable U_0 is the integral of the graph from the deflection of the loading point and the applied load, representing the energy required to break the specimen [21]. The deflection is registered with two LVDT-sensors (Linear Variable Differential Transformer), mounted on the top of the beam. The mean value of these deflections is the Load Point Deflections (LPD) in Figure 4-4.

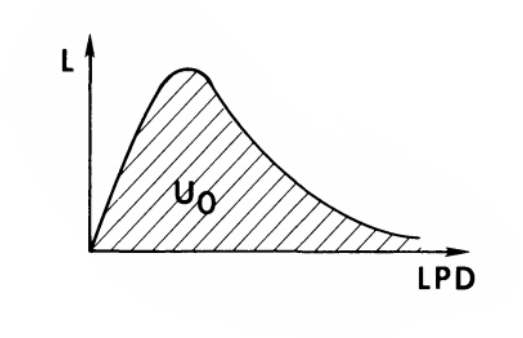

Figure 4-4: Load - Load Point Deflection graph [21]

4.1.2 Steel

The reinforcing steel was, as well as the concrete, graded before arrival from the distributor. To verify its material parameters a test was carried out. This test was performed for the primary reinforcement bars, assuming identical strength of the minimum reinforcement used.

The tensile strength of the reinforcement bars was tested using a hydraulic testing machine. The test specimen was mounted in between two wedges that grip on tight to the bar. The hydraulic testing machine pulls apart two ends of the bar, an elongation occurs and is registered [3]. The elongation is simultaneously logged with the applied tensile force. From this a stress-strain curve was assembled. An ideal elastic-plastic curve was derived from the material response and from this the ideal plastic strength was assessed.

The Young's modulus was also derived from the tests in the hydraulic MTS-machine according to Figure 4-5.

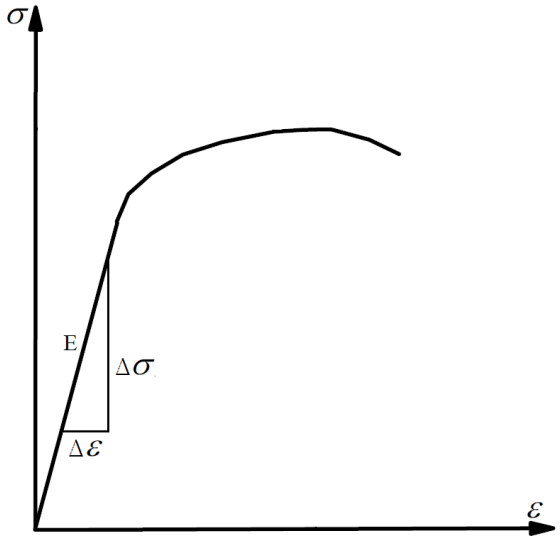

Figure 4-5: Determining the Young's modulus for steel

4.2 Manufacturing specimens

The dimensions of the specimens tested in this project can be seen schematically below in Figure 4-6.

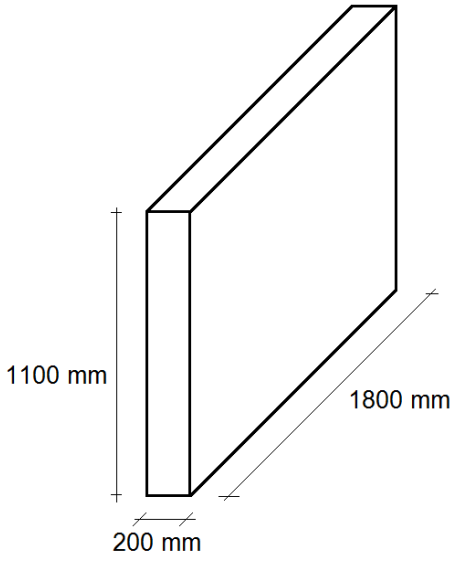

Figure 4-6: Dimensions of test specimen

4.2.1 Molding cast

The molds for the beam specimen were made using wooden planks of $45x95\ mm^2$ stiffening up the plywood especially made for casting concrete.

Figure 4-7: Molding cast for primary beam specimen

The cast were additionally stabilized with wooden planks at the gables and at the top to prevent deformations from the horizontal pressure when poring the concrete.

4.2.2 Reinforcement

The delivered reinforcement was measured, cut, bent and mounted according to layout decided upon, see APPENDIX A for drawings of the four different specimen. The ends of the bars were bent in order to provide anchorage length long enough to prevent any type of undesired failure. Some of the reinforcement bars are treated in order to fix the strain gauges – see subsection 4.2.2.

Strain gauges

The strain gauges used are of the brand *Tokyo Sokki Kenkyujo Co*, and register movements in longitudinal and transversal directions. Knowing how the reinforcement elongated gave information about whether it reaches plastic strains or not.

These strain gauges are mounted at two positions at each level of reinforcement levels, i.e. all tension rods in a layer are expected to have identical displacement. The elongation was also assumed to be symmetrical around the midpoint of the beam, reducing the number of strain gauges needed, Figure 4-8.

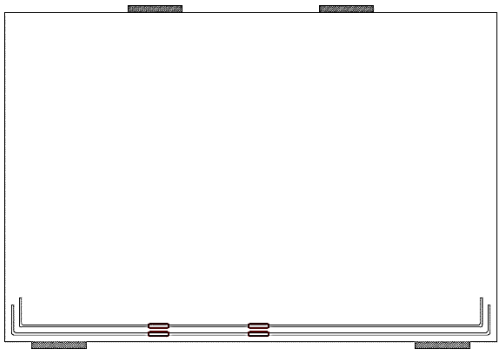

Figure 4-8: Setup for the laboratory process with placing of strain gauges

The strain gauges needed to be mounted on a flat surface, which meant the ribs had to be grinded flat in that region, Figure 4-9. Caution was taken in order not to reduce the cross-sectional area of the reinforcement bars any more than necessary. The strain gauge was glued into place, Figure 4-9, then soldered to a connector which later was soldered to a wire.

Figure 4-9: Strain gauge glued on grinded reinforcement bar

To protect the strain gauges and wire from short circuiting due to the moist concrete it was covered with silicon as well as a protective casing in form of a plastic pipe, Figure 4-10. Lastly the cable was fixed to secure it from ripping the strain gauge out of the casing when pouring concrete on top of them.

Figure 4-10 a) Cables soldered into place b) Protective plastic cap installed c) Cap filled with silicone

4.2.3 Material test specimen

A summary of the material test specimens are presented. The concrete specimens were cast at the same time, and with concrete from the same batch. A number of reinforcement bars were tested in tension to determine their properties as well. The specimens made for property testing were:

- 5 cubes for compressive testing, $150x150x150\ mm^3$
- 5 cylinders for tensile strength testing, $\phi = 150\ mm\ \ h = 300\ mm$
- 5 beams for testing of fracture energy, $100x100x1000\ mm^3$
- 4 reinforcement bars for strength testing

4.2.4 Concrete casting

The concrete, quality class C30, was delivered by a truck and poured into the casts. It was then compacted with a vibrator stick. Curing time was 28 days, which marks the point from where the properties of the concrete are assumed to be fully developed [3].

Following the casting process the molds were removed from the primary beams, covering them in plastic and keeping a high relative humidity to prevent any cracks due to drying. The beams were kept humid during the entire hardening process. The smaller specimens mentioned in subsection 4.2.3 were submerged in water.

A week prior the testing one side of the beams were painted in order to make the crack growth and propagation easier to spot and analyze.

4.3 Laboratory procedure

The testing of the beams was deformation controlled. The piston from the hydraulic press descended at a set rate of 0.01 mm/second, resulting in reaction forces at the supports.

The high beam specimen was placed on a test wagon which is shown in Figure 4-11. The test specimen was propped to prevent it from falling over, and then rolled into place underneath the hydraulic press. Maximum load of the wagon was about 1000 kN. This upper limit was decided by the research engineer.

Figure 4-11: Wagon for placing the beam under the hydraulic testing rig

Once the specimen is in place on top of its bearings the wagon is pushed into place underneath the hydraulic testing rig. The piston was slowly raised and the upper bearings were inserted, Figure 4-12. All desired measurements were prepared and started, consecutively the test may start.

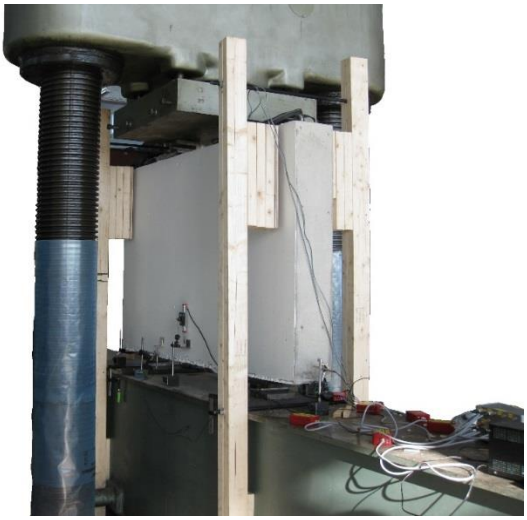

Figure 4-12: Testing setup; wagon, beam, supports and piston

4.4 Measurements

Several measurements and documentations were made. Some of the data achieved was used in this project but is available for future research. What was measured and documented were:

- Applied force
- Strain on the reinforcement, measured with strain gauges
- Deflection of beam, measured with deflection gauge
- Deflection of table where the beam is mounted
- Movement of the piston
- Crack propagation and size, photographed next to ruler to later determine crack growth on the painted face of the beam
- Filming as documentation as well as for use in education

5 COMPUTER MODELLING

This chapter is intended to give the reader an overview of the computer model used. From this description the interested reader should be able to reproduce the simulations.

5.1 Model

The following subsections present information needed to re-create this simulation, such as the material parameters and assumptions made.

5.1.1 Parts

A model consisting of two different parts were created; the high concrete beam member and the reinforcement bars. Naturally, these will have different material properties. The geometries of the models were the same as tested in the lab.

The beam was modelled as a 2D-planar shell element and given the depth of 0.2 m. The reinforcement bars were modelled as 2D-planar wire elements with a given cross-sectional area.

5.1.2 Material properties

Cracking of concrete affects the strength of the beam, therefore an effort to model this behavior has to be made. Several cracking models are available in the software. The one used for this project is the Concrete Damaged Plasticity model, CDP [22]. Basic material properties are presented in Table 5-1.

Table 5-1: Concrete properties, Density and Elasticity

Density, ρ	$2400\ kg/m^3$
Young's modulus, E	$33\ GPa$
Poisson's ratio, ν	0.2

The primary parameters in the CDP-modelling follows the recommendations in the Abaqus Manual [17], Table 5-2, and their features are explained in subsection 2.6.1. The dilation angle is chosen in conformation with literature, e.g. [13].

Table 5-2: Concrete properties, CDP Plasticity

Dilation angle (ψ)	Eccentricity (ϵ)	f_{b0}/f_{c0}	K_c	Viscosity Parameter μ
37°	0.1	1.16	0.667	$1 \cdot 10^{-6}$

From the tests in the lab, subsection 4.1.1, the compressive strength of the concrete were determined, subsection 6.1.1. The parameters entered in the computer model may be seen in Table 5-3. These are adopted from the curve expressed in Equation (2.2).

Table 5-3: Concrete properties, CDP Compressive behavior

Yield Stress [MPa]	Inelastic Strain [‰]
13.1	0
19.2	0.3
25.4	0.7
29.7	1
32.0	1.4
32.7	1.7
31.8	2.1
29.4	2.4
25.6	2.8
20.7	3.1

The tensile properties of the concrete were measured in the lab according to subsection 4.1.1. The tensile strength follows a bi-linear curve and the values entered are according to Table 5-4.

Table 5-4: Concrete properties, CDP Tensile behavior

Yield stress [MPa]	Displacement [m]
2.52	0
0.756	$3.87 \cdot 10^{-5}$
0	$1.74 \cdot 10^{-4}$

The reinforcement bars are modelled as elastic-plastic members. The data for the rebars are collected from the test results. Since no obvious yielding point is present the 0.2%-limit is used, se subsection 6.1.4, marked with a blue dot in Figure 5-1. The strain to the right of that point are considered as plastic deformations.

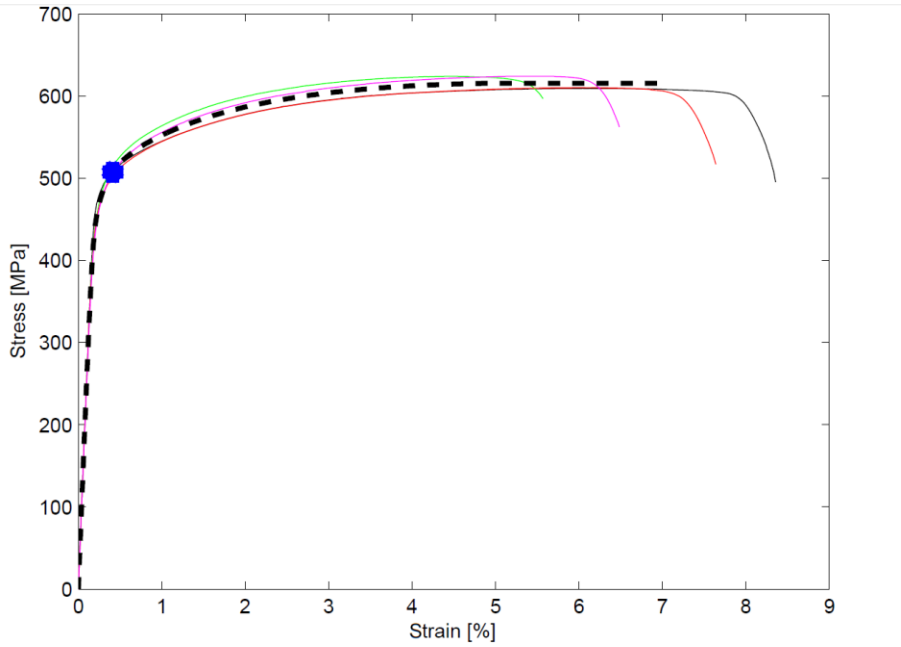

Figure 5-1: Mean stress-strain response curve for reinforcement, blue point indicates the assumed elastic limit

For strains above the yielding point, on the mean strength line, values were chosen to resemble the plastic behavior of the reinforcement. The values used can be seen in Table 5-5.

Table 5-5: Reinforcement response past the 'yielding point'

Yield Stress f_y $[MPa]$	Inelastic Strain, ε_{pl} [%]
507.2	0
516.6	0.0729
526.3	0.1735
534.4	0.2937
545.2	0.4538
555.2	0.653
570.4	1.032
590.1	1.75
610.0	3.224
615.4	4.539
615.3	6.61

The basic parameters used for the reinforcing steel Table 5-6.

Table 5-6: Steel properties, Density, Elasticity and Poisson's ratio

Density, ρ	$7850\ kg/m^3$
Young's modulus, E	$240\ GPa$
Poisson's ratio, ν	0.3

5.1.3 Loading and boundary conditions

Selected boundary conditions, which are supposed to represent reality, are presented in Figure 5-2. Three of the four nodes are constrained by a rolling support and the final one is pinned.

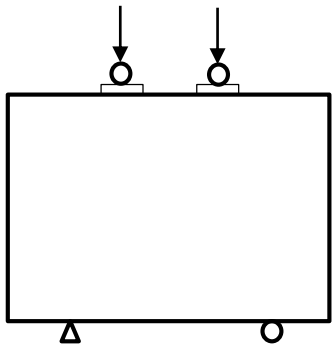

Figure 5-2: Schematic model, with boundary conditions

The loading plates are allowed to rotate and follow the deformation of the beam. In order to achieve displacement-controlled loading, a boundary displacement in the loading plates is prescribed. In order to calculate the corresponding force, reaction forces at the fixed boundary points are summarized.

5.1.4 Interaction between concrete and reinforcement bars

The interaction between the reinforcement and the concrete is modelled as an embedded region. Default values regarding the interaction behavior is used.

5.1.5 Time step

As dynamic effects are not taken into consideration and no kind of dynamic stabilization was used, time step was not used in order to capture any velocity, acceleration or similar. Instead, it was used as a factor to incrementally load the structure with a displacement. There exists some initial time step sensitivity in the model.

The time steps used are according to Table 5-7.

Table 5-7: Time step parameters used

Initial time step	$1 \cdot 10^{-4}$
Minimum time step	$1 \cdot 10^{-6}$
Maximum time step	$1 \cdot 10^{-4}$

Data is extracted every time unit of $1 \cdot 10^{-4}$ seconds in order to limit the amount of extracted data, generating faster data processing times. Thus, the maximum time step is $1 \cdot 10^{-4}$ seconds.

5.1.6 Mesh

In order to model stresses and force response accurately, a quite coarse mesh might be used according to Malm [15]. However, in order to model cracking behavior in an accurate way, finer mesh is preferable. In these studies, a coarse mesh has proven to capture the load-displacement behavior accurately.

Furthermore, shear locking is a phenomena associated with node types and is a risk when using isoparametric linear 4-node elements that might increase the stiffness of the model significantly. In order to avoid such response 'reduced integration' can be used. Also, the linear 4-node elements have proven insufficient when the deformations are simulated. Therefore quadratic 8-node elements were used.

The mesh size finally used in the models are of the size $0.1x0.1\ m^2$. This proved to yield good results in terms of forces.

6 RESULTS AND ANALYSIS

Results for each of the steps made regarding the beam specimen will be presented together with remarks in this chapter. The first section presents the properties of the materials used, based on the results reached in the laboratory tests, followed by the results of each of the methods used to attain the capacity of each specimen. Lastly, a comparison of the attained results for each of the four tested beams.

The results will be discussed throughout the chapter along each result where necessary.

6.1 Material properties

6.1.1 Concrete – compressive strength

The compressive strength of the concrete is tested according to subsection 4.1.1. Five cubes were tested, the results attained are presented in Table 6-1.

Table 6-1: Compressive strength of concrete, measured in lab

	Ultimate load [kN]	Strength f_{cu} $[MPa]$
Cube 1	730	32.4
Cube 2	720	32
Cube 3	830	36.9
Cube 4	760	33.8
Cube 5	640	28.4
Mean	736	32.7

6.1.2 Concrete – tensile strength

The tensile strength of the concrete is tested according to subsection 4.1.1. Five cylinders are tested and their results are evaluated to a corresponding tensile strength, as presented in Table 6-2.

Table 6-2: Tensile strength of concrete, measured in lab

	Ultimate load [kN]	Strength $f_{ct,sp}$ $[MPa]$	Strength f_{ct} $[MPa]$
Cylinder 1	78.5	2.50	2.25
Cylinder 2	103.4	3.29	3.06
Cylinder 3	81.5	2.59	2.33
Cylinder 4	88.8	2.83	2.54
Cylinder 5	88.3	2.81	2.53
Mean	88.1	2.80	2.52

6.1.3 Concrete – fracture energy

The fracture energy, G_f, was measured according to subsection 4.1.1. The results are presented in Table 6-3. The first beam, G_{f-1}, failed and therefore only the remaining beams are presented. The overall response from each beam tested is presented in Appendix C.

Table 6-3: Fracture energy results, measured in lab

	Fracture energy, G_f $[N/m]$
Beam 2	102.54
Beam 3	133.67
Beam 4	126.31
Beam 5	122.44
Mean	121.24

6.1.4 Reinforcement – tensile strength

The reinforcement were tested according to subsection 4.1.2. The results are presented in Table 6-4. The stress-strain behavior as well as the force-strain behavior is presented in graphs which can be found in Appendix C.

Table 6-4: Results from reinforcement tests, measured in lab

	Ultimate load [kN]	Strength f_y $[MPa]$	Strength f_u $[MPa]$
Rebar 1	30.63	506	609
Rebar 2	31.36	514	624
Rebar 3	30.67	502	610
Rebar 4	31.37	508	624
Mean	31.01	508	617

Since no obvious yielding point occurs in the stress-strain relationship, Figure 6-1, the yielding point is determined according to the standards [4]. To find the yield strength, a linear function is fitted to the elastic zone, then shifted 0.2% on the x-axis. The point of intersection is the yielding point.

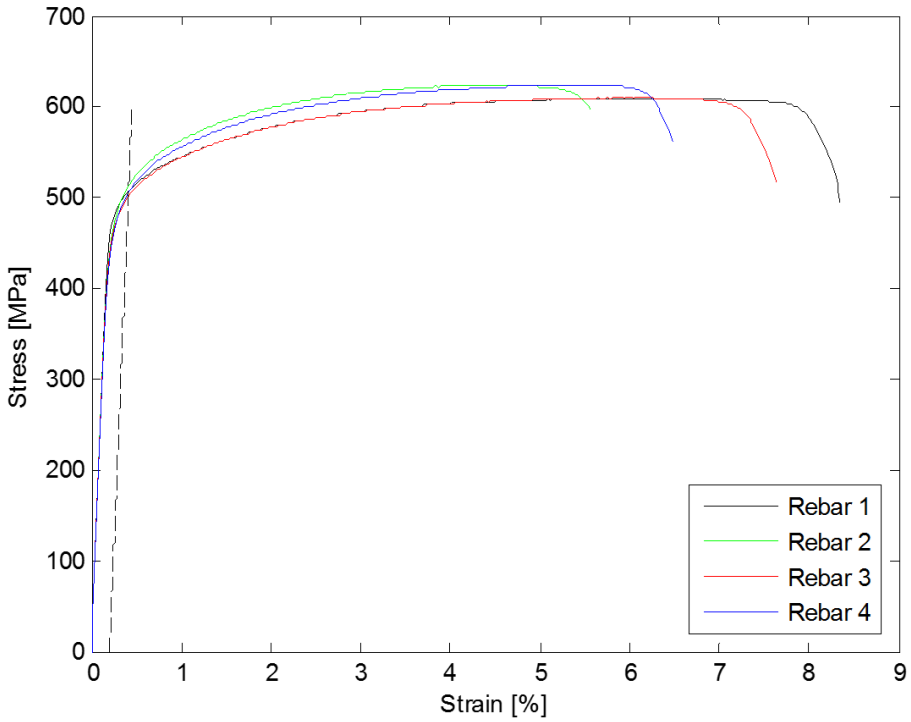

Figure 6-1: Stress-strain of reinforcement attained from testing

6.2 Load capacity

This section presents the calculated capacity for each of the specimen, as well as the measured strength from the laboration. A comparison of the results for each of the beam specimen is made in section 6.3.

6.2.1 Primary calculations

Determining the strength of the beams were made prior the testing of the materials strengths, i.e. the strength of the concrete and the reinforcement according to the standards, and are presented in Table 6-5. Calculations are presented in Appendix B.

Table 6-5: Total capacity of test specimens for different design angles according to hand calculations in Eurocode (primary)

	45°	60°	73.5°
T1	100 kN	174 kN	342 kN
T2	201 kN	348 kN	679 kN
T3	302 kN	522 kN	1018 kN
T4	201 kN	348 kN	679 kN

6.2.2 Revised calculations

Using the material parameters received from the material tests in the lab a revised set of calculations using the strut-and-tie method were made, Table 6-6.

Table 6-6: Total capacity with revised material strength parameters attained from laboratory tests

	45°	60°	73.5°
T1	102 kN	177 kN	347 kN
T2	204 kN	354 kN	690 kN
T3	306 kN	531 kN	1034 kN
T4	204 kN	354 kN	690 kN

6.2.3 Laboratory test results

Data regarding the testing of the four beam specimens are presented in Table 6-7.

Table 6-7: Total capacity of the specimen attained in the laboratory tests

	Highest applied load $[kN]$	Ultimate load $[kN]$	Cracking load $[kN]$	Deflection at highest load $[mm]$
T1	1000	1000	1000	2.14
T2	1000	-	1000	1.89
T3	1010	-	1010	2.19
T4	1200	-	850	4.19

A few short comments regarding the testing procedure for each beam is mentioned next.

Beam T1

Rather linear response until just about 1000 kN. Sudden crack pattern covering the entire height of the beam at mid span. The load was decreased and re-initiated, a sudden brittle failure occurred sending the two 500 kg halves one meter apart.

Beam T2

More or less linear response until 1000 kN, the upper limit set by the research engineer. Sudden cracks on both sides of the specimen, after aborting the test the crack pattern was filled in with a permanent marker.

Beam T3

Almost identical behavior as beam T2. Test was once again aborted at 1000 kN.

Beam T4

The first beam tested. Rather linear response until about 900 kN where the first visible cracks started to occur. Their development were tracked with close up photos and a ruler mounted next to it. The crack propagation is presented in Appendix C3.

6.2.4 Computer model results

The results from the computer models made in Abaqus/CAE are presented in Table 6-8.

Table 6-8: Capacity and behavior of computer modelled specimens

	$Ultimate\ load\ [kN]$	$Crack\ load\ [kN]$	$Deflection\ [mm]$
T1	763	690	0.10
T2	841	700	0.10
T3	1109	760	0.11
T4	1144	740	0.10

6.3 Comparison between model and laboration

This section presents a comparison of the results reached for each of the four beam specimen using computer simulations and the results from the lab.

6.3.1 T1 – Response curve

A comparison of the load-deflection response in configuration T1 is shown in Figure 6-2. The computer model is significantly stiffer than the beam specimen tested in the lab. In the model, when the tensile strength of the concrete is exceeded, just over 700 kN, the reinforcement yields instantaneously. The lab specimen follows a linear elastic response, some late cracking occur, just below 1000 kN, at which a brittle failure occur – separating the beam into two halves.

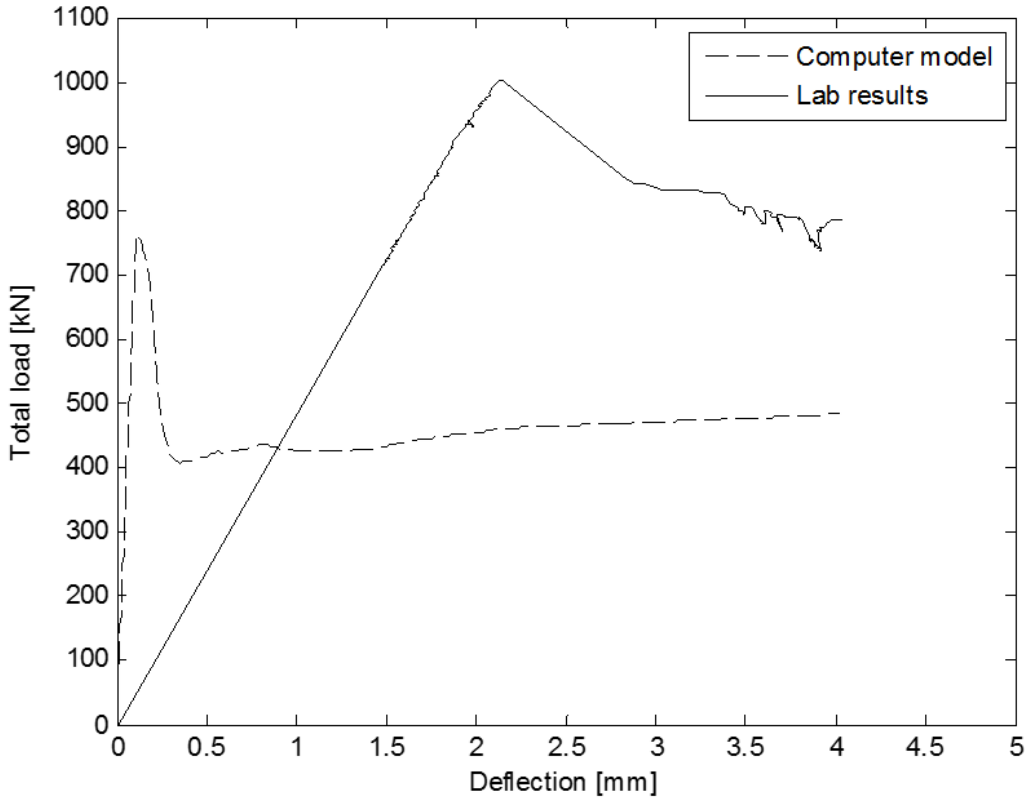

Figure 6-2: Comparison: Load-deflection, deflection measured at center of lower edge, T1

6.3.2 T1 – Force-strain in reinforcement

A graph comparing the results attained from the TTG-sensors mounted on the reinforcement and the strain from the computer model for beam T1 is presented in Figure 6-3. The results in this graph shows an infinitesimal strain in the specimen tested in the lab, indicating that the beam tested in the lab should be stiffer. However this contradicts the results presented in subsection 6.3.1, as well as the strain data from other beams. The author's speculations concerning this would be local strains in the laboration. The strains are believed to be concentrated to any area where the concrete have cracked, i.e. the TTG-sensor in Figure 6-3 may therefore be located relatively far from the weakening. In the computer model, the strains are more evenly spread out.

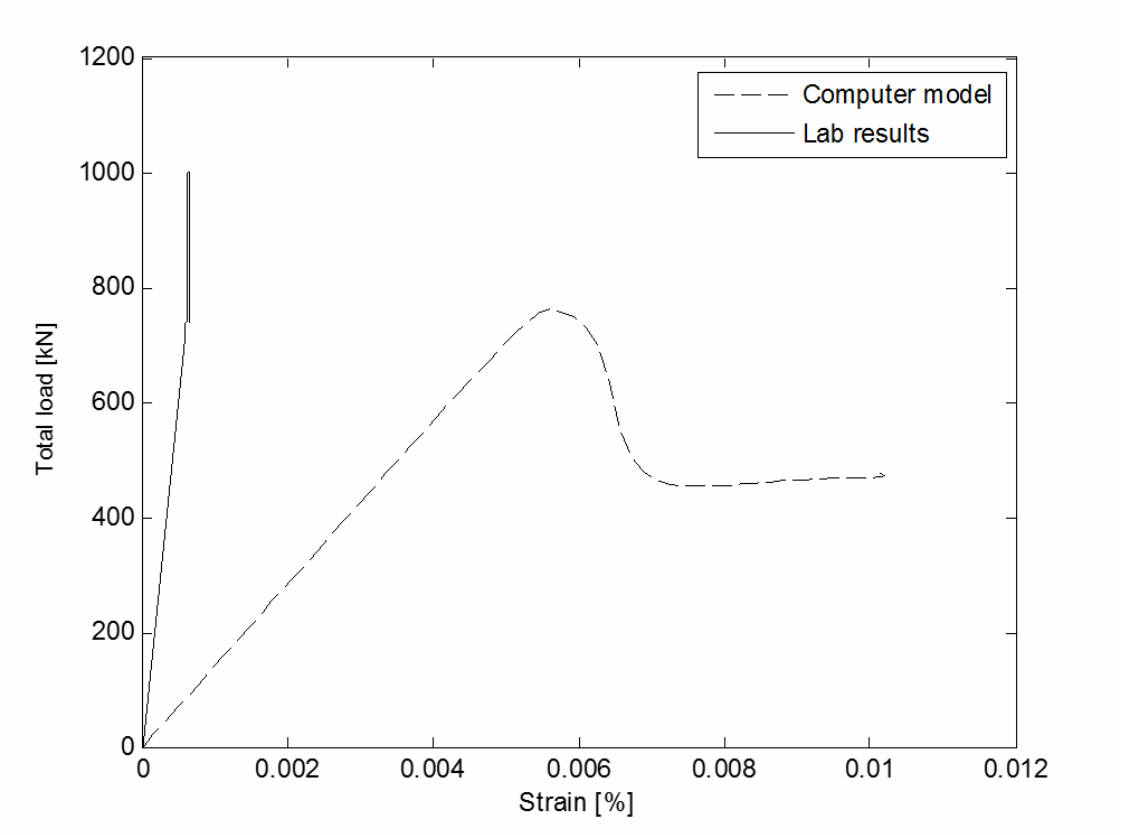

Figure 6-3: Comparison: Force-strain in reinforcement, center of rebar, T1

6.3.3 T2 – Response curve

A comparison of the load-deflection response in configuration T2 is shown in Figure 6-4. The behavior is similar to the previously shown T1. When the concrete in the computer model reaches its tensile strength cracking and some sudden deflection occur, followed by the reinforcement taking the load and starts to yield. The tested loading capacity exceeds the calculated capacity from the Abaqus model, loading stopped at 1000 kN, with no failure. However, cracks were detected.

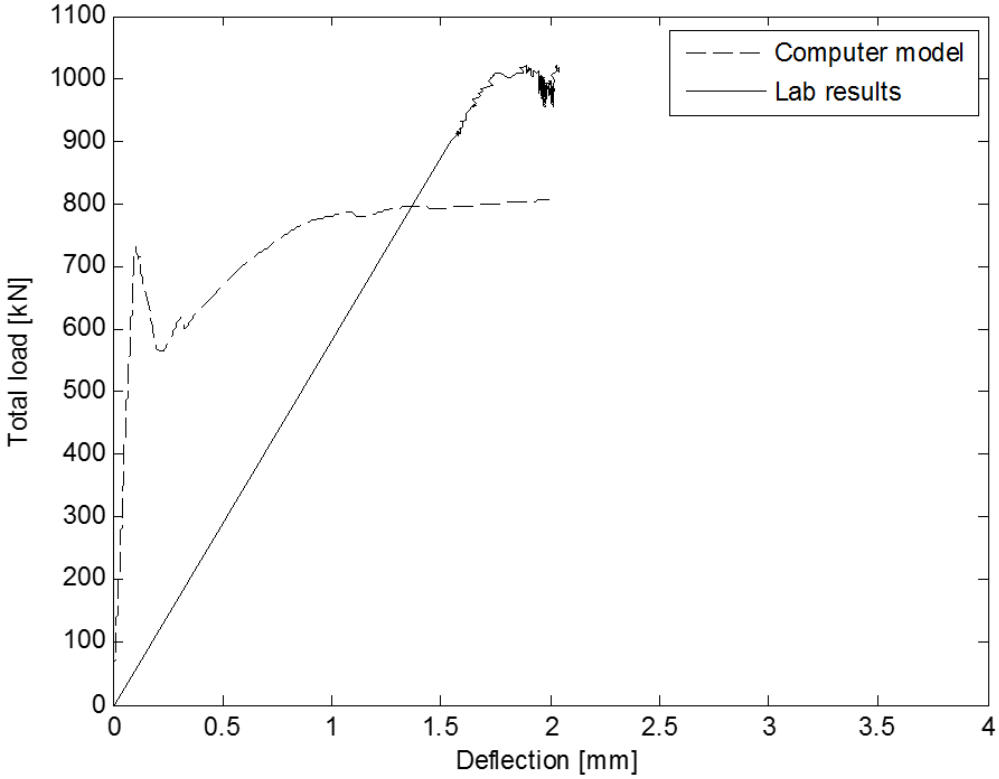

Figure 6-4: Comparison: Load-deflection, deflection measured at center of lower edge, T2

6.3.4 T2 – Force-strain in reinforcement

The results from the TTG-sensor from the lab as well as the computer modelled strains for specimen T2 are presented in Figure 6-5. The stiffness, i.e. inclination of the graphs, are similar. The laboratory specimen however did not start to yield. Strains might have been located close to cracks, or simply, the strains did not start to increase due to cracking, as cracks occurred when loading was stopped.

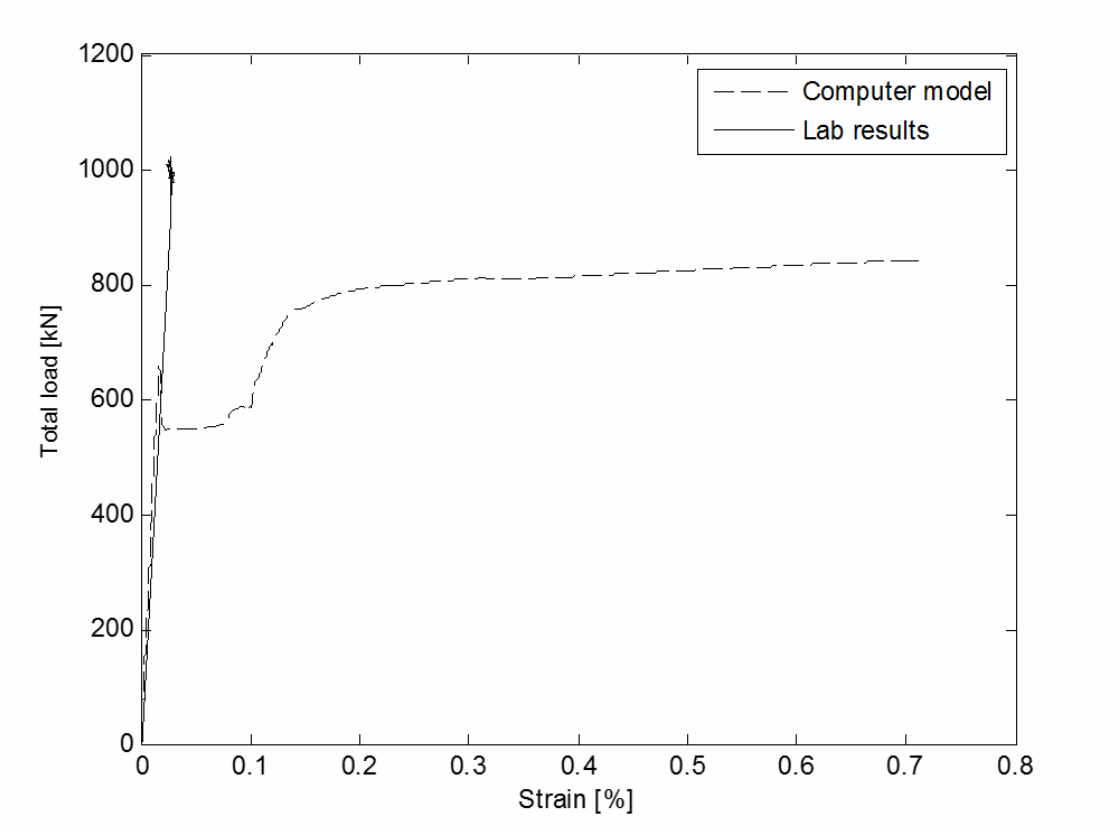

Figure 6-5: Comparison: Force-strain in reinforcement, center of lower rebar, T2

6.3.5 T3 – Response curve

A comparison of the load-deflection response in configuration T3 is shown in Figure 6-6. The behavior reminds of T1 and T2. The computer model is stiffer in the linear elastic zone. Past the tensile capacity of the concrete cracking occurs in the computer model, resulting in a redistribution of forces leaving the reinforcement being activated. The load may now be raised as high as about 1100 kN. The lab tested beam got visible cracks just about 1000 kN, where loading was stopped.

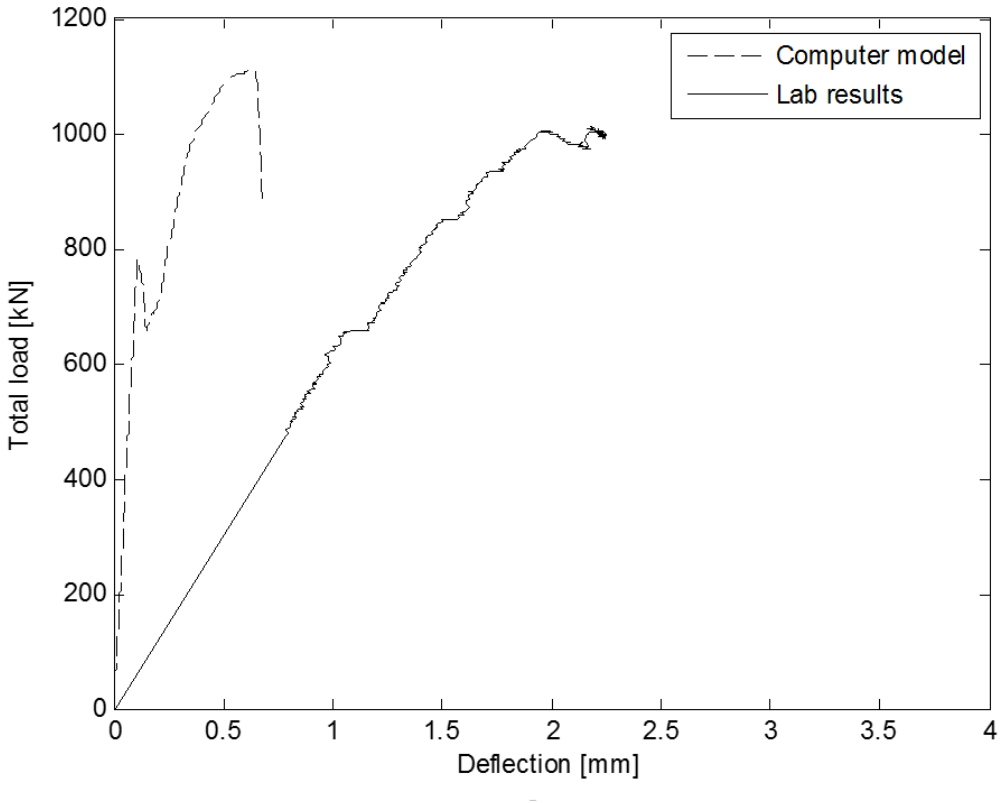

Figure 6-6: Comparison: Load-deflection, deflection measured at center of lower edge, T3

6.3.6 T3 – Force-strain in reinforcement

Results showing the force-strain relationship reached in the lab and the computer modelled for specimen T3 are compared in Figure 6-7. The stiffness of the two results seem similar, with what seems to be a yielding limit at just below 1000 kN in the lab.

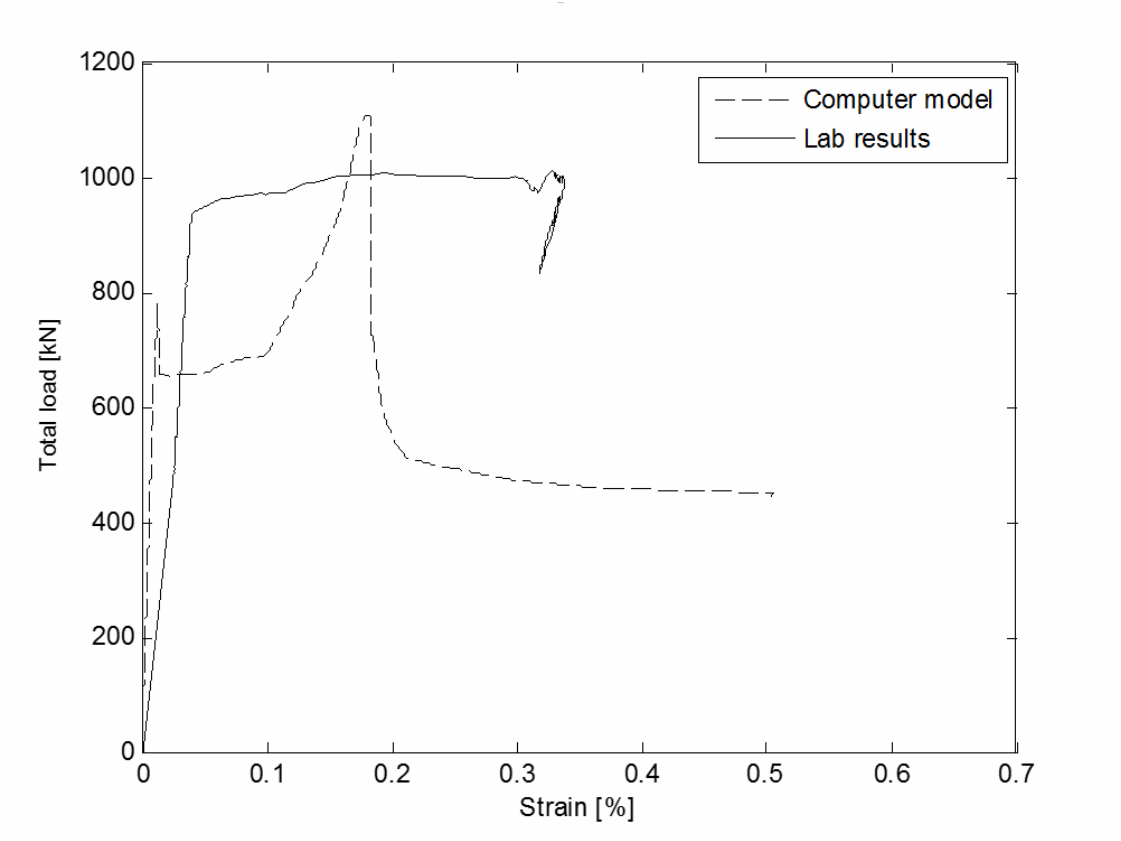

Figure 6-7: Comparison: Force-strain in reinforcement, center of lower rebar, T3

Some interesting behavior is observed in the graph above considering the computer model. The von Mises stress is shown, Figure 6-8 for a few steps in order to explain the curve. Sketch 1 and 2 are in the linear-elastic zone, stresses distributing and ending up in supports. Sketch 3 shows the stress distribution at cracking, i.e. about 800 kN. The 4:th sketch shows the stresses at about 1100 kN, when a shear failure occurs at the right support.

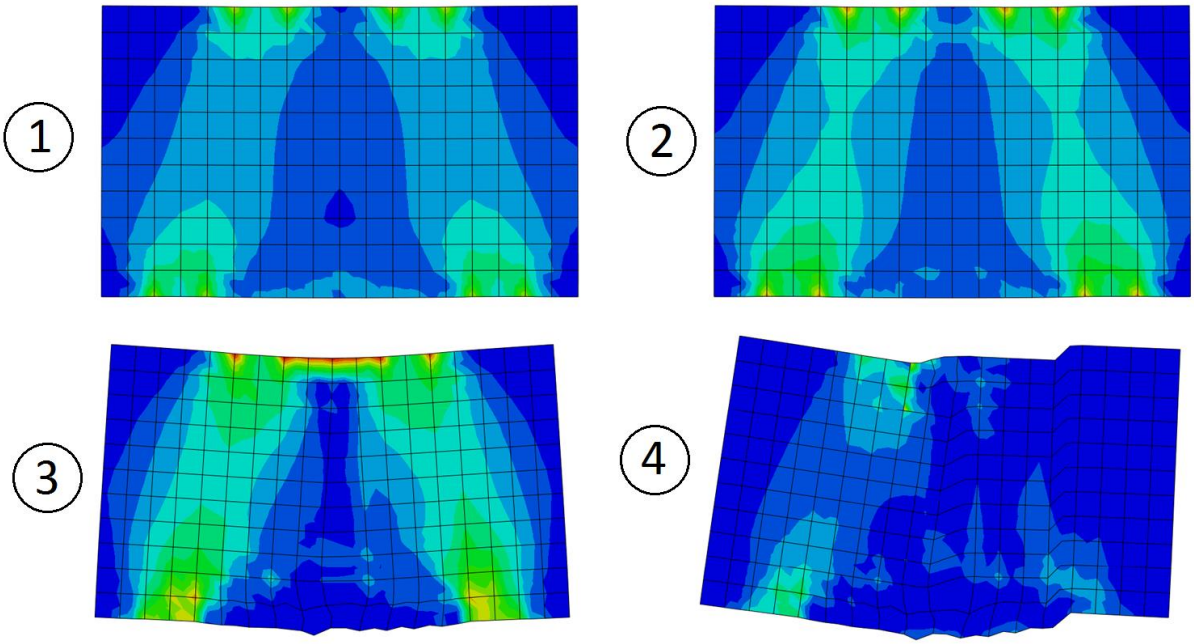

Figure 6-8: Stress distribution, T3 (Von Mises stress) at; 1:Intial stress ; 2: Stress increase; 3: Cracking in mid span; 4: Shear failure at support

6.3.7 T4 – Response curve

A comparison of the load-deflection response in configuration T4 is shown in Figure 6-9. The linear elastic response for the computer tested model exceeds the stiffness of the tested beam. Once the computer model reaches the tensile strength of the concrete a stress redistribution occurs and the reinforcement starts taking additional load.

In the laboratory practical visible cracks occurred at about 800 kN. The crack growth was photographed and measured, the growth of the width are shown in Appendix C3.

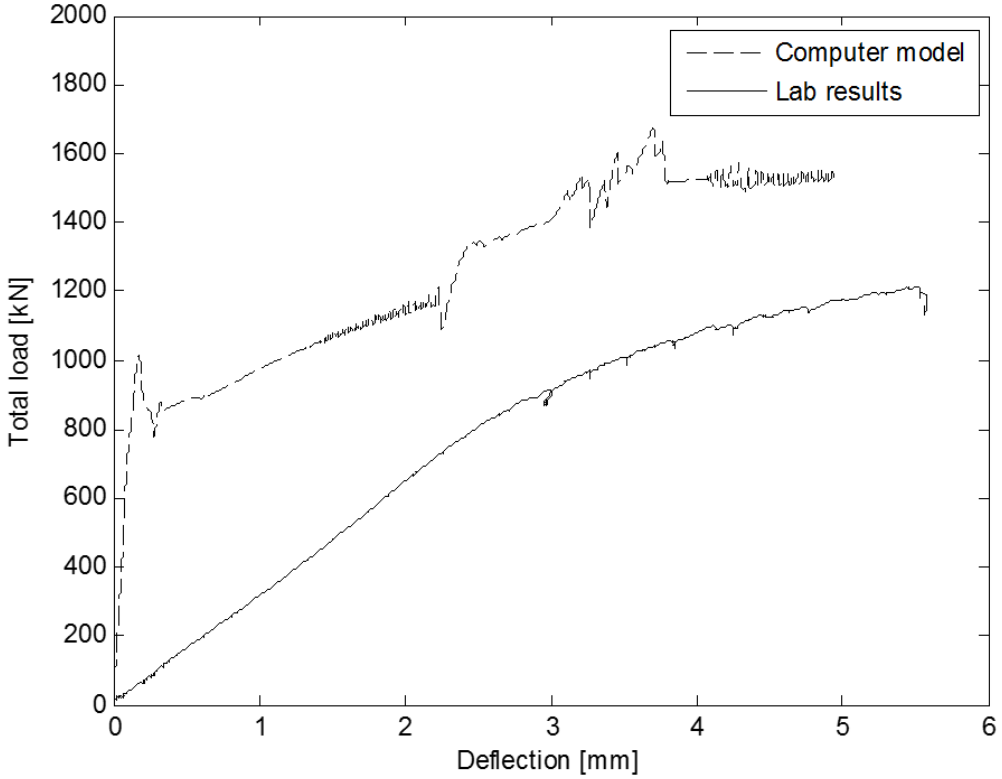

Figure 6-9: Comparison: Load-deflection, deflection measured at center of lower edge, T4

The failure that occurred in the computer simulation was of shear type, Figure 6-10, where the two compressive struts fails. One possible explanation is that the bending stiffness of this specimen is far greater than the similar T2 due to the minimum reinforcement. Instead of only having one internal lever arm (the primary reinforcement), the horizontal reinforcement bars contribute which an ‘extra’ lever arm increasing the flexural resistance. The struts are not significantly strengthened from the reinforcement mesh as the stiffness of the mesh, at the location of the struts, is low. The crack appears transversally to the horizontal bars. This is a possible explanation of the ‘shear’ behavior.

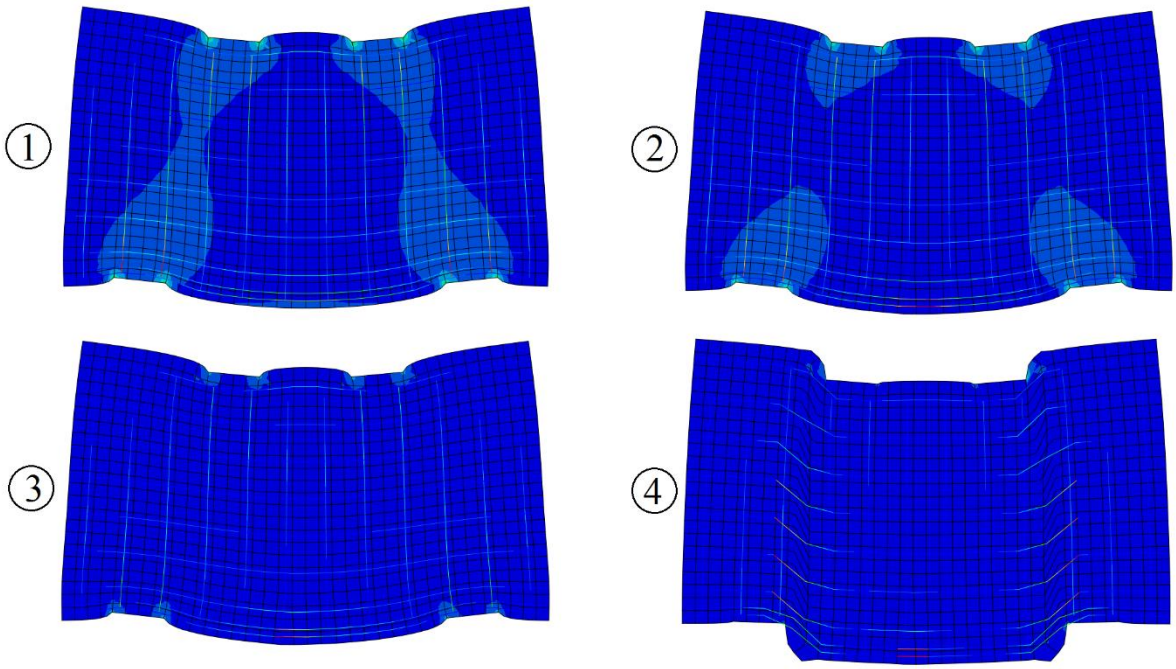

Figure 6-10: Simulated behavior for beam T4

6.3.8 T4 – Force-strain in reinforcement

A graph comparing the total load-strain relationship attained in the laboratory practical and the computer model for beam T4 are presented in Figure 6-11. The stiffness of beam T4 seems less than the model.

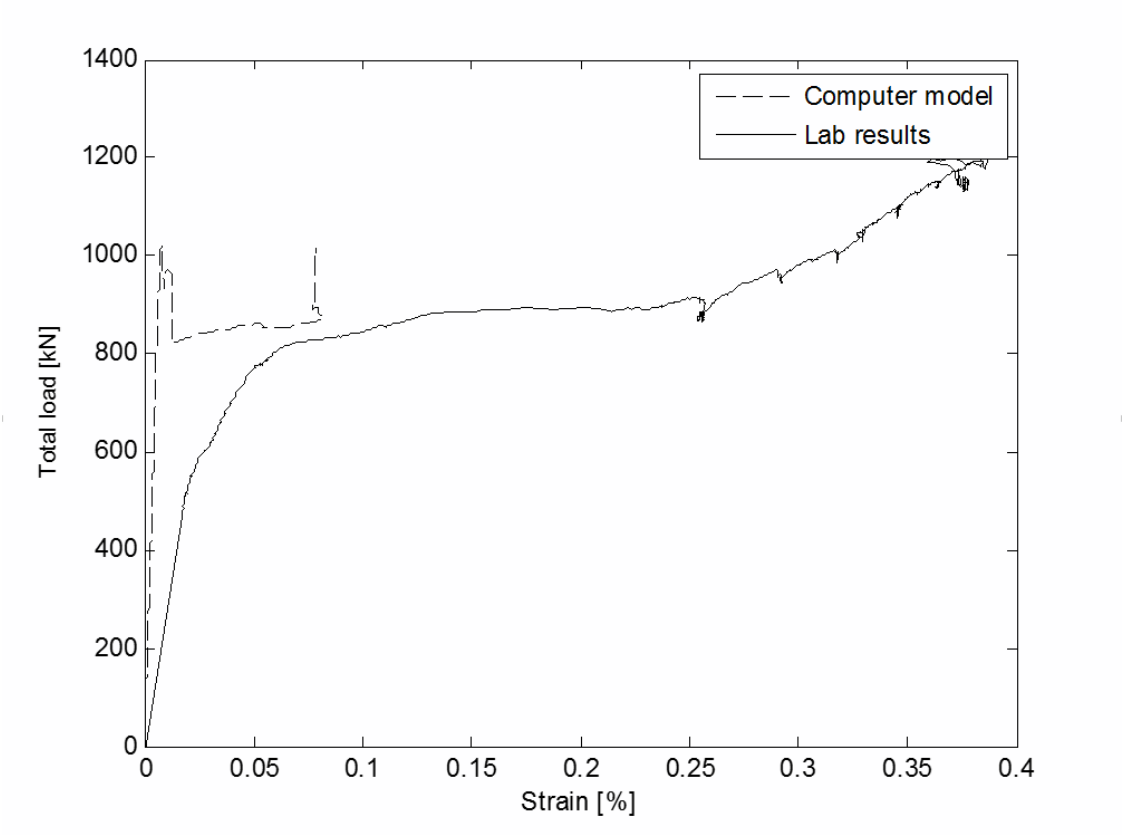

Figure 6-11: Comparison: Force-strain in reinforcement, center of lower rebar, T4

6.4 Comparisons between specimens

To more accurately get a clear picture of the behavior of the specimens comparisons are made.

6.4.1 Deflection - Laboration

The response curves from each of the in lab tested beam specimens are presented in Figure 6-12. Their initial responses may be considered rather similar. Beam specimen T1 failed at 1000 kN, beam T4 was tested as far as 1200 kN.

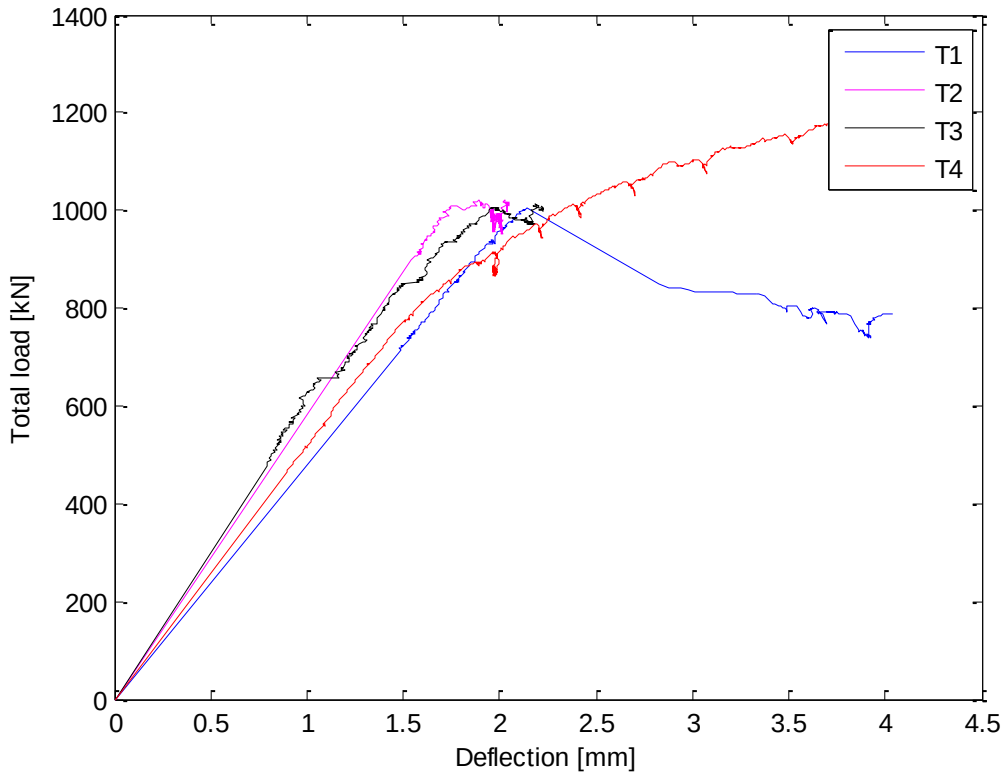

Figure 6-12: Comparison between specimens: Force-deflection curves from laborations, center of lower edge

6.4.2 Deflection – Computer model

Comparing the simulated response for each beam results according to Figure 6-13 are reached. From this the authors' explanation is that the concrete strength determines the linear-elastic zone.

The only difference between specimen T2 and T4 is the occurrence of minimum reinforcement according to current standards in the latter. This seem to almost offer an elongation of the linear elastic zone.

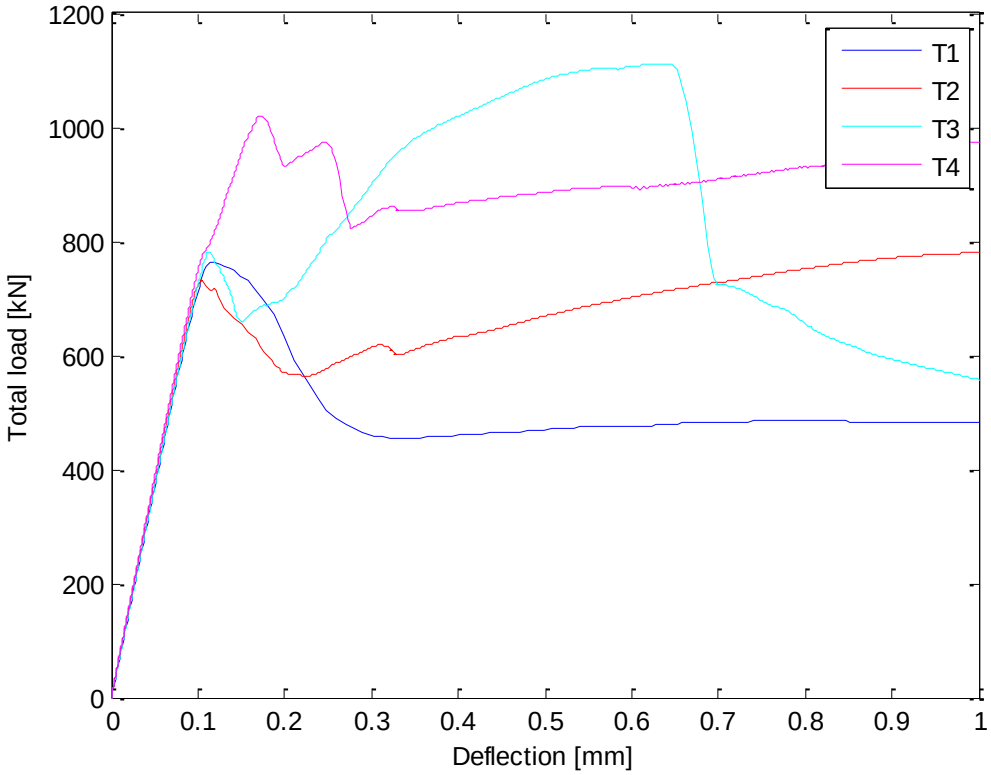

Figure 6-13: Comparison between specimens: Force-deflection curves from simulations, center of lower edge

6.4.3 Concrete stress field

The horizontal stresses in the concrete gives an indication of the plastic redistribution capacity. This should however be regarded as theoretical as results are from computer modelling. In Figure 6-14 the horizontal stresses S_{11} are shown over the height of the cross-section, clearly non-linear. This stress distribution will however change when the concrete begins to crack, resulting in a pressure zone located higher and with greater magnitude.

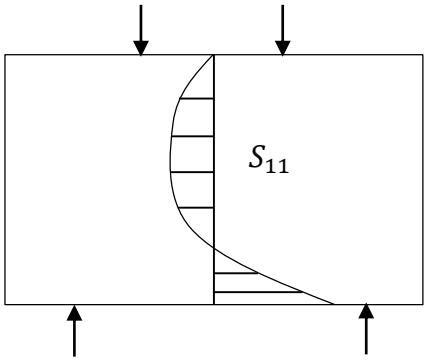

Figure 6-14: Sketch of horizontal stresses in high beam

The development of the horizontal stresses within the beams T1-T3 can be seen in Figure 6-15, Figure 6-17 and Figure 6-19. Here it is shown that there is a slight raise of the internal lever arm, i.e. the compressive zone of the concrete beyond the cracking limit. The loads for which the stresses are plotted are chosen according to the load-displacement graph in connection with each of the horizontal stress sketches, Figure 6-16, Figure 6-18 and Figure 6-20. The raise of the internal lever arm is an indication of the plastic redistribution capacity of the concrete, especially as T1-T3 has no minimum reinforcement.

T1

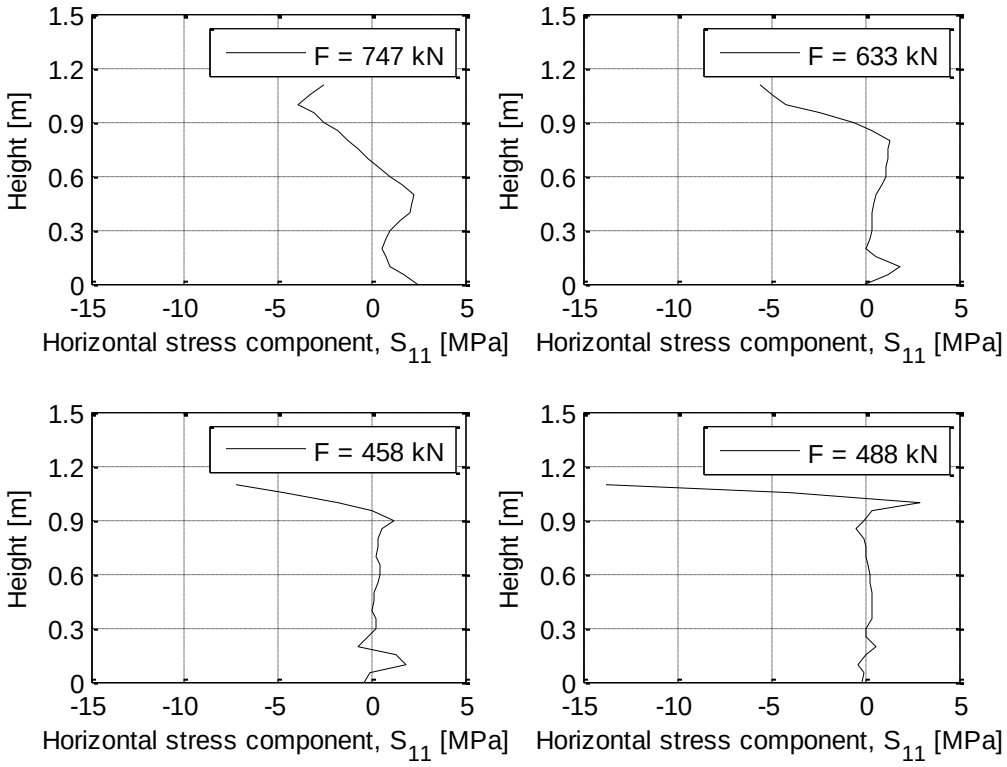

Figure 6-15: Concrete stresses in center of beam, T1

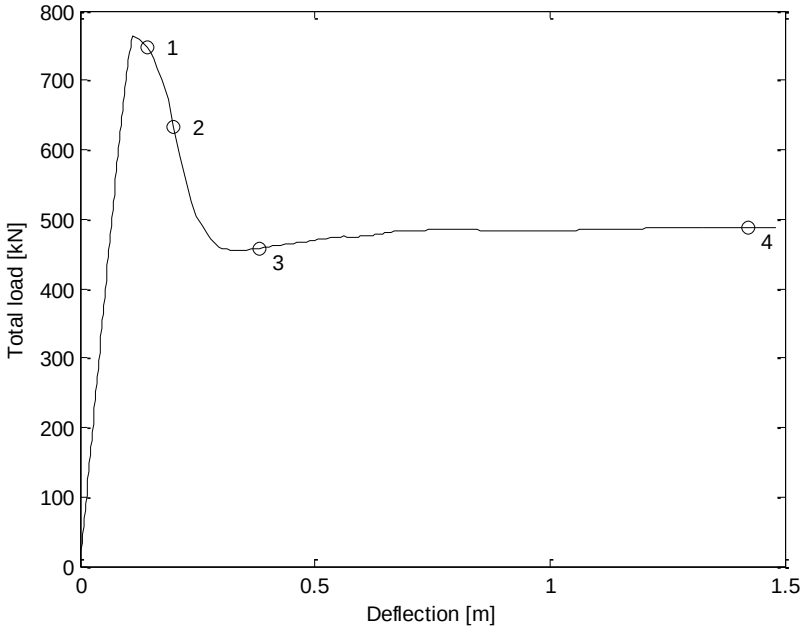

Figure 6-16: Forces of which concrete stresses are shown for T1

T2

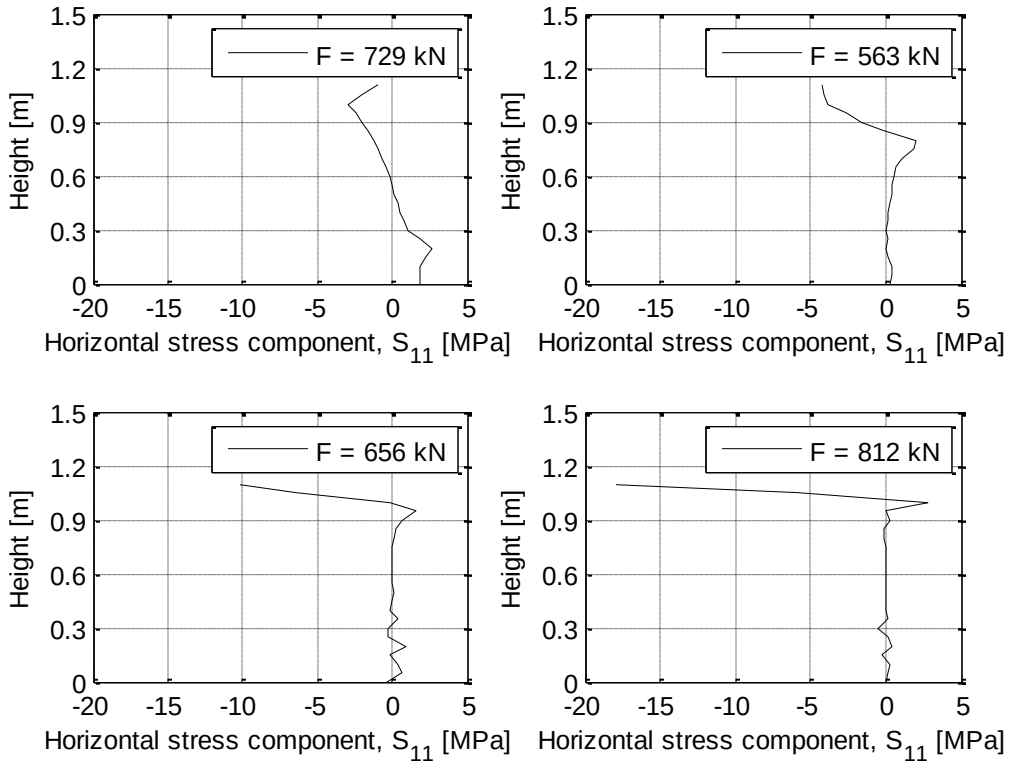

Figure 6-17: Concrete stresses in center of beam, T2

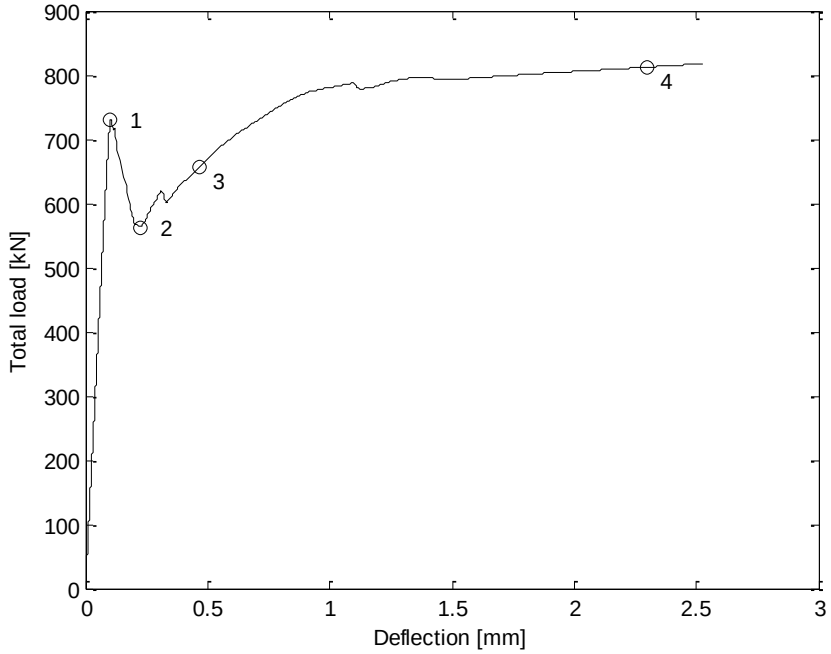

Figure 6-18: Forces of which concrete stresses are shown for beam T2

T3

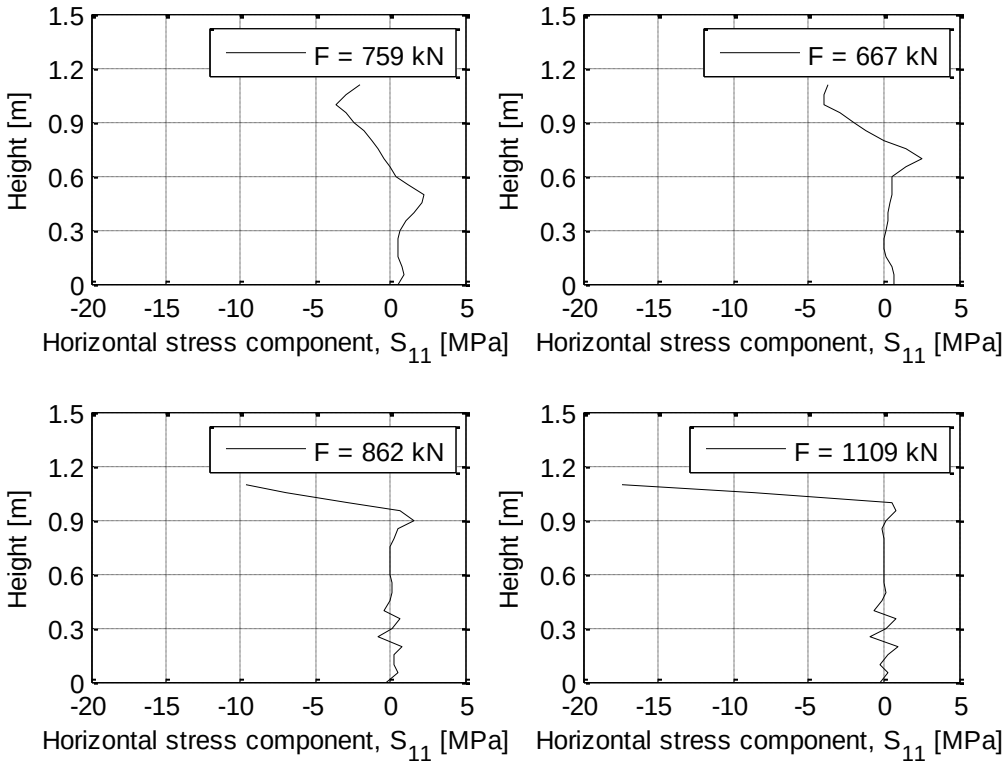

Figure 6-19: Concrete stresses in center of beam, T3

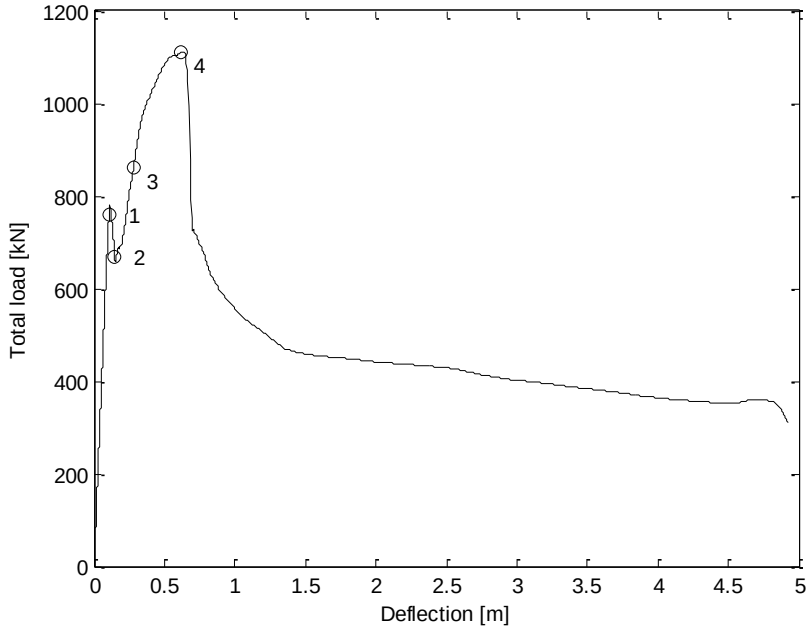

Figure 6-20: Forces of which concrete stresses are shown for beam T3

T4

Unlike T1-T3 the beam T4 does not crack in mid span during simulations. Therefore a stress distribution, and a rising lever arm in the center of the beam, is not of interest. However, a stress redistribution within the structure is obvious when studying the plotted stresses in each of the cases in Figure 6-21.

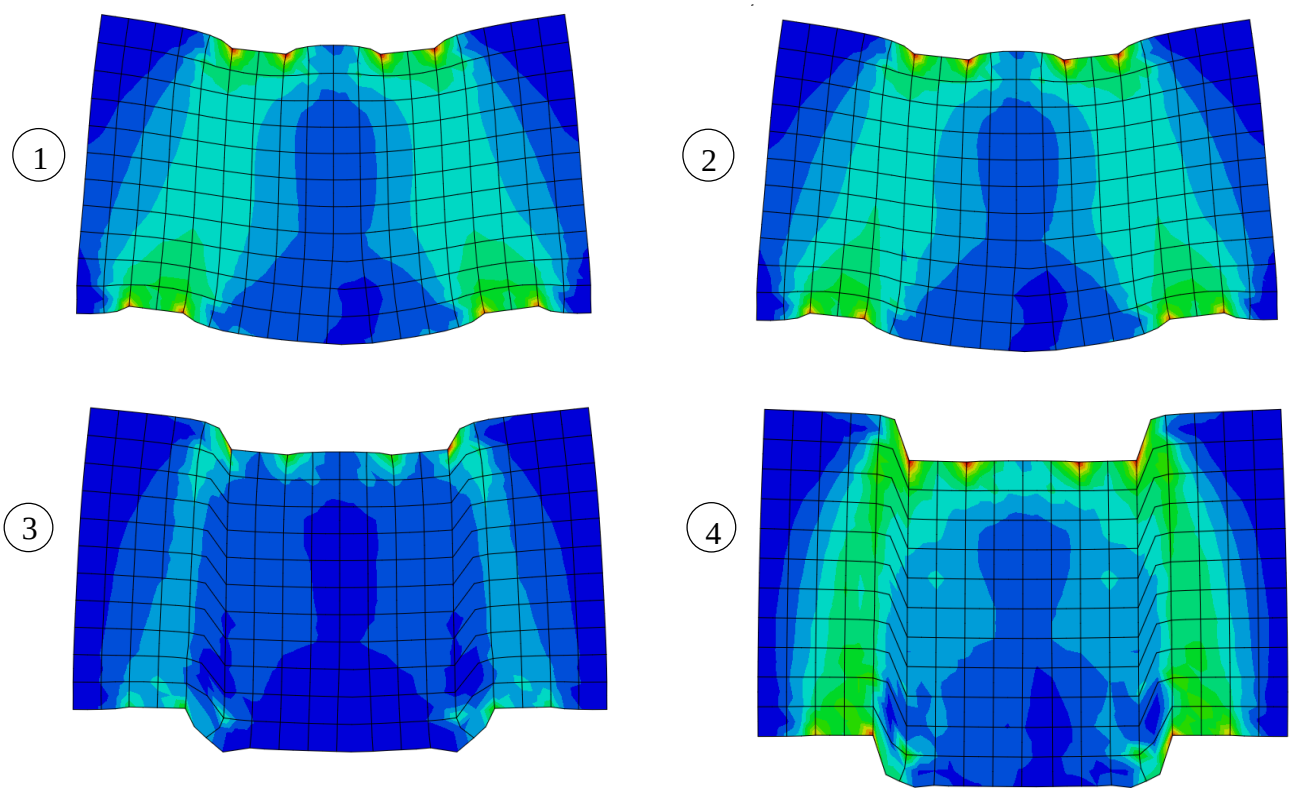

Figure 6-21: Stress distribution, T4 (Von Mises stress) at; 1: 928 kN; 2: 1094 kN; 3: 805 kN; 4: 1134 kN

Lever arm comparison

In Figure 6-22, the change in the internal lever arm for different forces is shown. The numbers 1-4 are presented on the force-deflection diagrams in Figure 6-16, Figure 6-18 and Figure 6-20. The lever arm is assumed to be the center of mass of the compressive stresses in the top of the beam.

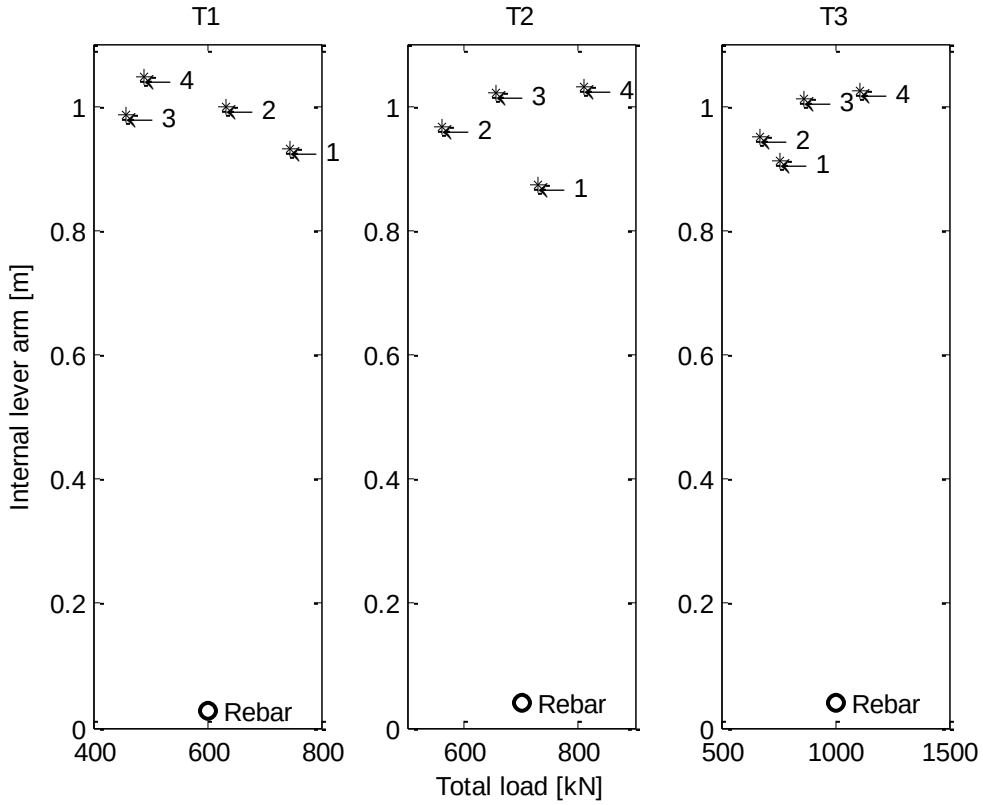

Figure 6-22: Internal lever arm variation from simulations, T1-T3

6.5 Discussion

Some difficulties encountered in the project are discussed below. They are divided in lab- and computer related difficulties.

Laboratory practical

- The small number of specimen leave a high insecurity in all results, since a large number of differences between specimen are possible. A larger number of tests would be preferable, but not realistic due to the size.
- Tensile strength of the concrete may be inconsistent. The theoretical tensile strength assumes the weakest link to be situated along the perimeter. Most tensile weaknesses are overlooked in a 'compressive test of the tensile strength' since cracks and other weaknesses are compressed and stabilized rather than exploited. A direct tensile test would have been preferable.
- Inaccurate measurements are unfortunately a major source of potential errors. Both in terms of the hydraulic load readings but also the deflections gauges (LVDT). For example some values from the LVDT's proved to be useless. A calibration was made whenever possible. There are also questions whether the deflection of the beam was properly measured.
- The casts were more or less identical in size when built, but at casting the horizontal pressure deformed the casts resulting in noticeable, but small, non-uniformities between the beam specimens. As a result of the risk of mold collapse, the vibration of the concrete may have been insufficient.
- Placement of the reinforcement bars is easily done in theory but difficult in practice. Small deviations have been made, since accuracy within millimeters is difficult to achieve, but the results should not be affected.
- In the initial steps of each test the system were 'compacted' prior the linear response of the beam. For example the dry cement applied on top. To compensate for this a linear approximation was made backwards. This linear approximation is sensitive to the choice of starting point selected and may give misleading results.
- In the design of the tests the authors chose to be conservative, e.g. using safety factors when calculating strut and node capacities. This resulted in a wide beam, with high concrete capacity. This lead to a very high crack-inducing load.

Computer simulation

- The number of parameters needed to model the beams in *BRIGADE/Plus* are overwhelming and the background theory is complex. The parameters which were not determined in the lab, i.e. the 'viscosity parameter', 'dilation angle', 'K', 'f_{b0}/f_{c0}' and the 'eccentricity', was either taken as the default value or from literature. Whether or not the values are good is difficult to tell.

- To determine the Young's modulus of the concrete it would have been more accurate to test a specimen in the hydraulic MTS. Even though it would not have been able to press the specimen to failure, the Young's modulus for the elastic zone would have been retrieved, rather than evaluating it according to the codes.
- The Young's modulus in the reinforcement bars might be too high. Sliding in the machine might yield misleading results. Also, the choice of the points on the graph for which Young's modulus may change the result.

7 CONCLUSIONS

7.1 Conclusions from work

1. When using the strut-and-tie method the tensile strength of the concrete as well as the strength of the minimum reinforcement is neglected. Questions may in some cases be raised whether or not this is accurate. Some analysis should also be done to check at which load the concrete starts to crack – as the strut-and-tie method models cracked behavior.

2. To assess a beam according to the strut-and-tie method it is important to understand the importance of crack behavior. To properly calculate the cracking load, a finite element analysis should be performed. Calculating cracking load according to basic beam theory gave a cracking load of about $338\ kN$, lower than the capacity of the weakest beam. A calculation replacing the tie consisting of reinforcement bars with a tie consisting of concrete, using the geometry given from node capacity calculations, gave a cracking load of about 296 kN. These simplifications are obviously not accurate.

3. Load bearing capacity calculations for the least reinforced beam, T1, according to the strut-and-tie model might be correct. The sudden, brittle, failure might be explained by the tensile capacity of the concrete. The capacity specimen T1 would have reached in the ultimate limit state, at yielding of the reinforcement, is less than the load required to induce cracks. When the first crack propagated, strains probably localized near the crack, and in this particular area the strength of the reinforcement bar was exceeded. When designing, a brittle failure should be avoided.

4. When evaluating failures of the tested beam specimens there are roughly two types of behavior. Those are; the brittle behavior of beam T1 and the ductile behavior of beam T4. T1 actually gave a stiffer response compared to the ductile beam T4. However, when failure occurred in beam T1 it was sudden and powerful. A structural element with such behavior would be dangerous to say the least. Therefore, it seems well motivated to use minimum reinforcement. Another advantage using minimum reinforcement is the reduction of crack widths. Studying Appendix D one may realize the increased number of cracks, but in theory they should be thinner compared to one single crack.

5. Laboratory results gave higher deflections than the computer model. Since all beams in laboratory and all beams in computer modelling showed similar force-deflection behavior, the errors probably were systematic. Therefore, some comparisons within modelling or laboratory work are valid. The cause of the differences has not been identified. Probably, a systematic measurement error exists, as the model should capture the behavior correctly in the linear-elastic stage. The results of the model might also be wrong, over-estimating the stiffness.

6. One of the scopes of the project, to investigate whether there exists a plastic redistribution capacity of the concrete specimen which might yield a higher design angles, cannot be determined. There exists indications from laboratory work in specimen T4. There is a contribution from the minimum reinforcement to the ductile behavior and redistribution ability, but as structures in reality always (at least when designing according to Eurocode) are constructed with minimum reinforcement, there are indications of a low design angle being over-conservative and that the structure has an ability to redistribute stresses. The computer models indicates a stress redistribution capacity.

7.2 Further research

Firstly, because of the some difficulties were encountered, further research with higher consideration for these difficulties and problems could yield more comparable results. Some suggestions are listed:

- In order to load the beams to failure a load distribution beam could be used. This may be placed on the rolling plate and positioned under the press, enabling a higher maximum force.
- Having smaller dimensions, more test specimens may be manufactured and tested which increases the reliability of the results.
- Measure deflections directly from an independent reference point, instead of measuring deformations indirectly including deformations of the wagon.

Secondly, the whole design of the test could be more relevant in terms of comparing reality and theory. Some suggestions are listed:

- If possible use uniformly distributed loading instead of two-point loading, as this corresponds to the most common load case.
- As minimum reinforcement is used in reality, this could be included in all specimens.

Thirdly, there are several interesting aspects to study in relation to the strut-and-tie method. Some suggestions are listed:

- Whether the contribution of minimum reinforcement to load-bearing capacity should be considered or not when regarding ultimate limit state is often debated. A study focusing on how this reinforcement affects ultimate limit state and serviceability limit state, and whether plastic redistribution in the concrete could actually be accounted for, might be interesting.

- Investigation of the use of fiber reinforcement instead of minimum reinforcement mesh, as it decreases time spent on placement of reinforcement and thereby work in situ. Aspects of interest are serviceability limit state (i.e. crack widths) and ductility compared to the use of minimum reinforcement mesh.
- A study on how different material parameters affects crack-growth in high concrete members. As designing according to the strut-and-tie method might make use of a large stress redistribution due to cracking, proper crack behavior is important to capture. A suggestion is to measure different material parameters included in a model, e.g. Concrete Damaged Plasticity, and how these affects model performance compared to real tests.

REFERENCES

[1] I. S. Newton, Philosophie Naturalis Principia Mathematica, London: Benediction Classics, 1687.

[2] W.-F. Chen, Plasticity in reinforced concrete, -: McGraw-Hill Inc., 1982.

[3] P. G. Burström, Byggnadsmaterial, Uppbyggnad, tillverkning och egenskaper, Pozkal: Studentlitteratur, 2007.

[4] Swedish Standard Institute, "Svensk standard SS-EN 1992-1-1:2005," SIS Förlag, Stockholm, 2008.

[5] A. M. Neville, Properties of Concrete, Longman Group Ltd, 1995.

[6] W.-F. Chen and D.-J. Han, Plasticity for Structural Engineers, New York: Springer-Verlag, 1988.

[7] P. K. Mehta, Concrete structure, properties, and materials, New Jersey: Prentice-Hall Inc., 1986.

[8] B. Engström, "Design and analysis of deep beams, plates and other discontinuity regions," Chalmers, Göteborg, 2011.

[9] T. Isaksson and A. Mårtensson, Byggkonstruktion Regel- och formelsamling, Lund: Studentlitteratur, 2010.

[10] J. Schlaich, K. Schäfer and M. Jennewein, "Toward a Consistent Design of Structural Concrete," Presstressed concrete institute, Stuttgart, -.

[11] N. Saabye Ottosen and H. Petersson, Introduction to the finite element method, Bungay: Prentice Hall Europe, 1992.

[12] A. Hillerborg, "Application of Fracture Mechanics to Concrete," Lund, 1988.

[13] R. Malm, "Shear cracks in concrete structures subjected to in-plane stresses," Royal Institute of Technology (KTH), Stockholm, 2006.

[14] A. Hillerborg, "The theoretical basis of a method to determine the fracutre energy Gf of concrete," Rilem Technical Committees, Lund, 1985.

[15] R. Malm, Predicting shear type crack initiation and growth in concrete with non-linear finite element method, Stockholm: Royal Institute of Technology (KTH), 2009.

[16] H. Hibbitt, B. Karlsson and E. Sorensen, ABAQUS version 6.7 finite element program - standard user's manual, 2007.

[17] Dassault Systèmes, "Abaqus/CAE Users's Guide," Dassault Systèms Simulia Corp, Providence, 2013.

[18] J. Lubliner, J. Oliver, S. Oller and E. Oñate, "A Plastic-Damage Model for Concrete," *International Journal of Solids and Structures*, pp. 299-326, 6 April 1989.

[19] Building Research Institute, "Material Testing," Building Research Institute, [Online]. Available: http://www.buildingresearch.com.np/services/mt/mt2.php. [Accessed 08 02 2016].

[20] P. Bamforth, D. Chisholm, J. Gibbs and T. Harrison, "Properties of Concrete for use in Eurocode 2," The Concrete Centre, Camberley, 2008.

[21] J. Malvar and G. Warren, "Fracture Energy for Three-Point Bend Tests on Single-Edge Notched Beams," NCEL Technical Report, Port Hueneme, 1988.

[22] M. Szcecina and A. Winnicki, "Calibration of the CDP model parameters in Abaqus," The 2015 World Congress on Advances in Structural Engineering and MEchanics (ASEM15), Incheon, 2015.

APPENDIX A - DRAWINGS

This Appendix contains drawings for each of the beam configurations used. The drawings included are:

- A1 – Beam T1
- A2 – Beam T2
- A3 – Beam T3
- A4 – Beam T4

A1 – Beam T1

Beam number 1, *T1*, contains 2 reinforcement bars placed in 1 layer with the diameter of $\phi 8\ mm$. The placement of the reinforcement and overall design of the beam is shown in Figure A-1.

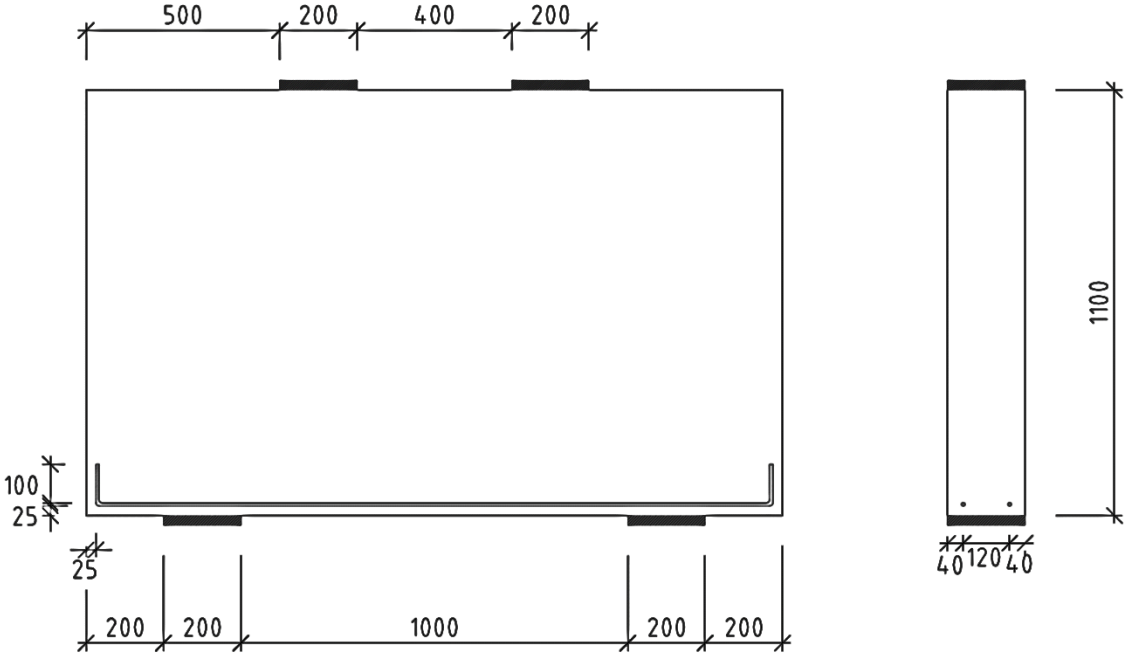

Figure A-1: Beam configuration 1

A2 – Beam T2

Beam number 2, *T2*, contains 4 reinforcement bars divided in 2 layers with the diameter of $\phi 8\ mm$. The placement of the reinforcement and overall design of the beam is shown in Figure A-2.

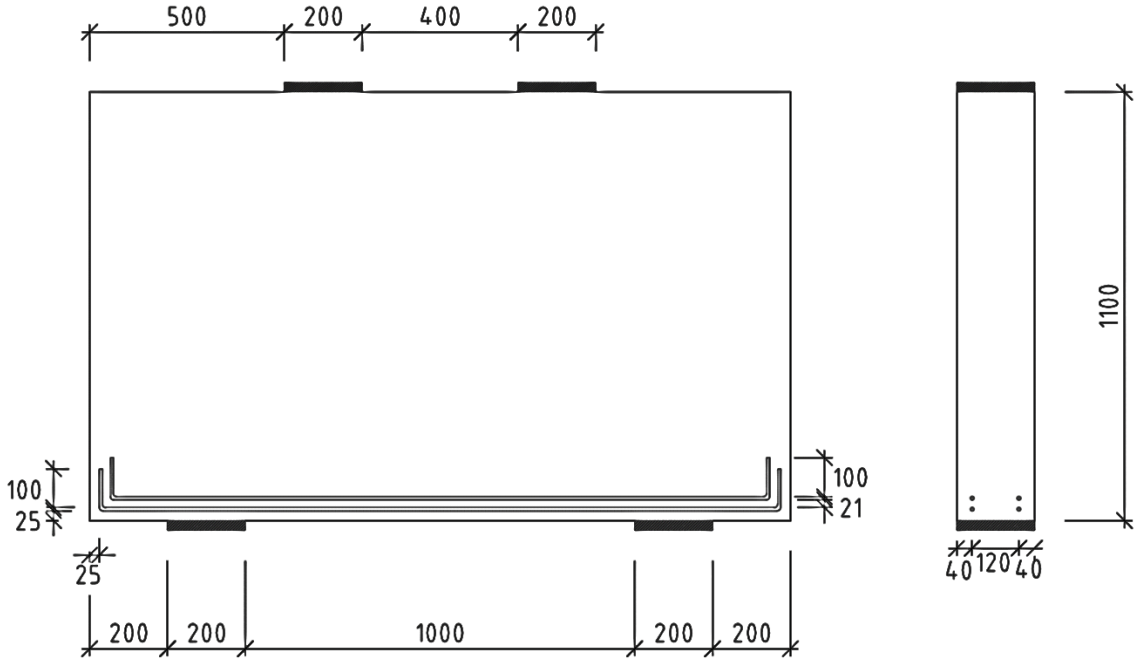

Figure A-2: Beam configuration 2

A3 – Beam T3

Beam number 3, *T3*, contains 6 reinforcement bars divided in 2 layers with the diameter $\phi 8\ mm$. The placement of the reinforcement and overall design of the beam is shown in Figure A-3.

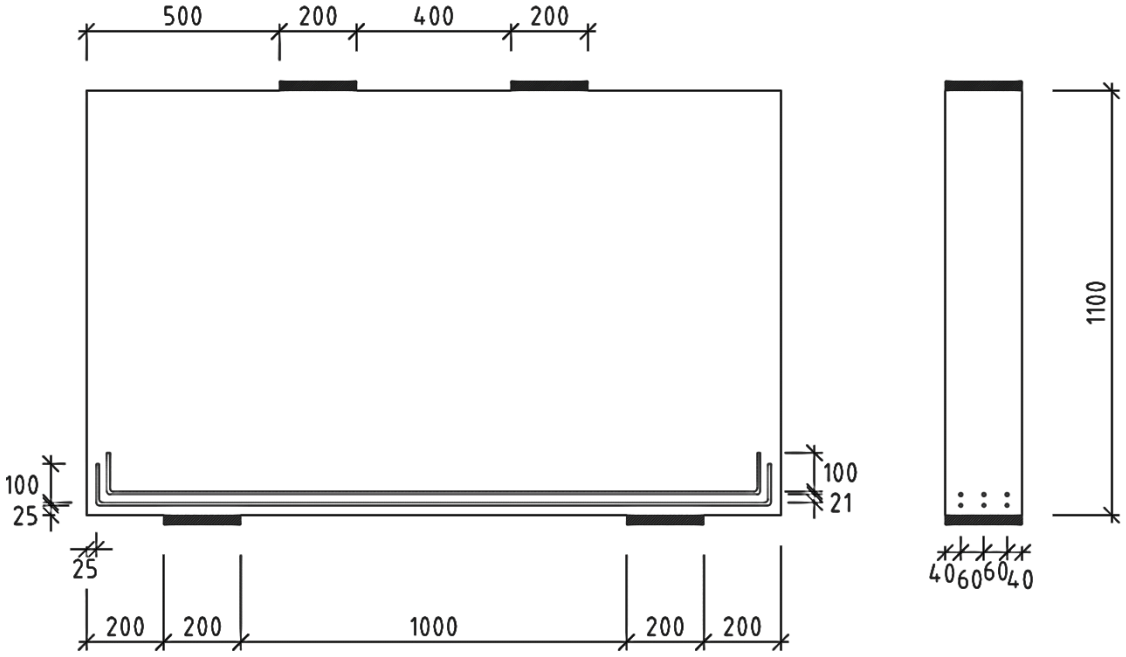

Figure A-3: Beam configuration 3

A4 – Beam T4

Beam number 4, *T4*, contains 4 reinforcement bars divided in 2 layers with the diameter of $\phi 8\ mm$, this beam is also equipped with minimum reinforcement in accordance with current standards. The placement of the primary reinforcement, minimum reinforcement and the overall design of the beam is shown in Figure A-4.

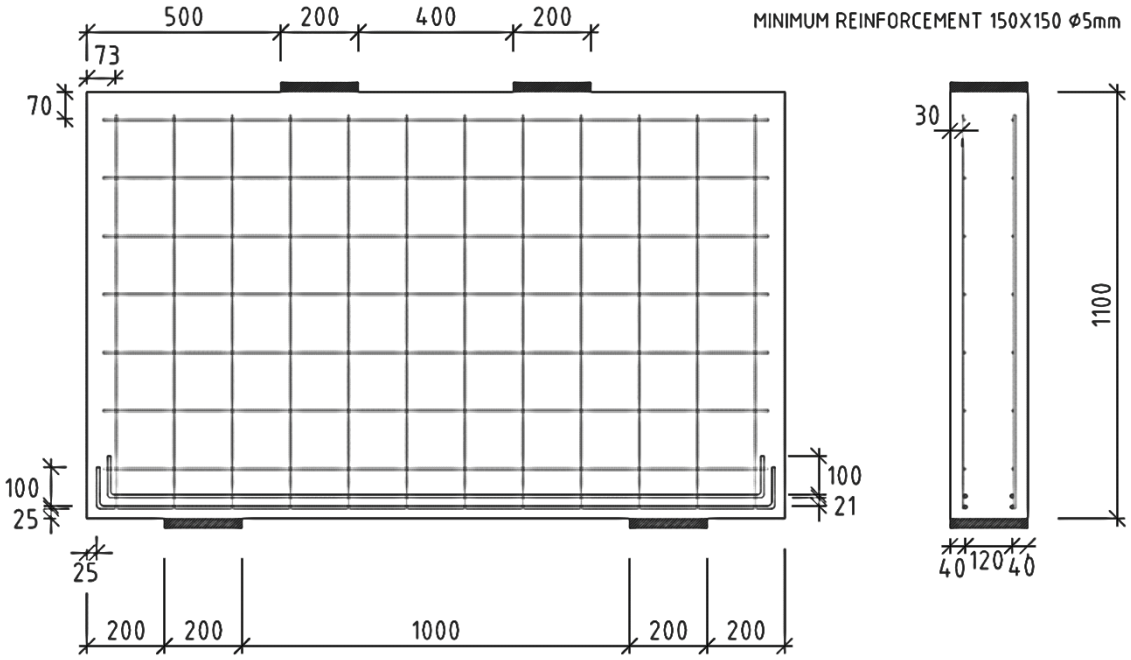

Figure A-4: Beam configuration 4

APPENDIX B - CALCULATIONS

This Appendix contains several sections, one for each of the calculations made. The sections included are the following:

- B1 – Struts
- B2 – Nodes
- B3 – Ties
- B4 – Anchorage Length
- B5 – Load Capacity
- B6 – Revised Load Capacity

The equations used have been showed and motivated in chapter 3 in the report. *Appendix B* will only show the calculations made.

General values:

$$f_{cm} = f_{ck} + 8\ MPa = 38\ MPa\ (Equation\ (2.16))$$

$$f_{cd} = \frac{f_{cm}}{\gamma_C} = \frac{38}{1.5} = 25.3\ MPa\ (Equation\ (2.15))$$

$$v' = 1 - \frac{f_{cm}}{250} = 0.848\ (Equation\ (3.6))$$

B1 – Struts

Strut forces

The calculations are carried out using the highest applicable capacities presented in subsection 3.1.2.

$$C_1 = \frac{F}{2\sin\alpha} = \frac{1012}{2\sin 73.4} = 528\ kN\ (Equation\ (3.1))$$

$$C_2 = \frac{F}{2} = \frac{1012}{2} = 506\ kN\ (Equation\ (3.2))$$

$$C_3 = \frac{F}{2\tan\alpha} = \frac{1012}{2\tan 73.4} = 151\ kN\ (Equation\ (3.3))$$

Strut control of capacity

From Appendix B2 it is shown that the maximum stress in a strut is $\sigma_C = 12.6\ MPa$. This stress appears at the lower loading plate as well as the upper loading plate. The stress is verified according to the maximum capacity:

$$\sigma_{Rd,max} = 0{,}6 \cdot \nu' \cdot f_{cd}\ (Equation\ (3.4))$$

$$\sigma_{Rd,max} = 0{,}6 \cdot 0{,}848 \cdot 25{,}3 = 12{,}87\ [MPa]$$

Since $\sigma_{c,max} < \sigma_{Rd,max}$ the struts are OK!

B2 – Nodes

To calculate the strength of the nodes the dimensions of them needs to be determined. The controls are carried out using the highest applicable strut forces C_1, C_2, C_3 presented in Appendix B1. Placement of the two nodes may be seen in Figure 3-1. Some values are valid for both nodes, see Appendix B1.

Since the highest forces appear in T3, design is based upon this configuration. Thus the internal angle becomes $\alpha = 73.4°$.

Control of the upper (CCC) node

Geometry and placing of forces acting on the upper node are presented in Figure 3-3.

$$\sigma_{Rd,max} = k \cdot \nu' \cdot f_{cd} = 1 \cdot 0.848 \cdot 25.3 = 22.3\ MPa\ (Equation\ (3.5))$$

$$a_1 = \sqrt{a_2^2 + a_3^2} = 0.209\ m\ (Equation\ (3.7))$$

$$a_2 = b_{lp} = 0.2\ m\ (Equation\ (3.8))$$

$$a_3 = \frac{a_2}{\tan \alpha} = \frac{0.2}{\tan 73.4} = 0.0596\ m\ (Equation\ (3.9))$$

The node resistance is compared with the forces:

$$\sigma_{Rd,max} \geq \sigma_{Ci} = \frac{C_i}{a_i b}\ (Equation\ (3.10))$$

$$\sigma_{C1} = \frac{C_1}{a_1 \cdot b} = \frac{528 \cdot 10^3}{200 \cdot 209} = 12.6\ MPa\ (Equation\ (3.10))$$

$$\sigma_{C2} = \frac{C_2}{a_2 \cdot b} = \frac{506 \cdot 10^3}{200 \cdot 200} = 12.6\ MPa\ (Equation\ (3.10))$$

$$\sigma_{C3} = \frac{C_3}{a_3 \cdot b} = \frac{151 \cdot 10^3}{200 \cdot 59{,}6} = 12.6\ MPa\ (Equation\ (3.10))$$

Since $\sigma_{Rd,max} > \sigma_{C1}, \sigma_{C2}, \sigma_{C3}$ the nodes are OK.

Control of the lower (CCT) node

The node capacity is calculated according to:

$$\sigma_{Rd,max} = k_2 \nu' f_{cd} = 0.85 \cdot 0.848 \cdot 25.3 = 18.26\ MPa\ (Equation\ (3.11))$$

Where $k_2 = 0{,}85$ (National recommendation, due to biaxial tensile stress state)

Geometry of the node is needed to calculate the stresses, Figure 3-4.

$$a_s = r_{tp} = 43.5\ mm\ (Equation\ (3.12))$$

$$u = 2a_s = 2 \cdot 43.5 = 87\ mm\ (Equation\ (3.13))$$

$$a_2 = \left(a_1 + \frac{u}{\tan\alpha}\right)\sin\alpha = \left(200 + \frac{87}{\tan 73.4°}\right) \cdot \sin 73.4° = 216.5\ mm\ (Equation\ (3.14))$$

$$a_1 = b_{up} = 200\ mm = (Equation\ (3.15))$$

The node resistances are compared with the stresses:

$$\sigma_{Rd,max} \geq \sigma_{Ci} = \frac{C_i}{a_i b}\ (Equation\ (3.10))$$

$$\sigma_1 = \frac{C_1}{b_{up} \cdot b} = \frac{506 \cdot 10^3}{200 \cdot 200} = 12.6\ [MPa]\ (Equation\ (3.10))$$

$$\sigma_2 = \frac{C_2}{a_2 \cdot b} = \frac{528 \cdot 10^3}{216.5 \cdot 200} = 12.2\ [MPa]\ (Equation\ (3.10))$$

Since $\sigma_{Rd,max} > \sigma_{C1}, \sigma_{C2}$ the nodes are OK!

B3 – Minimum concrete covering

Since the concrete coverage should not affect the strength of the beam these calculations are not referred to in the report. But since the coverage must be made big enough to prevent failure and follow the codes a design have of course been made, and shown in the following section.

The concrete coverage is controlled both in terms of coverage between the reinforcement bars as well as from the reinforcement to the face of the beam.

Cover to beam edge

The calculations regarding minimum concrete covering of the reinforcement is done according to the standards in the Eurocode [4], subsection 4.4.1.

Minimum coverage is calculated according to Equation (B.1)

$$c_{nom} = c_{min} + \Delta c_{dev} \tag{B.1}$$

Where c_{min} is defined as a minimum coverage and Δc_{dev} offers a margin for error.

$$c_{min} = \max \begin{cases} c_{\min,b} \\ c_{\min,dur} + \Delta c_{dur,\gamma} - \Delta c_{dur,add} = 10\ mm \\ 10\ mm \end{cases} \tag{B.2}$$

Where the included parameters vary as follows:

$c_{\min,b} = 8\ mm$ since reinforcement bars are separated

$c_{\min,dur} = 10\ mm$ since exposure class $X0$ is chosen (no risk for corrosion or attack) and structural class S1 which is the recommended minimum class.

$\Delta c_{dur,\gamma} = 0\ mm$ recommended value

$\Delta c_{dur,add} = 0\ mm$ recommended value

$\Delta c_{dev} = 10\ mm$ recommended minimum value

This assumptions and recommendations yields the total minimum concrete coverage to be a minimum of Equation (B.3).

$$c_{nom} = c_{min} + \Delta c_{dev} = 10 + 10 = 20\ mm \tag{B.3}$$

Cover between reinforcement bars

The calculations regarding minimum concrete covering of the reinforcement is done according to the standards in the Eurocode [4], section 8.2. See Equation (B.4) for the three requirements.

$$c_{between} = max \begin{cases} k_1 \cdot \phi_{bar} \\ d_g + k_2 \\ 20 \end{cases} = \max \begin{cases} 1 \cdot 8 \\ 16 + 5 = 21\ mm \\ 20 \end{cases} \quad (B.4)$$

Where the variable d_g is the maximum aggregate size, in this case $16\ mm$. $k_1 = 1$ and $k_2 = 5$ mm respectively, according to recommendations.

B4 – Anchorage Length

The calculation of the anchorage length is done in accordance with Eurocode [4]. These are fully presented in the appendix as they are not essential for the strut-and-tie method. Two cases are relevant; either 2 or 3 reinforcement bars per layer.

Two reinforcement bars

Anchorage length is calculated according to:

$$l_{b,rqd} = \frac{\phi}{4}\frac{\sigma}{f_{bd}} \tag{B.5}$$

$$f_{bd} = 2.25\eta_1\eta_2 f_{ctd} \tag{B.6}$$

Assuming good anchorage conditions yields:

$$\eta_1 = 1.0$$
$$\phi \leq 32\ mm \rightarrow \eta_2 = 1.0$$

Mean values are used for strengths of concrete.

$$f_{ctd} = \frac{f_{ctm}}{\gamma_C} = \frac{f_{ctm}}{1.5} = 1.9\ [MPa] (Equation\ (2.17))$$

$\sigma = 500\ [MPa]$ due to yielding of reinforcement

$$l_{b,rqd} = \frac{\phi}{4}\frac{\sigma}{f_{bd}} = \frac{0.008}{4}\frac{500}{1.9} = 526\ mm$$

The design value of anchorage length is calculated according to:

$$l_{bd} = \alpha_1\alpha_2\alpha_3\alpha_4\alpha_5 l_{b,rqd} \geq l_{b,\min} \tag{B.7}$$

Where α_1 considers the effect of the shape of the rebars assuming enough concrete cover is provided, see Figure B-1 for dimension specifications.

$$\alpha_1 = 0.7 \text{ as } c_d > 3\phi = 24mm$$

$$c_d = \min\begin{cases} a/2 \\ c_1 \end{cases} = \min\begin{cases} 112/2 \\ 36 \end{cases} = 36 \tag{B.8}$$

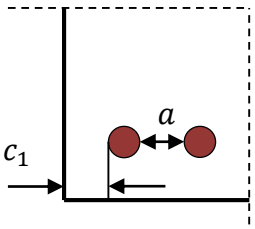

$$c_d = \min\left(\frac{a}{2}.c_1\right)$$

Figure B-1: Effect of concrete cover, adopted from [4]

α_2 considers the effect of concrete cover:

$$\alpha_2 = 1 - 0.15 \cdot \frac{c_d - 3\phi}{\phi} = 0.775 \qquad (B.9)$$

Where

α_3 considers the confinement of vertical shear reinforcement: $\alpha_3 = 1$

α_4 considers the effect of one or several vertical rebars welded to the reinforcement bar: $\alpha_4 = 1$

α_5 considers the effect of compression perpendicular to the chipping plane within the design anchorage length: $\alpha_5 = 1$ assumption on safe side

$$l_{b,min} = \max\begin{cases} 0.3 \cdot l_{b,rqd} \\ 10\phi \\ 100 \end{cases} = \max\begin{cases} 103.5mm \\ 80mm \\ 100mm \end{cases} = 103.5\ mm \qquad (B.10)$$

$$l_{bd} = \alpha_1\alpha_2\alpha_3\alpha_4\alpha_5 l_{b,rqd} = 0{,}7 \cdot 0{,}775 \cdot 1 \cdot 1 \cdot 1 \cdot 526 = 286\ mm \geq l_{b,\min} = 103.5\ mm$$

$$l_{b,rqd} = 286\ mm$$

Three reinforcement bars

Anchorage length is calculated according to Equation (B.5) and (B.6).

Assuming good anchorage conditions yields:

$$\eta_1 = 1.0$$
$$\phi \leq 32\ mm \rightarrow \eta_2 = 1.0$$

Mean values are used for strengths of concrete.

$$f_{ctd} = 1.9\ [MPa]\ (Equation\ (2.17))$$

$\sigma = 500\ [MPa]$ due to assumed yielding of reinforcement

$$l_{b,rqd} = \frac{\phi}{4}\frac{\sigma}{f_{bd}} = \frac{0.008}{4}\frac{500}{1.9} = 526\ mm$$

The design value of anchorage length is calculated according to:

$$l_{bd} = \alpha_1\alpha_2\alpha_3\alpha_4\alpha_5 l_{b,rqd} \geq l_{b,\min}$$

Where α_1 considers the effect of the shape of the rebars assuming enough concrete cover is provided

$$\alpha_1 = 0.7 \text{ as } c_d > 3\phi = 24mm$$

$$c_d = \min\begin{cases} a/2 \\ c_1 \end{cases} = \min\begin{cases} \frac{112}{2} - \frac{8}{2} \\ \frac{2}{36} \end{cases} = 26\ mm$$

α_2 considers the effect of concrete cover:

$$\alpha_2 = 1 - 0.15 \cdot \frac{c_d - 3\phi}{\phi} = 0.9625$$

α_3 considers the confinement of vertical shear reinforcement: $\alpha_3 = 1$

α_4 considers the effect of one or several vertical rebars welded to the reinforcement bar: $\alpha_4 = 1$

α_5 considers the effect of compression perpendicular to the chipping plane within the design anchorage length: $\alpha_5 = 1$ assumption on safe side

$$l_{b,min} = \max\begin{cases} 0.3 \cdot l_{b,rqd} \\ 10\phi \\ 100 \end{cases} = \max\begin{cases} 103.5mm \\ 80mm \\ 100mm \end{cases} = 103.5\ mm$$

$$l_{bd} = \alpha_1\alpha_2\alpha_3\alpha_4\alpha_5 l_{b,rqd} = 0.7 \cdot 0.9625 \cdot 1 \cdot 1 \cdot 1 \cdot 526 = 354\ mm \geq l_{b,\min} = 103.5\ mm$$

$$l_{b,rqd} = 354\ mm$$

B5– Load Bearing Capacity

The load bearing capacity of the beams are calculated in accordance with chapter 3. The calculations are divided into specimens T1, T2, T3 and T4. The load placement is shown in Figure 1-1 and the equilibrium is shown in Figure 3-5. Calculations are made for angles of $\alpha = 73.4° \; or \; 73.6°, \alpha = 60°$ and $\alpha = 45°$ for all specimens. All calculations are based on Equation (3.21).

T1

$$A_s = 2 \cdot \phi 8$$

$$\alpha = 73{,}6\,°$$

$$F = 2 \cdot 500 \cdot 2 \cdot \frac{0.008^2 \cdot \pi}{4} \cdot \tan 73{,}6 = 342\ kN$$

$$\alpha = 60\,°$$

$$F = 2 \cdot 500 \cdot 2 \cdot \frac{0.008^2 \cdot \pi}{4} \cdot \tan 60 = 201\ kN$$

$$\alpha = 45\,°$$

$$F = 2 \cdot 500 \cdot 2 \cdot \frac{0.008^2 \cdot \pi}{4} \cdot \tan 45 = 174\ kN$$

T2

$$A_s = 4 \cdot \phi 8$$

$$\alpha = 73{,}4\,°$$

$$F = 2 \cdot 500 \cdot 4 \cdot \frac{0.008^2 \cdot \pi}{4} \cdot \tan 73{,}4 = 674\ kN$$

$$\alpha = 60\,°$$

$$F = 2 \cdot 500 \cdot 4 \cdot \frac{0.008^2 \cdot \pi}{4} \cdot \tan 60 = 348\ kN$$

$$\alpha = 45\,°$$

$$F = 2 \cdot 500 \cdot 4 \cdot \frac{0.008^2 \cdot \pi}{4} \cdot \tan 45 = 201\ kN$$

T3

$$A_s = 6 \cdot \phi 8$$

$$\alpha = 73{,}4\,°$$

$$F = 2 \cdot 500 \cdot 6 \cdot \frac{0.008^2 \cdot \pi}{4} \cdot \tan 73{,}4 = 1012\ kN$$

$$\alpha = 60\,°$$

$$F = 2 \cdot 500 \cdot 6 \cdot \frac{0.008^2 \cdot \pi}{4} \cdot \tan 60 = 522\ kN$$

$$\alpha = 45\ °$$

$$F = 2 \cdot 500 \cdot 6 \cdot \frac{0.008^2 \cdot \pi}{4} \cdot \tan 45 = 302\ kN$$

T4

As T4 has the same primary reinforcement as T2, and the minimum-reinforcement is assumed not to provide any additional strength, this specimen is assumed to withstand the same load as T2.

APPENDIX C – DETAILED RESULTS FROM LABORATION

This Appendix contains some detailed results from the laborations. The results included are the following:

- C1 – Tensile test of reinforcement
- C2 – Fracture energy of concrete
- C3 – Crack width growth, beam T4

C1– Tension test of reinforcement

Figure C-1 shows the response curves for the reinforcement. The dashed line shows the 0.2 %-limit.

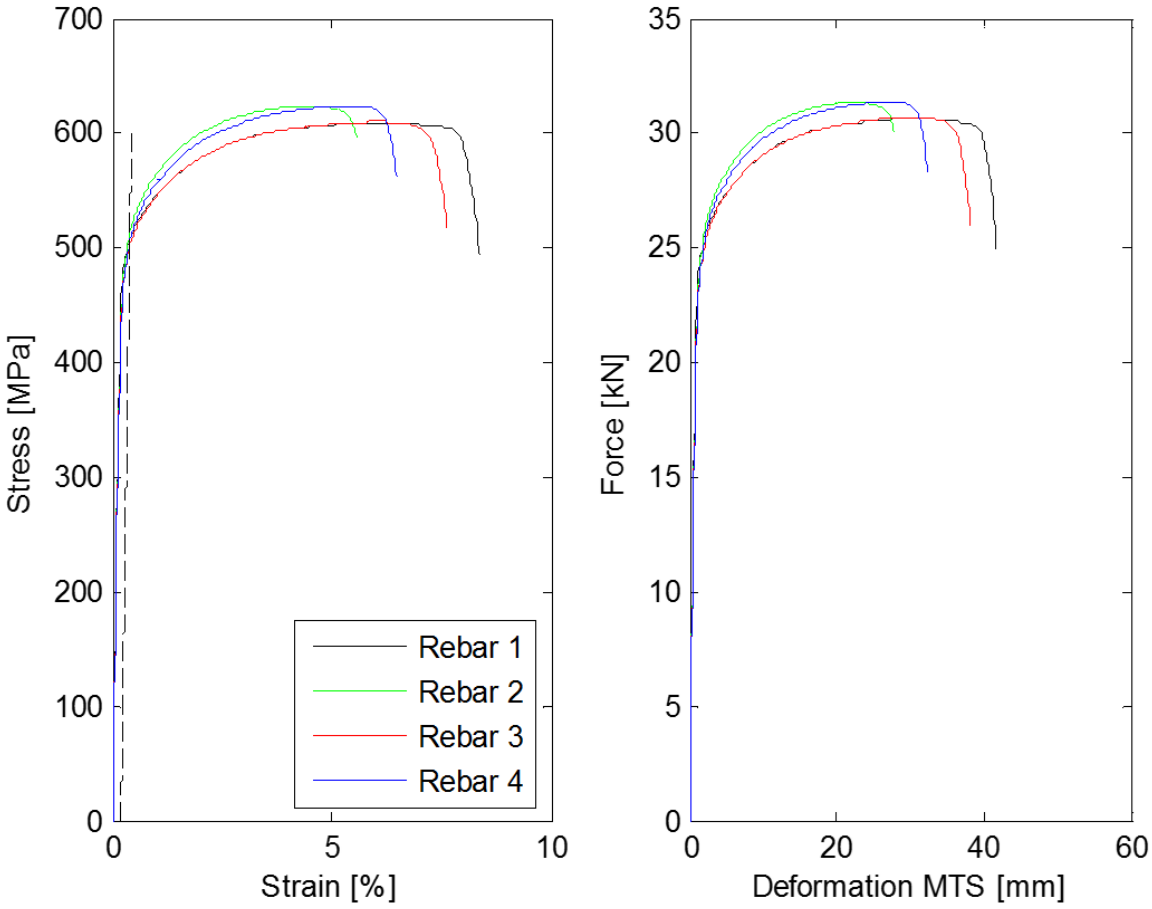

Figure C-1: a) Stress-strain curves for the 4 tested specimens b) Force-strain curves for the 4 tested specimen

C2– Fracture energy

To achieve the fracture energy G_f the variable U_0 primarily must be found. U_0 is the mean integral of the curves shown in Figure C-2.

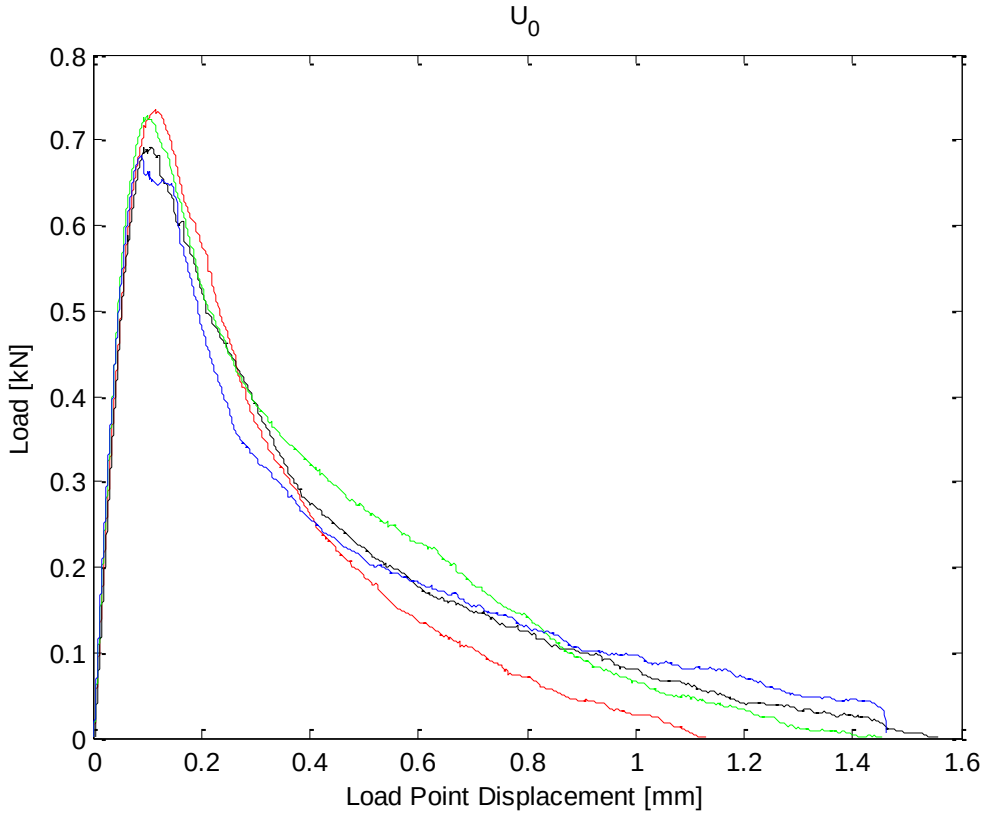

Figure C-2: Graph of U_0 from the 4 successful tests

C3– Crack growth, beam T4

A camera was fixed on a tripod close to the specimen as soon as a crack were seen. A ruler was placed within frame and a photo was taken. At a few load levels the test were paused, notes were made on the beam and photos taken. Evaluating these pictures gave the crack width growth, the data extracted is shown in Figure C-3.

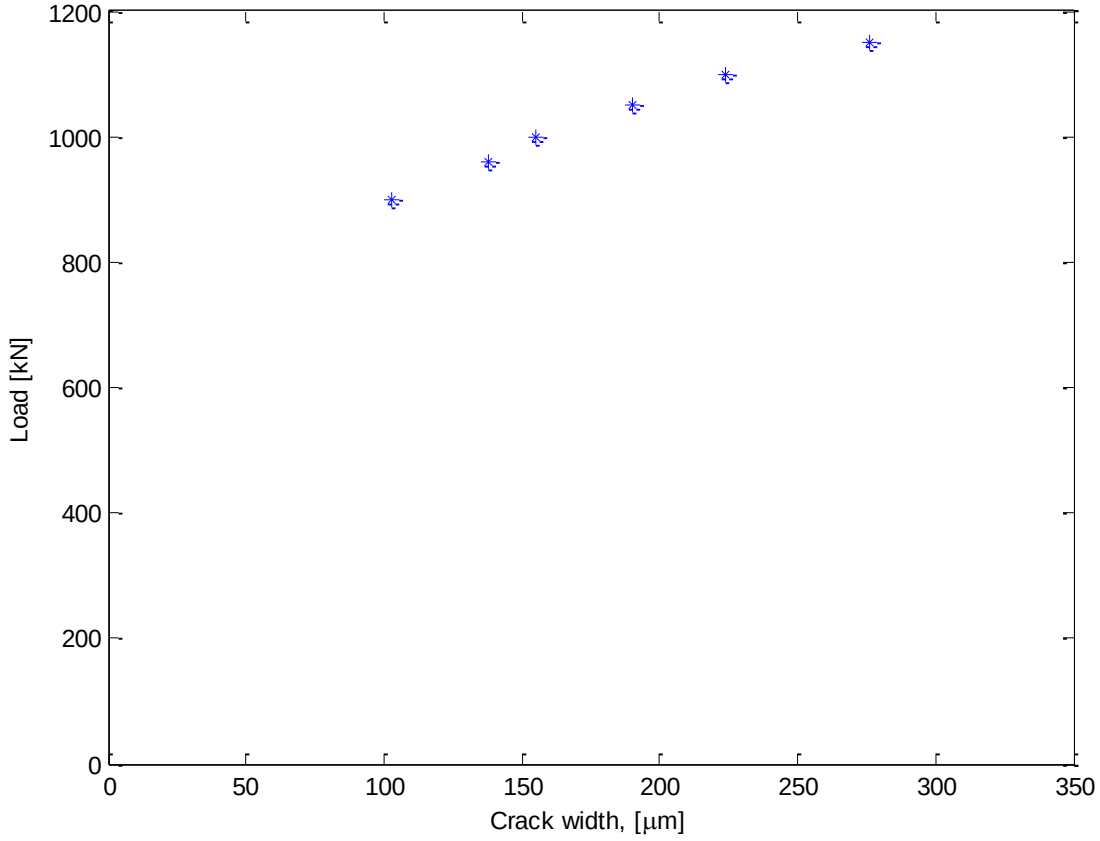

Figure C-3: Crack growth, beam T4

APPENDIX D – Crack patterns

Crack patterns visible for the naked eye at close range, were filled with a permanent marker and then later re-created according to Figure D-1 - Figure D-4. These representations of the cracks are schematic.

D1– Crack pattern, beam T1

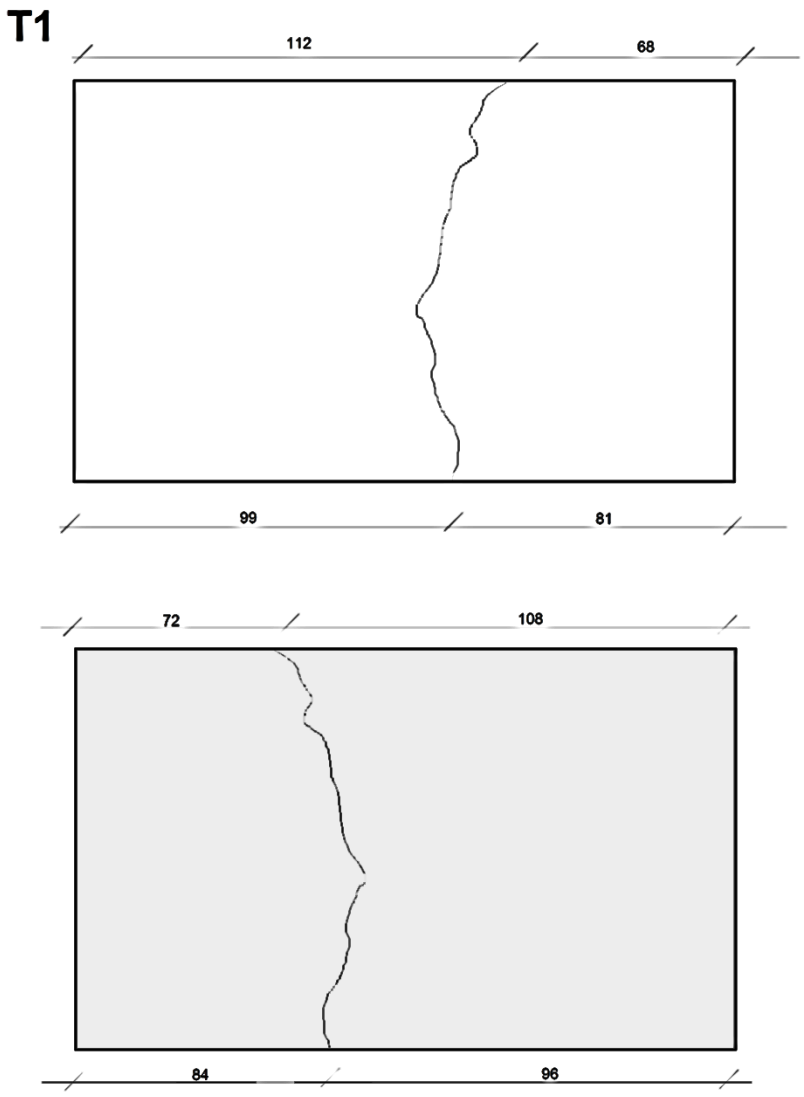

Figure D-1: Crack pattern, T1

D2– Crack pattern, beam T2

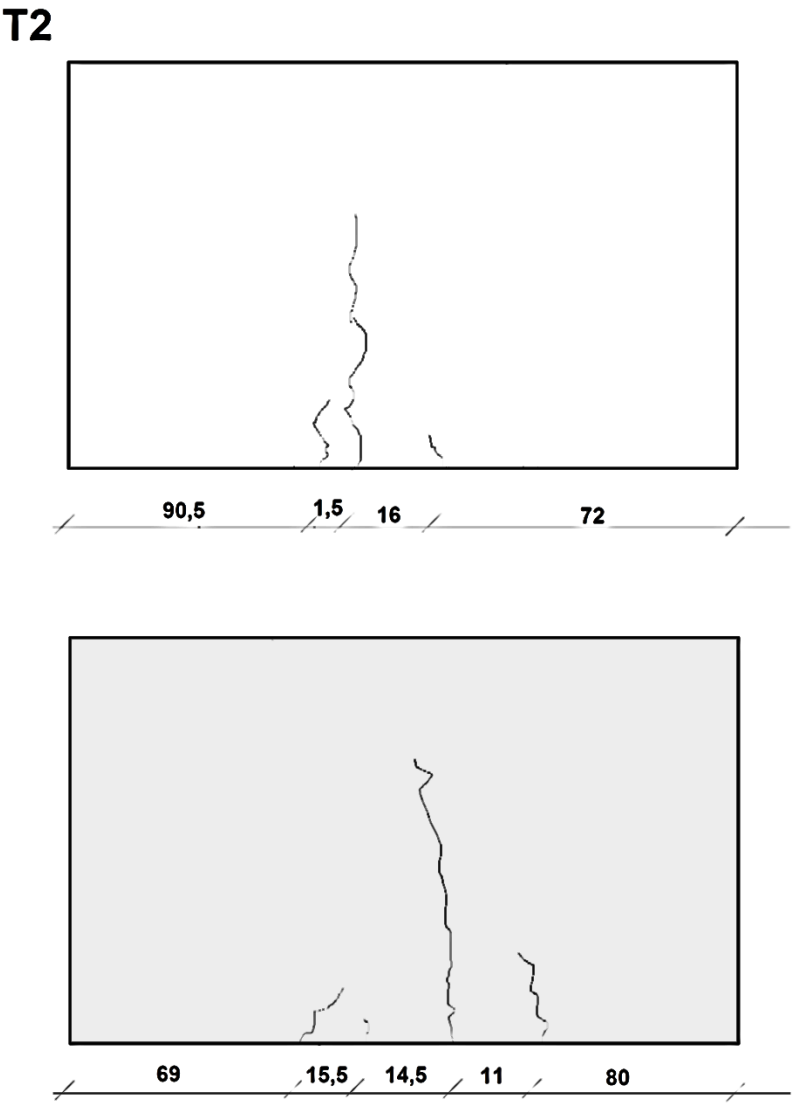

Figure D-2: Crack pattern, T2

D3– Crack pattern, beam T3

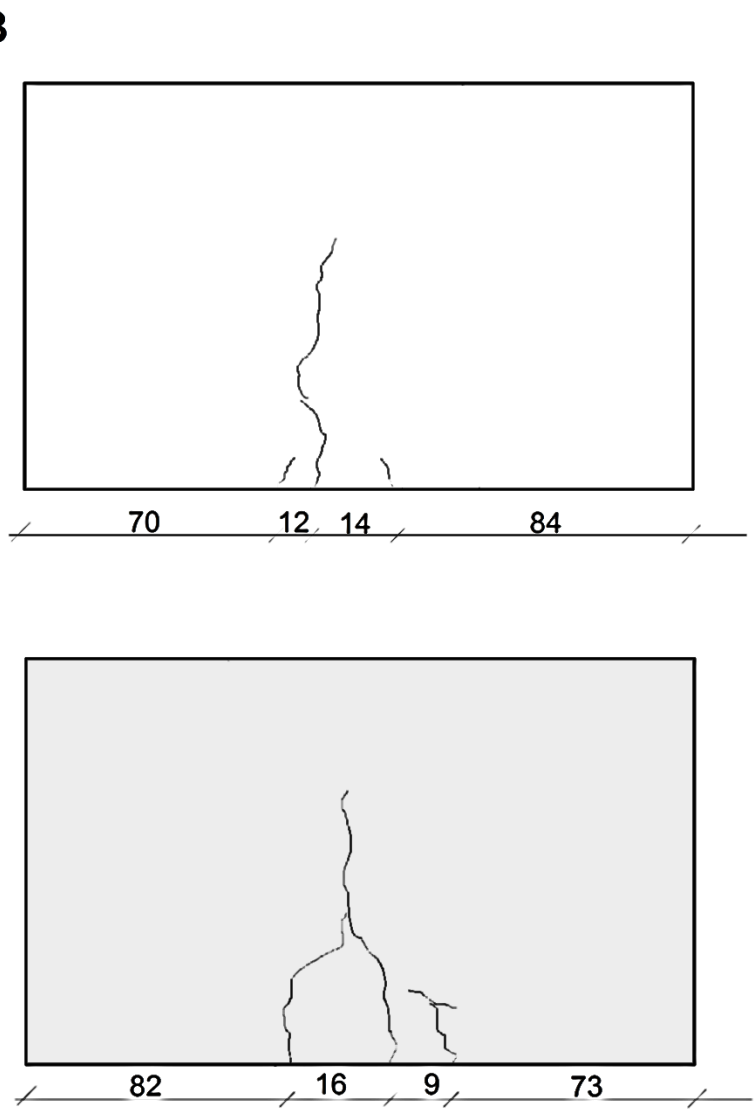

Figure D-3: Crack pattern, T3

D4– Crack pattern, beam T4

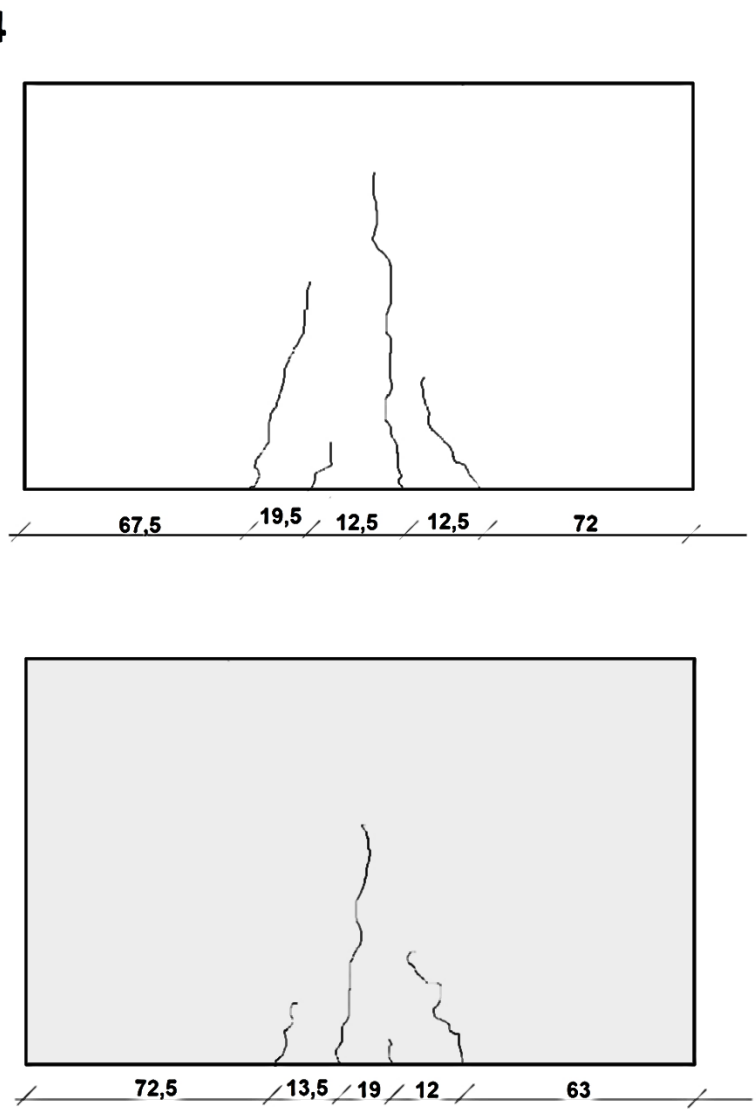

Figure D-4: Crack pattern, T4